IN-18

182479

108 P

Feasibility Study of an Orbiting Laboratory for Testing CSI Technology

Andrew S. Bicos and Gregory G. Loboda

McDonnell Douglas Aerospace
Huntington Beach, California

(NASA-CR-191524) FEASIBILITY STUDY
OF AN ORBITING LABORATORY FOR
TESTING CSI TECHNOLOGY Final Report
(McDonnell-Douglas Corp.) 108 p

N94-13016

Unclas

G3/18 0182479

NASA

National Aeronautics and
Space Administration

Langley Research Center
Hampton, Virginia 23681-0001

TABLE OF CONTENTS

ACRONYMS

ACE	Advanced Composition Explorer
ACS	Attitude Control System
ACTEX	Advanced Controls Technology Experiment
ADACS	Attitude Determination and Control Subsystem
ASTREX	Advanced Space Structures Technology Research Experiments
CEM	CSI Evolutionary Model
CER	Cost Estimating Relations
CSI	Controls-Structures Integration
CT&R	Command, Telemetry and Ranging
ELV	Expendable Launch Vehicle
EOS	Earth Observation System
FEM	Finite Element Model
GI	Guest Investigator
GTF	Ground Test Facility
HIRIS	High-Resolution Imaging Spectrometer
INFLEX	Inexpensive Structures & Materials Flight Experiment
JPL	Jet Propulsion Laboratory
LACE	Laser Atmospheric Compensation Experiment
LaRC	Langley Research Center
LAWS	Laser Atmospheric Wind Sounder
LEO	Low Earth Orbit
LOS	Line of Sight
LSS	Large Space Structures
MACE	Middeck Active Control Experiment
MFLOPS	Millions of Floating Point Operations Per Second
MIPS	Millions of Instructions Per Second
MODE	Middeck 0-gravity Dynamics Experiment
MSFC	Marshall Space Flight Center
PACOSS	Passive and Active Control of Space Structures
SAFE	Solar Array Flight Experiment
SDIO	Strategic Defense Initiative Office
SID	System Identification
SSF	Space Station Freedom
STA	Structural Test Article

BACKGROUND AND JUSTIFICATION

Controls-Structures Integration (CSI) technology is enabling or enhancing for many future NASA missions, and as such, considerable resources have been expended in the last decade in advancing the state of the art. Applications of CSI technology will benefit future systems such as an evolving Space Station Freedom (SSF), an Earth Observation System (EOS), and other science systems that include large interferometers and large diameter telescopes. CSI technology will allow these kinds of systems to meet stringent performance requirements on their pointing and tracking, jitter, and vibration settling time. Almost all of the CSI-related research, however, has been analytical and ground-test research; there have been very few flight test programs. The flight test programs to date have investigated orbital structural dynamics issues, not CSI issues. There is a need for a flight test program because this technology will not be used by future systems programs if it is not first convincingly demonstrated under orbital conditions. Many of the CSI technologies developed so far have been demonstrated on the ground, but because the dynamics of spacecraft change due to the absence of gravity and prolonged exposure to the space environment, flight demonstration is essential. Previously proposed, dedicated free-flying CSI experiment programs have been canceled when their costs escalated beyond $100M. Successful flight demonstrations should be able to be accomplished by smaller and less expensive programs that provide enough demonstration capability to justify their costs. This study evaluated the feasibility of just such a concept.

CSI-STAR CONCEPT

CSI-Star is envisioned as an orbiting CSI facility for guest investigators. It will be affordable enough to fly yet have sufficient capability for demonstrating technologies that have been developed on the ground and are now ready to be demonstrated in space. The CSI-Star concept is unique in that it proposes to operate as a free-flying CSI laboratory for at least one year in low earth orbit (LEO) by using a flight-proven small spacecraft bus (smallsat) launched as a secondary payload. This will enable the costs of the program to remain far below those of previously proposed CSI free-flyers. For this study, we baselined the use of the Ball QuickStar spacecraft bus integrated with a CSI experiment payload. This payload, to be assembled using commercial and flight-proven hardware satisfying typical guest investigator (GI) requirements, will provide GIs great flexibility to perform various experimental demonstrations of CSI technology. The spacecraft and its CSI payload will be launched on a McDonnell Douglas Delta II launch vehicle as a secondary payload. During the initial on-orbit period, the correct operation

of the spacecraft and experiment payload systems will be checked out by conducting baseline CSI experiments, after which the facility will be turned over to NASA for GI use. Over the next year, several GI groups will perform their own experiments to investigate the CSI-related issues of their choice. A schematic of the concept is shown in Figure 1.

The CSI-Star facility is made up of a flight segment and a ground segment. The flight segment consists of a CSI experiment payload that is highly integrated into the QuickStar smallsat bus. The integration of the payload into the bus is such that the existing bus subsystems are used to the greatest extent possible so as to maximize the number and variety of the payload components. The QuickStar was baselined for the CSI-Star because it is an existing, flight-demonstrated design that has more weight, power and computational capability than most other smallsats. The prototype QuickStar was the bus for the SDIO LOSAT-X mission that was launched as a Delta secondary payload in July 1991. Using this smallsat bus launched in the same way will minimize the cost and risk to a CSI-Star program. The use of the Delta II expendable launch vehicle (ELV), which is the most reliable ELV in the world and has five to ten launches per year, allows for several flight opportunities for secondary payloads per year. The CSI-Star ground segment consists of a single, portable PC-based ground station. This was also used successfully on the LOSAT-X mission and will provide the required telemetry capability for the CSI-Star mission.
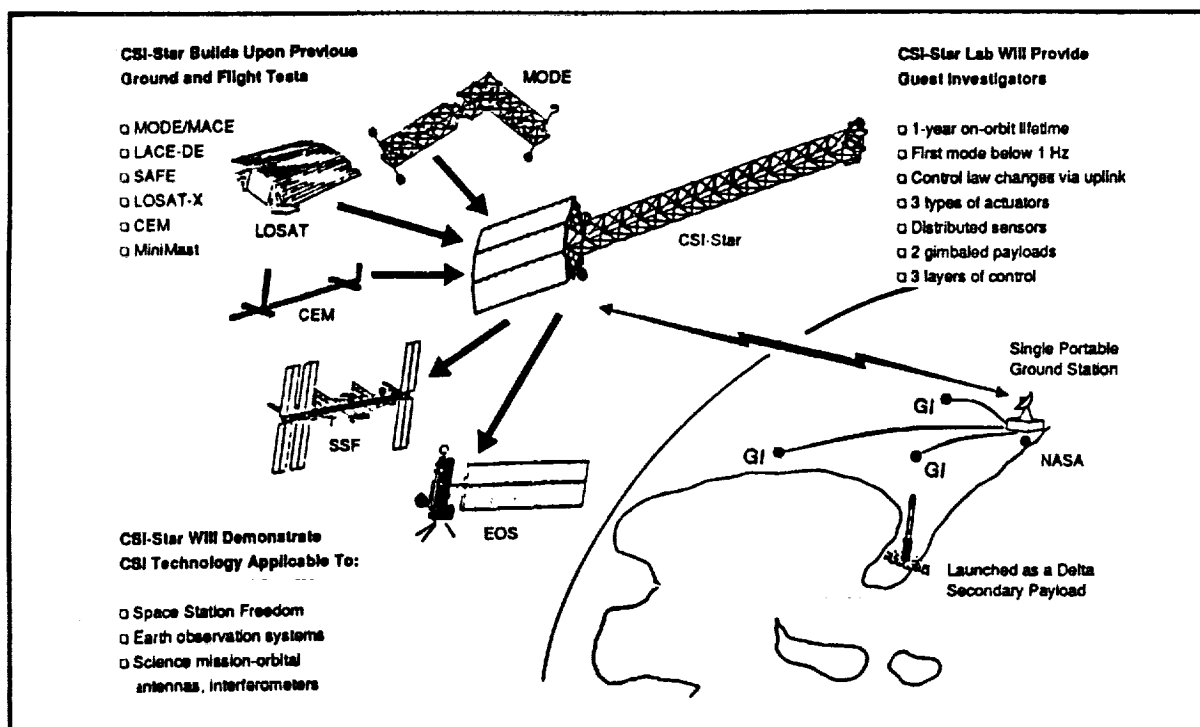

Figure 1. Schematic of CSI-Star System.

The baseline CSI experiment payload components were selected based on cost. availability, reliability, and how well each component helps the payload meet the desired CSI technology demonstration objectives. These objectives include demonstration of system identification techniques for updating spacecraft models and for monitoring the health of the spacecraft structure, and methods for operating several payload systems on a multibody platform using various local, global and hierarchical control architectures with several types of sensors and actuators. Figure 2 shows a summary of the baseline CSI-Star components and their arrangement on the QuickStar bus. The types of experiments that can be supported by CSI-Star include, but are not limited to, the following.

- Measurement of the dynamic response of the structure caused by one or more programmable disturbance sources.
- Control of the dynamic response of the structure caused by one or more programmable disturbance sources.
- Control of the pointing line-of-sight (LOS) of a gimbaled payload during the operation of one or more programmable disturbance sources.

Depending on the objectives of an experiment, the combination of disturbance sources, control actuators, and sensors can be varied among all of the available components. This will allow GIs the flexibility to tailor their experiments to achieve their specific objectives.

The QuickStar bus provides adequate capabilities for the CSI experiment payload and for a wide range of experiment options. For the baseline CSI payload, Table 2 lists the CSI-Star requirements, the QuickStar capabilities and the margins.
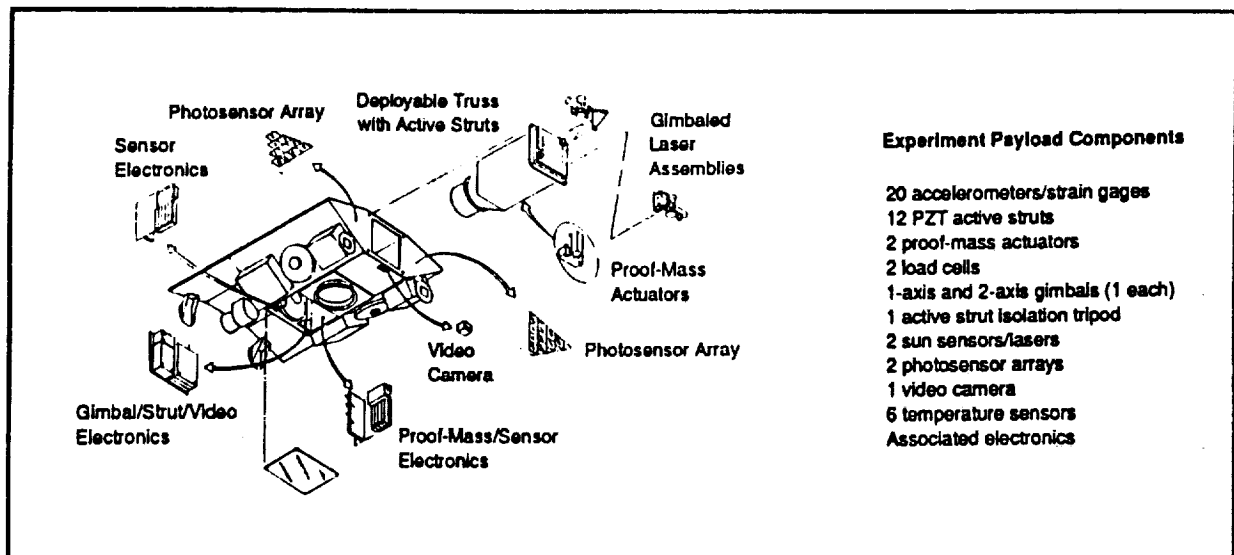

Figure 2. CSI-Star Orbiting Laboratory Components and Configuration.

Table 2. CSI-Star Requirements are Satisfied by QuickStar Capabilities

Item	QuickStar Capability	CSI-Star Requirement	Margin
Payload weight	70 lbs	59 lbs	19%

Payload power
  Peak
  Orbit Average
	140 W
	44 W
		69 W
		16 W to 38 W
			51%
			175 % to 16 %

Data
  Storage
  Downlink
	1 to 2 Gbits
	1 Mbps
		0.72 Gbit (orbit ave)
		0.56 Mbps (orbit ave)
			39 % to 178 %
			79 %

Processor Speed	0.6 MFLOPS	0.44 MFLOPS (nom)	36 %

COST, RISK AND SCHEDULE

The study estimated that a CSI-Star orbiting facility capable of meeting GI science requirements can be developed, manufactured, tested and launched by July 1997 for a total program cost of $20M to $26M. Of this total cost, the experiment payload and initial orbital operations are estimated to cost $8M to $10M. The cost of the spacecraft bus, launch services, and a single PC-based ground station is estimated to be $12M to $16M. Because this latter figure is based on a recent flight program (LOSAT-X) we believe it to be an excellent estimate. The former figure has more uncertainty in it, however, if a low-cost, fast-track program approach similar to LOSAT-X is applied to the CSI-Star program, we believe that the total cost estimate is reasonable. An estimate based on NASA experience on previous programs gave a considerably higher cost of about $40M.

A reliability analysis was performed and reliability and effectiveness estimates were derived. The reliability estimate is the probability that no failure will occur in one year in orbit and the effectiveness estimate is the probability that the mission objectives can still be met after a single experiment component failure. For the baseline experiment payload the reliability is estimated at 0.86 and the effectiveness is 0.90. We evaluated several options to boost these numbers higher. The best options considered added some internal redundancy to the bus CPUs and had no significant cost, weight, or power impact and increased the reliability and effectiveness estimates to about 0.90 and 0.95, respectively.

The schedule for a CSI-Star program Phase C/D was determined to be driven by the spacecraft bus schedule, which Ball has baselined at 24 months but can be accelerated to 18

months, if desired. Based on inputs from NASA, we baselined a 1997 launch date and identified two NASA launch opportunities during that year. This resulted in a 48 to 60 month program starting with Phase A in the last quarter of CY1993.

CONCLUSIONS AND RECOMMENDATIONS

CSI-Star is a technology demonstration and validation program, not a technology development program. The current state of the art for CSI technology is such that it is ready to be demonstrated in space. This is absolutely essential if this technology is to be integrated into the designs of planned systems needed for future missions. It was determined that it is feasible to put into orbit a relatively low-cost CSI facility that the government and nongovernment CSI community can use to demonstrate CSI technology. It is our belief, based on past experience and this study, that the best way to do this is to use the QuickStar bus launched as a Delta secondary payload. CSI-Star fills the gap between current ground-test facilities and Shuttle middeck and other secondary non-free-flying experiments and the future NASA science mission systems such as the planned Earth Observation System.

It is recommended that a CSI-Star or similar program be initiated with a Phase A study to further define and develop a concept or several concepts for an affordable CSI facility in orbit. The most affordable concept that provides the most demonstration potential should be carried into a Phase B to develop the concept into a realistic design. It is also recommended that beginning in Phase A, potential GI inputs be considered in the design process so as to ensure the greatest usefulness to the CSI community.

1.0 INTRODUCTION

1.1 STUDY SCOPE AND OBJECTIVES

This study considered the feasibility of a low-cost orbiting laboratory for conducting CSI demonstration experiments by a number of guest investigators (GI). The majority of the study concentrated on hardware issues. This was done in order to identify candidate experiment payload components needed for a facility that can be used remotely for conducting typical controls-related experiments. The study was restricted to using the Ball Aerospace QuickStar small satellite (smallsat) bus into which the experiment payload components would be mounted. This provided a basis for determining the capability of the orbital laboratory for conducting CSI experiments and estimating the other relevant technical and programmatic parameters, such as weight, power and computational requirements, cost, reliability, and scheduling.

The overall objective was to define a feasible and affordable CSI orbital facility concept by using the QuickStar bus. The QuickStar is designed to be launched as a secondary payload on a McDonnell Douglas Delta II expendable launch vehicle (ELV). This system will build on and extend the database provided by previous ground and flight testbeds. The cost and the reliability of the conceptual system will be estimated. The concept will be designed to the following requirements:

1. on-orbit life of at least one year
2. first flexible mode below one Hertz -
3. closely-spaced and coupled flexible modes
4. sufficient sensors for quality system identification
5. control algorithms reprogramable via uplink
6. multiple, interacting control systems
7. optical path-length or line-of-sight control
8. sub-arcminute payload or spacecraft pointing.

These requirements were selected based on the characteristics of planned NASA missions and the space systems envisioned to support them. Also important in these requirements is the goal of keeping program costs to a minimum while providing a facility that many guest investigators can use. The CSI-Star system meeting these requirements will be a testbed that represents an actively-controlled, flexible, multibody platform with multiple instrument payloads. Future systems that can be thus represented include Space Station Freedom (SSF), the Earth Observation System (EOS) platforms, and several other science mission spacecraft, such as large interferometers and large-diameter telescopes. It should be noted that CSI technology is

not only applicable to large systems--CSI also can be useful on more compact systems, such as the Hubble Space Telescope, that have very stringent performance and stability requirements.

1.2 STUDY GROUNDRULES

The following groundrules guided the study effort and were designed to minimize program costs.

1. Single-string design will be used with options for selected redundancy considered with cost, mass, and power impacts estimated.

2. NASA MIL-STD 975 Class "B" electronic parts will be used.

3. Protoflight hardware development will be assumed--no qualification units or electronic breadboards.

4. Minimum program documentation will be assumed.

5. No dynamic ground test program in baseline--assumed that will be covered by a separate investigator program.

6. Single ground receiver station will be assumed.

7. No ground-based computational facilities in baseline for system identification or derivation of control system parameters during flight operations--assumed that will be covered by a separate investigator program.

8. Low study priority on slewing experiments--slewing should not size reaction wheels.

These guidelines and the requirements discussed above were used to select experiment component hardware candidates, conduct design studies, and estimate the cost and reliability of the CSI-Star system.

2.0 BACKGROUND AND JUSTIFICATION

2.1 BACKGROUND

The concept for CSI-Star was born out of both the technical requirements for a CSI demonstration facility in space and the programmatic requirements for affordable flight experiments.

2.1.1 Technical

The traditional design approach for spacecraft uses frequency separation to prevent the dynamic interaction between the structure and the control system. This is accomplished by attempting to design into the spacecraft a sufficiently large frequency separation between the flexible spacecraft modes and the control system bandwidth. This is shown in Figure 2-1a. Some planned spacecraft, such as orbital antennas that require large diameters, will be large and flexible with many closely-spaced modes. Many smaller spacecraft that are planned will have stringent instrument pointing and tracking accuracy, jitter, and settling requirements. This evolution has spacecraft structures evolving to lower modal frequencies, while controllers are
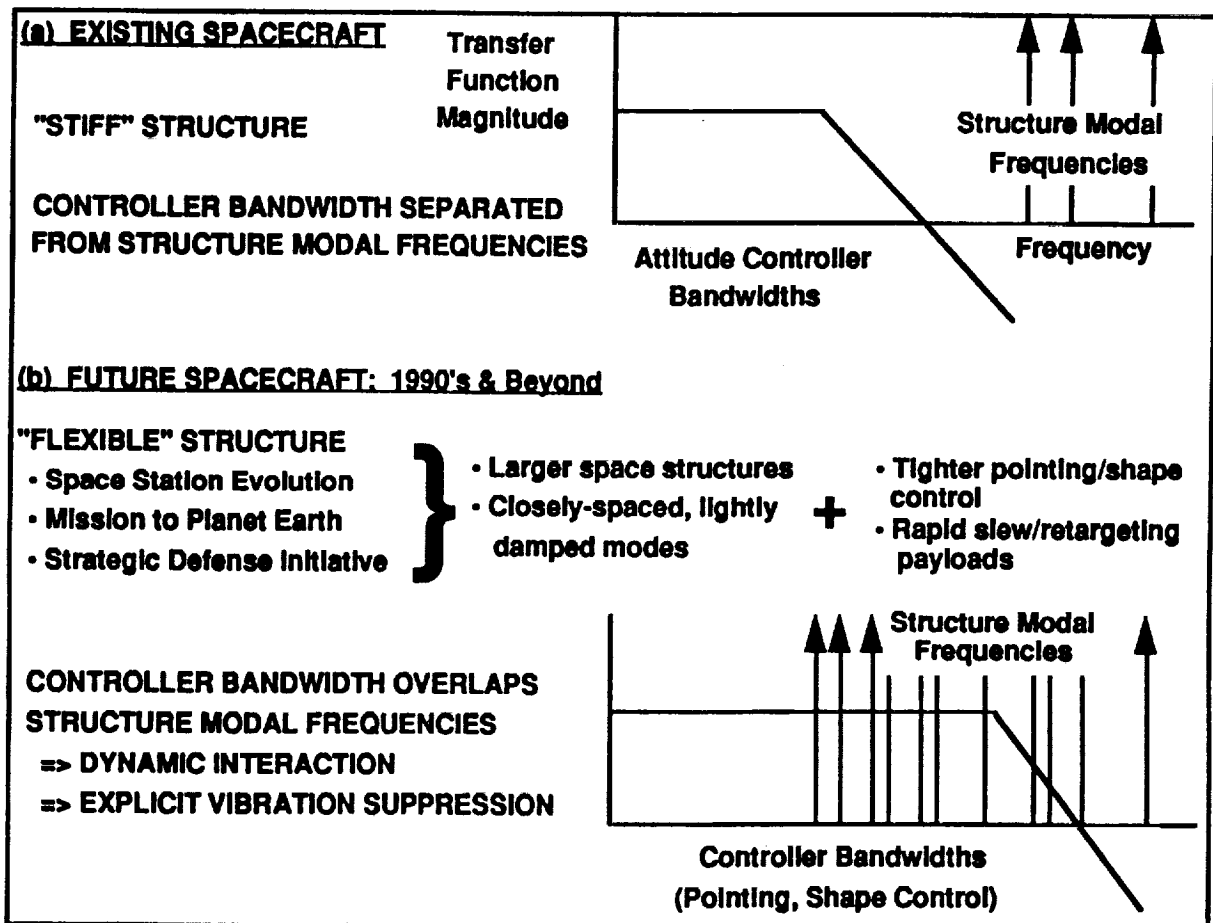
Figure 2-1. Dynamic Interaction Occurs When the Structure's Modes Overlap the Controller Bandwidth.

evolving to higher bandwidth. This leads to an overlap of the two, as shown in Figure 2-1b, which can result in a dynamic interaction. In cases where this overlap is present, as will be the case in many future designs for both large and small spacecraft, CSI technology is required to maintain stability while meeting mission performance requirements.

In order to meet their goals many planned NASA missions will require space systems that incorporate CSI technologies. It is the requirements of these systems that determine what CSI technologies must be demonstrated. CSI demonstration objectives will be selected to investigate important elements of a variety of future NASA missions. CSI technology is either enabling or enhancing technology for many planned missions. For example, CSI technology will enable such far-term projects as optical interferometers where the individual telescopes/siderostats are mounted on long, thin beam structures to achieve the needed baseline separation. The technology will be used to keep each telescopes/siderostats precisely aligned and the structure they are mounted on free from misaligning vibrations. Other far-term missions requiring CSI technology include large diameter astrophysics telescopes with sub-arcsecond pointing requirements. Near-term missions requiring CSI technology are represented by multi-instrument platforms. CSI technology will prevent the disturbances created by the operational motions of one instrument from degrading the performance of another instrument. Near-term systems that will benefit from this flight-validated technology are the planned EOS and an evolving SSF.

The specific objectives that are desired for a CSI testbed are the demonstration of:

1. Health monitoring and system identification methods for initial and changing on-orbit dynamic characteristics

2. Global vibration control techniques for a test article with fixed geometry using several types of actuators

3. Global vibration control techniques allowing precision pointing of multiple instruments and payloads on the test article

4. Micro-amplitude vibration control techniques allowing precision payload pointing

5. Global vibration control techniques during large-angle reorientation slewing of the whole test article

6. Global vibration control techniques for a test article during large-angle articulation of a payload with flexible appendages

7. Multi-level vibration control techniques using active truss members for suppression, an active tripod for isolation, and gimbals for compensation.

Objective 6 is not being considered for this study and objective 5 has a low priority.

Experiments that have conducted these types of demonstrations to varying degrees of

complexity have been performed in many ground testbeds. However, even though future NASA missions will need CSI technology for meeting performance goals, program managers will not consider using this technology if it is not first convincingly demonstrated in space. Many analytical and ground-test programs have been conducted, and are continuing, in CSI and related technology areas. There have, however, been no free-flying CSI flight demonstrations.

In the past, DoD and NASA have planned several CSI flight experiments. SDIO has several small experiments that piggyback on existing spacecraft to demonstrate adaptive structures technology. None of these has yet flown. The result is that there is limited on-orbit data for a CSI investigator to use. These data are made up entirely of dynamics data, mostly from the Solar Array Flight Experiment (SAFE), the Laser Atmospheric Compensation Experiment (LACE), and the Middeck 0-gravity Dynamics Experiment (MODE).

2.1.2 Programmatic

The CSI community has been eager to have a free-flying CSI testbed in orbit. Previously designed free-flying CSI experiment programs have been very expensive (>$100M) and this is a major reason for none having actually made it to orbit. Experiments proposed for the shuttle cargo bay are somewhat less expensive (~$50M to $100M - still too expensive) but have a short on-orbit time of several days, which does not allow enough time to even conduct experiment checkout and thorough system identification. Also, the number of guest investigators is limited on a shuttle experiment. Small secondary experiments are relatively low cost (<$10M) and several have flown (e.g., MODE and LACE-Dynamics Experiment) and others are planned to fly in the near future (MACE and ACTEX). The opportunities for flying experiments as secondary payloads are very attractive from a cost point of view, however, there are many constraints that are imposed on the experiment design. These include restrictions on weight, volume, power, communications, and computational capability, plus primary payload mission schedule variations. This is true for both Shuttle and ELV secondary payloads. However, a well-designed experiment can be flown within these constraints and provide cost-effective results. It seems that to fly a technology demonstration experiment or testbed in today's economic environment, the proposed experiment's cost must be brought down to affordable levels and it must be well-designed to produce the maximum return within any imposed constraints. It is probably better to fly a lower-cost, smaller experiment with satisfactory capability than to design an expensive, full-capability experiment that will never fly.

The traditional method of designing a spacecraft from scratch around the experiment requirements results in a very capable system but a very expensive program. It can be much less expensive to use an existing spacecraft bus and design an experiment that fits this bus. Several low-cost options are available and others will become available in the near future. The most

affordable are in the form of low-cost smallsats that are launched as primary payloads on small ELVs or secondary payloads on larger ELVs and the Shuttle. One consequence of using a smallsat is that probably everything that is wanted by the experiment investigators cannot be fully accommodated. Another consequence of using an existing smallsat bus is that, in general, lower reliability must be expected and accepted by the program and its investigators.

2.2 FLIGHT TEST JUSTIFICATION

Planned NASA spacecraft will require high performance control systems with good stability margins. This requires analytical models of the combined dynamics of the structural and control system components of the spacecraft. The prediction of the on-orbit dynamic response of a flexible spacecraft by analytical models is very difficult, as has been demonstrated in the past by several on-orbit systems. For example, the MSFC SAFE, flown on the Shuttle in 1984, was predicted to have vibrational modes that did not appear in the flight data and the predicted damping of some modes was off by a factor of five. The SDIO LACE spacecraft has exhibited unpredicted modes of vibration. There are also examples of more compact and less flexible spacecraft, e.g., Galileo and the Hubble Space Telescope, exhibiting unanticipated structural dynamics problems. Repeated attempts to predict the dynamics of various CSI ground testbeds have also demonstrated the difficulty of analytical predictions. In almost all cases, the measured response is significantly different from predicted response. These analytical model inaccuracies usually result in either poor control system performance or control system instability. The controller design is usually improved by measuring the actual dynamics and updating the analytical model used to design the controller. This works well for ground testbeds, however, if the controller is being designed for a spacecraft operating in 0 g the ground test measurements that will be used to update the model are contaminated by gravity. Gravity loading stiffens joints and alters the damping characteristics of the spacecraft. Suspension systems are required to ground test flexible test articles and gravity interacts with the suspension system to produce extraneous suspension system modes, e.g., pendulum and violin modes, which intermix with the test article modes. Also, gravity loading of a suspended flexible test article results in static sag that produces unrealistic modal coupling. Therefore, these gravity-induced effects must be analytically removed from the ground-based measurement model if this model is to be used for accurate on-orbit performance/stability predictions. However, for some types of spacecraft the analytical removal of the gravity-induced effects may not be easy and in many cases may be very difficult.

There has been much work done in the last decade on developing the CSI tools to solve these problems, but it will never be known how adequate these tools are in addressing these problems until both open and closed loop testing of the same test article both on the ground and on orbit is

accomplished. Guest investigator studies on CSI-Star will be able to address these issues when augmented with the required ground testing. There is an alternative approach to improving the spacecraft controller, especially for spacecraft in which the analytical removal of the gravity-induced effects from ground-test data may not be easy or not even possible. In this approach, the spacecraft dynamics are measured once the spacecraft is in orbit, the test data is downlinked to the ground where it is processed and used to determine updated controller parameters to further improve on-orbit performance/stability. These techniques form the basis of new methods for flight qualification of spacecraft exhibiting CSI characteristics. These new techniques are being developed and require on-orbit validation testing.

Spacecraft qualification tests are usually performed on the ground where gravity and suspension effects as discussed above will cause the qualification testing dynamics to be different from the operational on-orbit dynamics. The differences between the ground and on-orbit environments can significantly alter the open and closed loop behavior of a spacecraft, both in the short and long term. Controller stability and performance robustness require model fidelity that is intimately related to the level of applied control authority, which will be different in 1 g and 0 g. The CSI-Star is part of a group of experiments, both ground and flight, that attempt to develop and demonstrate technologies that address these issues. CSI-Star is designed to build on the successes of previous ground and flight testbeds, some of which are listed below.

Ground
- CSI Evolutionary Model (CEM) Phases 0, 1,2 - LaRC
- JPL Testbeds
- Large Space Structures Ground Test Facility - MSFC
- Advanced Space Structures Technology Research Experiments (ASTREX) - AF Phillips Lab

Flight
- Solar Array Flight Experiment (SAFE) - flown in 1984
- Laser Atmospheric Compensation Experiment (LACE) - currently in orbit
- Middeck 0-g Dynamics Experiment (MODE) - flown in 1991, reflight in 1994
- Middeck Active Control Experiment (MACE) - planned 1994 Shuttle flight
- Active Control Technology Experiment (ACTEX) - planned 1993 flight
- Jitter Suppression Experiment (Jitter) - planned 1995 flight
- Inexpensive Flight Experiment (INFLEX) - planned

This is not meant to be an all-inclusive list - there are other ground testbeds operating. There are several flight tests being planned and some are in the initial design stages, however, the ones listed have either already flown or will fly in the near future, with the exception of INFLEX, which currently is not funded beyond the preliminary design review. CSI-Star is designed to build upon these testbeds and add to the database of the funded testbeds, as illustrated in Figure 2-2. MODE/MACE is a series of shuttle middeck experiments that investigate the zero-gravity behavior of critical spacecraft dynamic systems, first passive (MODE) and then active (MACE). ACTEX is a small secondary payload attached to a Navy spacecraft that investigates control of structures in space with embedded sensors and actuators. The next step in this progression, e.g., CSI-Star, is to have a space testbed that can address the issues of the MODE/MACE experiments but for longer durations in space like the ACTEX experiment by using test articles that are traceable to the spacecraft components of future missions.
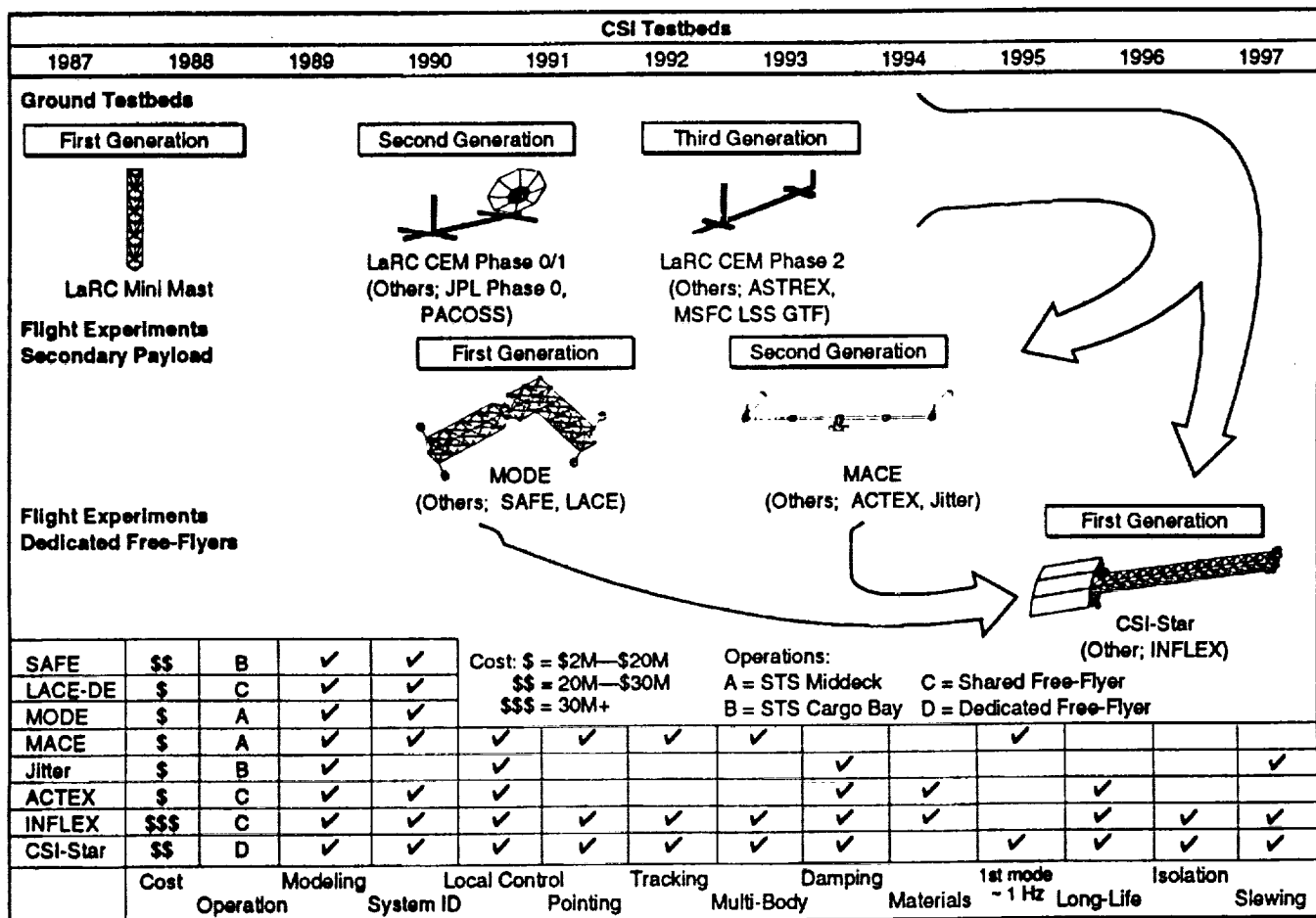
CSI Testbeds

1987	1988	1989	1990	1991	1992	1993	1994	1995	1996	1997

Ground Testbeds

First Generation — LaRC Mini Mast

Second Generation — LaRC CEM Phase 0/1 (Others; JPL Phase 0, PACOSS)

Third Generation — LaRC CEM Phase 2 (Others; ASTREX, MSFC LSS GTF)

Flight Experiments Secondary Payload

First Generation — MODE (Others; SAFE, LACE)

Second Generation — MACE (Others; ACTEX, Jitter)

Flight Experiments Dedicated Free-Flyers

First Generation — CSI-Star (Other; INFLEX)

Name	Cost	Op	1987	1988	1989	1990	1991	1992	1993	1994	1995	1996	1997
SAFE	$$	B			✔	✔							
LACE-DE	$	C			✔	✔							
MODE	$	A			✔	✔							
MACE	$	A			✔	✔	✔	✔	✔	✔	✔		
Jitter	$	B			✔		✔			✔			✔
ACTEX	$	C			✔	✔	✔			✔	✔	✔	
INFLEX	$$$	C			✔	✔	✔	✔	✔	✔	✔	✔	✔
CSI-Star	$$	D			✔	✔	✔	✔	✔	✔		✔	✔

Cost: $ = $2M—$20M
$$ = 20M—$30M
$$$ = 30M+

Operations:
A = STS Middeck   C = Shared Free-Flyer
B = STS Cargo Bay   D = Dedicated Free-Flyer

Cost — Modeling — Local Control — Tracking — Damping — 1st mode ~1 Hz — Isolation
Operation — System ID — Pointing — Multi-Body — Materials — Long-Life — Slewing

Figure 2-2. CSI-Star Extends the Database Provided by Previous Ground and Flight Tests.

3.0 CSI-Star CONCEPT

CSI-Star is envisioned as an orbiting CSI laboratory that is affordable enough to fly yet has sufficient capability for demonstrating technologies that have been developed on the ground and are now ready to be demonstrated in space. The CSI-Star concept is unique in that it proposes to operate as a free-flying CSI facility available for guest investigators for at least one year in low earth orbit (LEO). It will use a flight-proven smallsat bus launched as a secondary payload. This will enable the costs of the program to remain far below those of previously proposed CSI free-flyers. The CSI-Star facility is made up of a flight segment and a ground segment. The flight segment consists of a CSI experiment payload that is highly integrated into the smallsat bus. The integration of the payload into the bus is such that the existing bus subsystems are used to the greatest extent possible so as to maximize the number and variety of the payload components. This payload, to be assembled using commercial and flight-proven hardware satisfying typical guest investigator (GI) requirements, will provide GIs great flexibility to perform various experimental demonstrations of CSI technology. The Ball QuickStar was baselined for the CSI-Star because it is an existing, flight-demonstrated design and has more weight, power and computational capability than other smallsats. The smallsat and its CSI payload will be launched on a McDonnell Douglas Delta II launch vehicle as a secondary payload attached to the Delta second stage (Figure 3-1). The prototype QuickStar was the bus for the SDIO LOSAT-X mission that was launched as a Delta secondary payload in July 1991. Using this smallsat bus launched in the same way will minimize the cost and risk to a CSI-Star program. The use of the Delta II ELV, which is the most reliable ELV in the world and has five to ten launches per year, allows for several flight opportunities for secondary payloads per year. The CSI-Star ground segment consists of a single, portable PC-based ground station. This was also used successfully on the LOSAT-X mission and will provide the required telemetry capability for the CSI-Star mission.
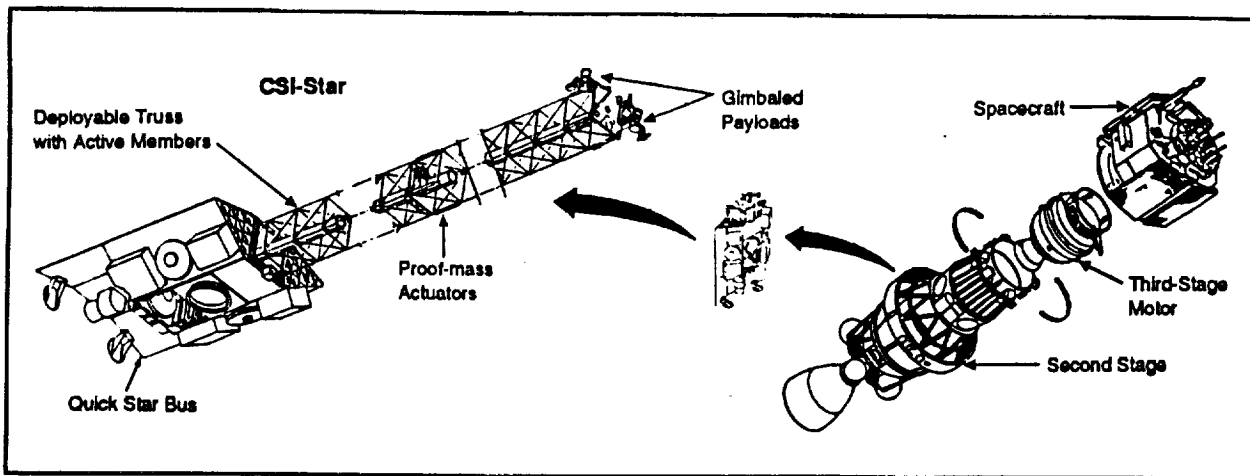

Figure 3-1. CSI-Star is Launched as a Delta Secondary Payload.

3.1 OBJECTIVES

The overall objective of the CSI-Star system is to provide an orbital testbed that will be affordable enough to fly and have sufficient capability for guest investigators from NASA, DoD, industry, and universities to develop and demonstrate CSI technology tools. This overall objective is made up of engineering science objectives and programmatic objectives. Traditionally, the approach to designing a orbital demonstration has been to start with the science objectives and develop the required hardware/software to meet those objectives subject to some programmatic parameters. Here, the programmatic parameter of cost has been included in the statement of the overall objective because it is cost more than any other parameter that determines if a worthwhile technology experiment will fly. The engineering science objectives and to what extent they can be satisfied within all programmatic constraints will determine how worthwhile the demonstration testbed is and if sufficient capability exists.

3.2 SYSTEM DRIVERS AND CONSTRAINTS

The experiment design and candidate configurations depend on the launch vehicle's primary payload characteristics, bus capabilities, cost constraints, and the engineering science requirements. The launch vehicle's primary payload characteristics determine the weight and the final orbit of CSI-Star. The launch vehicle primary mission weight margin and the launch vehicle interface clampband and c.g. limits determine the total CSI experiment payload weight and its distribution within the spacecraft bus. The launch vehicle's primary mission orbital parameters will dictate the orbits that are available to place CSI-Star in. The QuickStar spacecraft bus capabilities also provide input into the definition of the design space. The payload volume available within and on the bus, the power, and the computational throughput available for use by the CSI experiment payload play very important parts in the configuration design. Imposed cost constraint measures, such as using "off-the-shelf" hardware as much as possible and minimal hardware development, are needed to keep the CSI-Star mission costs at an affordable level. Within all these design "parameters," the engineering science requirements must be met to the greatest extent possible so as to insure a worthwhile CSI orbital facility.

For the purposes of this study, we baselined two Delta II launch opportunities in 1997. In July 1997, the ACE mission is scheduled to be launched into a highly elliptical orbit, having a perigee at 167 km and an apogee at the earth-moon L1 point (~352,000 km), inclined at 28.7°. The ACE mission has a weight margin of 1,415 lbs. A secondary payload attached to the Delta second stage, like CSI-Star, can be put into an approximately circular orbit at an altitude between 500 km and 1000 km by the second stage depletion burn after the primary payload has been released. In October of 1997, the ATMOS mission is scheduled to be launched into a 792 km circular, sun-synchronous (98.5° inclination) orbit. This is approximately the orbit that CSI-Star

will be placed into as an ATMOS secondary payload. The ATMOS has an available weight margin of 400 lbs. This is probably the minimum primary mission weight margin that CSI-Star could use since up to 67% of the secondary payload weight must be added as ballast on the opposite side of the Delta second stage to maintain proper launch vehicle c.g. location. The orbit altitudes available from both the ACE and ATMOS missions are sufficient to provide CSI-Star with an orbital lifetime of more than one year. The solar minimum will occur in 1996-97 and as can be seen from Figure 3-2, a CSI-Star in an orbit of more than about 250 miles will stay in orbit at least one year.

The Delta II - secondary payload interface clampband capability determines that maximum CSI-Star total weight allowable within the launch weight margin for the primary mission. The current clampband design, shown in Figure 3-3, was designed and qualified for the LOSAT-X secondary payload, which weighed 160 lbs. The current design could be requalified to 200 lbs and a c.g. envelope (x,y,z) of (±1.0", ±1.0",-6.0") with only a static load test required at a minimal cost impact. If it is required to increase the clampband capability to 220 lbs, then there will need to be a modification to the current design and a static load qualification test. The cost of the redesign and testing is in the range of $200,000. If it is required to increase the clampband capability beyond 220 lbs, a redesign and test of the clampband would be needed, as well as a study of the structural impact to the second stage guidance section to which the clampband is mounted. There could be a significant cost impact due to this. Based on these facts the CSI-Star baseline was selected to be the 220 lbs option.
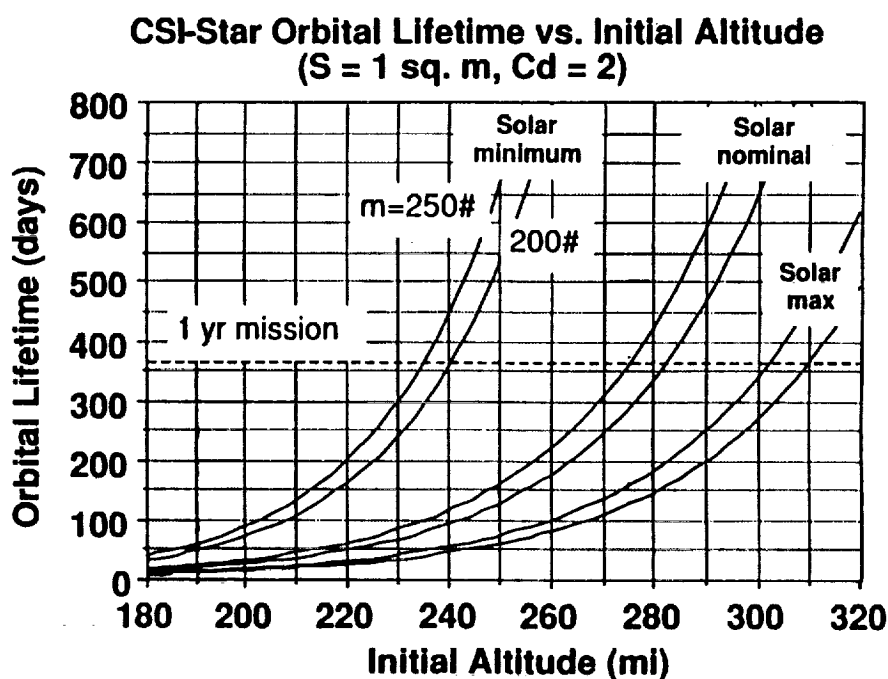

Figure 3-2. CSI-Star Can Achieve Orbital Lifetime of More Than One Year at Altitudes Greater Than 240 Miles.

- **CLAMPBAND CAPABILITY DETERMINES MAX PAYLOAD WEIGHT**

- **CURRENT CLAMPBAND DESIGN (LOSAT)**
  - **200 LBS PAYLOAD**
  - **±1.0", ±1.0", -6.0" PAYLOAD C.G. ENVELOPE**
  - **STATIC LOAD TEST REQUIRED - MINIMAL COST IMPACT**

- **REDESIGNED CLAMPBAND**
  - **220 LBS PAYLOAD**
  - **±1.0", ±1.0", -6.0" PAYLOAD C.G. ENVELOPE**
  - **REDESIGN EFFORT & STATIC LOAD TEST REQUIRED - MINIMAL COST IMPACT**

- **GREATER THAN 220 LBS PAYLOAD REQUIRES GUIDANCE SECTION IMPACT TO BE CONSIDERED - SIGNIFICANT COSTS POSSIBLE**
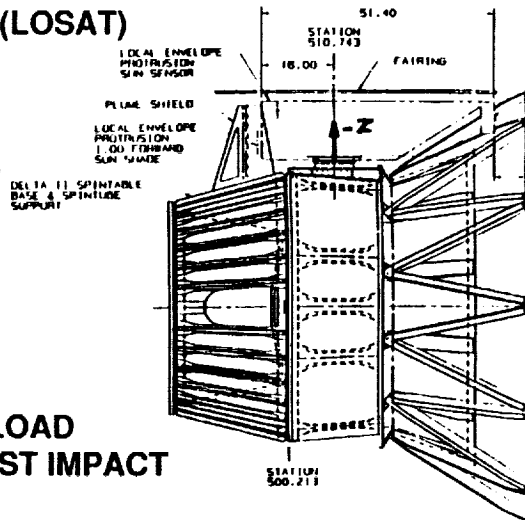
Figure 3-3. Delta II-QuickStar Interface Capability Can Support a 220 lbs CSI-Star Laboratory.

3.3 DESCRIPTION

The CSI-Star concept was developed in a design-to-cost approach in which existing hardware is to be used as much as possible. This included trying to find an existing low-cost, small spacecraft bus that can accommodate a CSI experiment payload and that can be launched into orbit at relatively low cost. As discussed above, the Ball QuickStar spacecraft bus was selected because it was a relatively low-cost spacecraft bus (<$15M) that has flown before as a secondary payload aboard a Delta II launch vehicle. This is very important because the previous flight experience gained on the SDIO LOSAT-X mission in 1991 resolved the issue of how this type of Delta II secondary payload would impact the launch vehicle's primary payload. The result was that it had no measurable impact. This spacecraft bus can support a relatively large experiment payload of up to 70 pounds (compared to microsats and most smallsats) and launch as a secondary payload results in relatively low launch service costs (<$2M).

The concept was developed based on the requirements listed in Section 1.0. A long on-orbit life of at least one year and a capability to reprogram control algorithms via uplink will allow several different GIs to use the facility. Sufficient sensors for quality system identification will facilitate the job of the GIs. Many planned missions use large flexible structures and these

systems will have closely-spaced and coupled flexible modes with fundamental modal frequencies below one Hz. These structures may have many different instruments mounted on them. These instruments will have varying performance requirements, such as pointing, and may have control systems that will interact with each other and the spacecraft controller. These characteristics of planned NASA missions and the space systems envisioned to support them drove the selection of CSI-Star requirements. From an engineering science perspective, the fundamental mode and pointing requirements could have been lower, however, these values were selected to minimize program costs yet to be representative of planned missions.

CSI-Star is composed of the CSI experiment payload and the QuickStar spacecraft bus. The experiment payload is highly integrated into the spacecraft bus so as to make maximum use of the bus capabilities. The spacecraft bus provides the experiment payload with power, onboard processing, data storage, and telecommunications. The experiment payload can also use the spacecraft bus 3-axes stabilization system reaction wheels and gyros as additional experiment actuators and sensors. Figure 3-4 shows a schematic of the CSI laboratory elements of CSI-Star and which are provided by the bus and which by the CSI experiment payload.

The CSI-Star concept consists of a structural test article (STA), which together with the spacecraft bus represents a space platform on which multiple instrument payloads can be mounted, as would be the case on Space Station Freedom or an EOS platform. On the STA will be mounted two or more simulated EOS-type instruments and the associated sensors and actuators needed to conduct CSI technology demonstrations. There can also be a video system to observe STA deployment and other significant dynamic events. Two concept configuration options are shown in Figures 3-5 and 3-6. Each of the components is discussed below.

The STA will be, by necessity, a deployable truss-type structure that can be stowed inside the QuickStar bus for launch. Once in orbit, the STA will deploy to its operational length. There are some deployable truss designs that allow partial deployment. If one of these designs can be used then different configurations and the corresponding on-orbit adjustment of the system controllers can be investigated. The baseline STA is a 20 ft long deployable truss structure mounted in a cantilevered configuration to the QuickStar bus.

The STA will be instrumented with a suite of accelerometers, strain gages, and temperature sensors. The number of accelerometers will be selected to provide good identification of the expected number of significant modes. For the baseline configuration, 20 accelerometers and strain gages were selected. There are six temperature sensors baselined to provide information at critical locations along the STA.

The candidate EOS instrument payloads that could be represented on CSI-Star include the Laser Atmospheric Wind Sounder (LAWS), which is a coherent Doppler lidar using a 1.6 m diameter, continuously scanning (0.1 to 0.2 Hz) transmit and receive telescope, and the High-
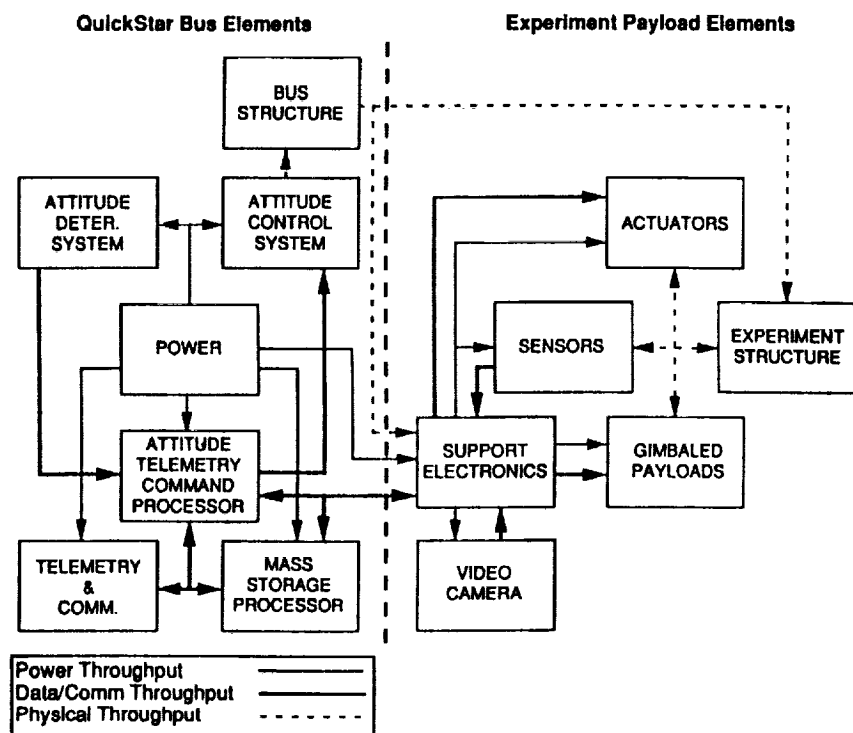
QuickStar Bus Elements   **Experiment Payload Elements**

BUS STRUCTURE

ATTITUDE DETER. SYSTEM

ATTITUDE CONTROL SYSTEM

ACTUATORS

POWER

SENSORS

EXPERIMENT STRUCTURE

ATTITUDE TELEMETRY COMMAND PROCESSOR

SUPPORT ELECTRONICS

GIMBALED PAYLOADS

TELEMETRY & COMM.

MASS STORAGE PROCESSOR

VIDEO CAMERA

Power Throughput ————
Data/Comm Throughput ————
Physical Throughput - - - - - -

Figure 3-4. The CSI-Star Orbital Laboratory has Experiment Elements That are Highly Integrated with the Spacecraft Bus Elements to Maximize CSI Capabilities.

PHOTOSENSOR ARRAY

DEPLOYABLE TRUSS W/ ACTIVE STRUTS

GIMBALED LASER ASSEMBLIES

SENSOR ELECTRONICS

PROOF-MASS ACTUATORS

PHOTOSENSOR ARRAY

GIMBAL/STRUT/VIDEO ELECTRONICS

PROOF-MASS/SENSOR ELECTRONICS
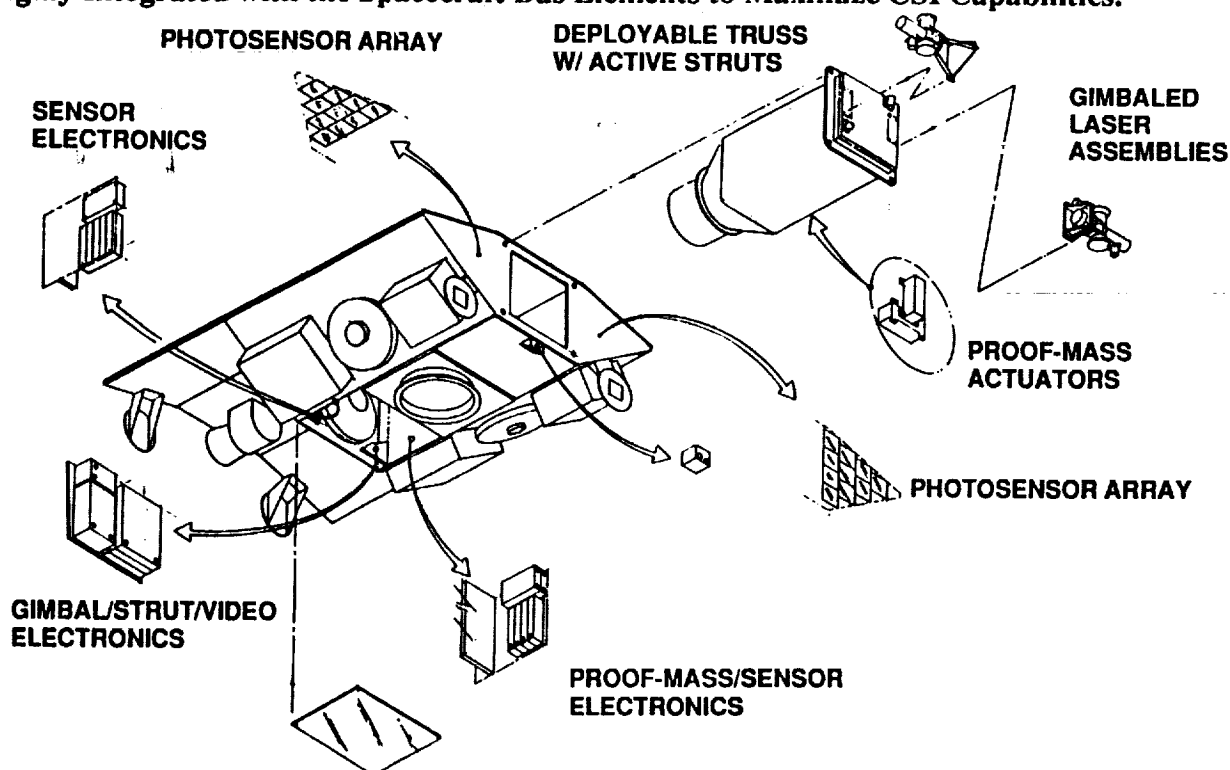
Figure 3-5. Conceptual Design of the CSI-Star Laboratory Configuration A, Showing the Major Experiment Payload Hardware Elements.
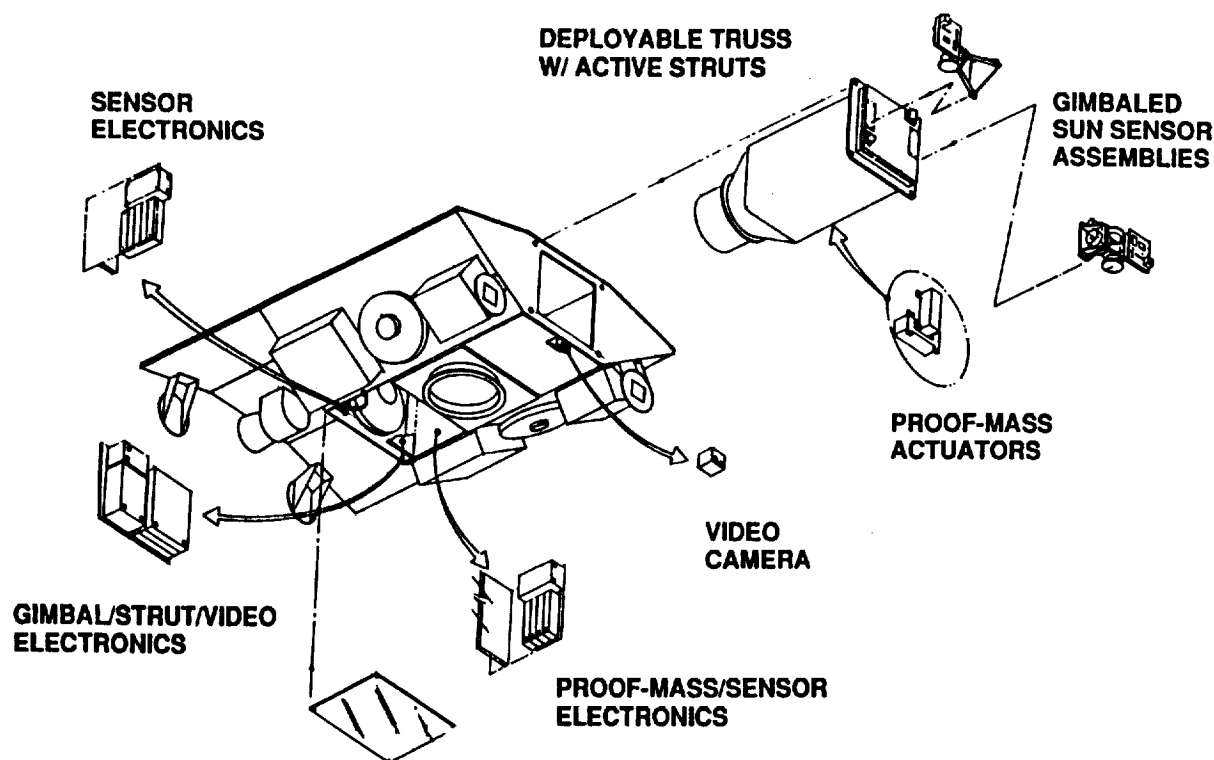
Figure 3-6. Conceptual Design of the CSI-Star Laboratory Configuration B, Showing the Major Experiment Payload Hardware Elements.

Resolution Imaging Spectrometer (HIRIS), which is provides high spatial resolution images of the Earth and has sub-arcminute pointing stability and jitter requirements. If both of these instruments were mounted on the same platform, as proposed for EOS-B, the operation of the scanning LAWS payload could affect the pointing performance of the HIRIS payload. Flight-demonstrated CSI technology can prevent this. The CSI-Star will have components that can represent these types of instruments for CSI technology validation purposes. The LAWS-type payloads, which provide disturbances into the platform, can be represented by a slewing mass on a gimbal system or proof-mass actuator(s) and the HIRIS-type payload can be represented by a pointing mass or instrument on a gimbal system. These mass/instrument and gimbal systems will be mounted on the structural test article. The baseline configuration has at the tip of the STA a disturbance laser payload sized to provide the required excitation of the structure on a 1-axis gimbal and a laser simulating a pointing payload mounted on a 2-axes gimbal. At the base of the STA mounted on the face of the spacecraft bus are photosensor arrays for detecting and determining the pointing of the lasers. The configuration options arise by replacing the laser/photosensor system (called Configuration A) with a precision sun sensor system (called Configuration B).

The STA has active members distributed along it to provide vibration control capabilities. The type, number and location will be determined by the expected dynamic response of the structure and the required nominal performance.

An active member tripod is included to augment the pointing laser mounting (in addition to the 2-axes gimbal) and provide for three layers of control, if desired. The three layers of control being suppression by the STA struts, isolation by the tripod, and compensation by the gimbals. The tripod elements are envisioned to be piezoelectric or electrostrictive active members.

At approximately the mid-bay of the STA there will be two proof-mass actuators (PMA) and loadcell sensors for additional excitation capability. If used for control then additional sensors (position sensors) will be required. The PMAs will be sized for 1 Hz operation. These will be oriented in two orthogonal directions normal to the STA longitudinal axis.

At the base of the STA on the face of the spacecraft bus a video camera will be added for visual inspection capability during deployment of the STA, as well as at other desired events.

All required electronics are housed inside the QuickStar bus and positioned with consideration to the spacecraft c.g. limits.

3.4 EXPERIMENT HARDWARE

The following is a discussion of the CSI-Star experiment hardware to be provided for direct experiment support in addition to the spacecraft bus supplied by Ball. Ball will customize its QuickStar spacecraft bus to provide the necessary interfaces to the electronic functions described in the following sections. For example, Ball will provide dedicated experiment power conditioning (+/-15V and +5Vdc) in the Power Distribution Unit.

The supporting electronics circuit card assembly (CCA) volume and weight is estimated for each component if not supplied with the unit. The component total peak power and cost is determined from the vendor or estimated based on data from similar units. A generally-accepted factor of 0.035lb/cubic-inch is used to convert volumes into weights for circuit cards. It is assumed that each circuit card has a depth of 1 inch.

3.4.1 Structural Test Article

Several deployable articulated-longeron truss designs from Astro Aerospace and Able Engineering have been considered for the CSI-Star structural test article (STA). These include the FASTMAST and ADAM structures from Able and the X-Beam from Astro. The ADAM has been baselined, however, the others seem to be equally feasible for use on CSI-Star at this time. The ADAM deployable mast assembly manufactured by Able Engineering, Inc. consists of a deployable mast, mast canister, and deployment motor (if necessary). The Able Deployable Articulated Mast (ADAM) is an articulated four-longeron truss-type mast. When deployed from the canister by the deployment motor, the mast extends from a twisted compressed configuration

to an erect position via diagonal cable members. In the fully deployed position, the mast is held erect by latch mechanisms which fix the positions of the diagonal cables (Figure 3-7). Because the ADAM mast designed is deployed by a motor, it can be partially deployed and maintain a degree of stiffness.

Because of the space and mass restrictions of the QuickStar bus, the entire mast assembly is required to fit within a 9x9x24 inch rectangular volume and weigh less than 25 pounds. The fully deployed mast is 20 feet long with a first bending mode below 1 Hz. The first several modes of the CSI-Star with deployed STA were calculated and are shown in Figure 3-8. The STA model used for these calculations was such that the results do not show bending-torsion coupling modes that would be present in the real STA. The degree of this coupling can be designed into the STA by adding offset dummy masses to the STA, provided this extra mass does not exceed weight restrictions. The preliminary design offered by Able is a square cross section mast approximately 8.5 inches in diameter. The longerons are made of aluminum, giving the mast a total weight of 5.3 lbs. The canister is also aluminum, conforming to the 9x9 dimensional limits of the bus, with a length of approximately 16 inches. The canister weight is 12 lbs. The deployment motor is located behind the canister within the body of the spacecraft bus. Requiring 14 W for operation, the motor extends the mast at a rate of 2 inches per second. The motor weight is 5.5 lbs, raising the total mast assembly weight to 22.8 pounds. The RDT&E cost of the mast structure is estimated at $900K, and the combined cost of the motor/canister assembly is $100K.
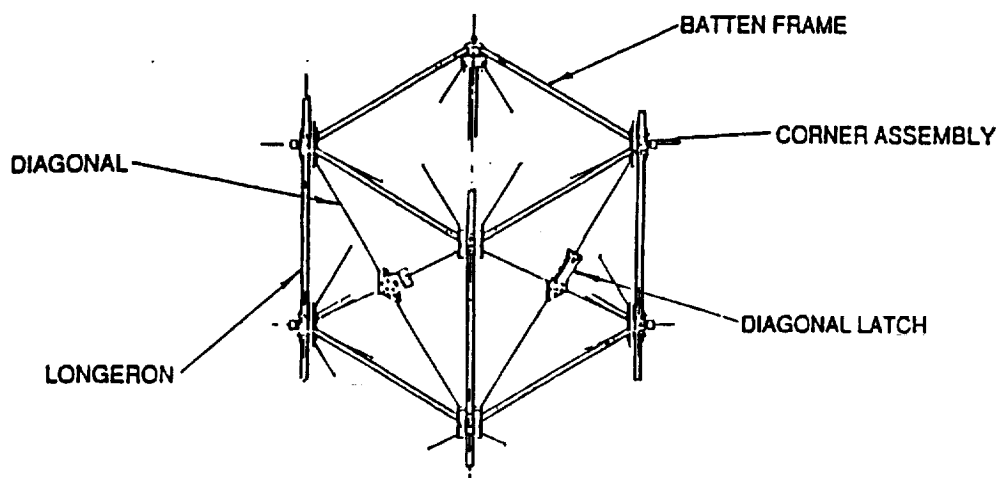

Figure 3-7. A Flight-Proven Deployable Structural Test Article will be Used - One Bay of a Candidate Structure is Shown.
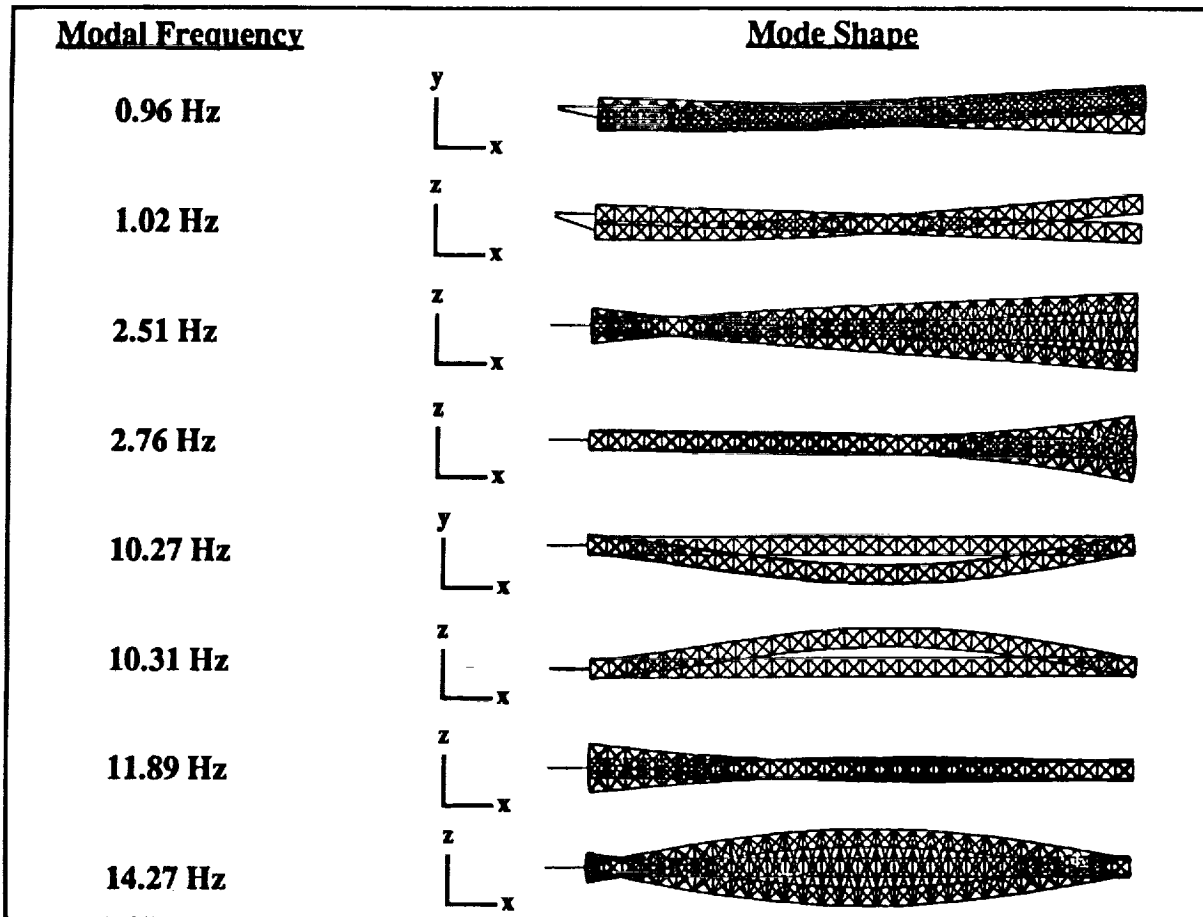
Modal Frequency	Mode Shape
0.96 Hz	
1.02 Hz	
2.51 Hz	
2.76 Hz	
10.27 Hz	
10.31 Hz	
11.89 Hz	
14.27 Hz	

Figure 3-8. CSI-Star STA Modes Calculated with a Finite Element Model.

3.4.2 Accelerometers

The accelerometers studied for CSI-Star experiment integration are Flexcels model 336A built by PCB. These are low impedance voltage mode sensors with the signal conditioning built into the piezoelectric device. These devices have a 0-5V output scaled at 1000mV/g, with the scale chosen for a low-acceleration environment as expected during on-orbit operations. PCB also supplies a model 495B amplifier unit for use with these accelerometers. These amplifier units perform the input constant current regulation function as well as the output signal conditioning function including removal of the signal DC bias. The conditioned accelerometer signals will be input to a Ball Special Function Interface (SFI) card for use in the control algorithms.

3.4.3 Load Cells

The load cells (combined force/accelerometer transducer) studied for the CSI-Star experiment integration are model 288A11 also built by PCB. The sensitivities of this device are

1000mV/lb force and 100mV/g acceleration. This device has a built-in microelectronics charge to voltage converter to condition the output signals similar to the model 336A accelerometers. Each load cell requires two channels of constant current source power/output signal conditioning such as supplied by the model 495B amplifier unit. Again the conditioned accelerometer/force signals will be input to a Ball SFI card for use in the control algorithms.

3.4.4 Strain Gauges

To plan for up to 20 channels of strain gauge signal conditioning a 25V, 5000 ohm gauge is assumed (based upon typical values). Each strain gauge channel has a dedicated amplifier circuit, and the Ball SFI card would have to be built with bipolar analog to digital converters. The strain gauge CCA sizing was performed as follows;

- 20 ea. 14 pin DIPs (Matched Instrumentation Amplifiers, e.g. PMI OP-10)
- 20 ea. 8 pin DIPs (Output stage op amps, e.g. PMI OP-01)
- 80 ea. resistors
- Results in an approximate board area of 27.5 sq. in.

If the amplifier circuits will perform adequately with +/-5V supplies, then the power consumed by this board will be approximately 1.4 Watts. Otherwise, for +/-15V operation the board power will go up to 5.2 Watts.

3.4.5 Temperature Sensors

To plan for 6 channels of temperature sensor signal conditioning, a 4-wire resistance temperature detector (RTD) sensor was assumed, with each sensor requiring a constant current source and an amplifier. The RTD value used is 1000 ohms +/-50% over temperature at a constant current of 1mA to provide a voltage change of 1V with temperature. The temperature conditioning circuitry sizing is as follows;

- 6 ea. 8 pin DIPs (Voltage Reference IC's for constant current source)
- 6 ea. 8 pin DIPs (Amplifier IC's e.g. PMI AMP-02)
- 12 ea. resistors
- Results in an approximate board area of 4.5 sq. in.

The power dissipation would be 1 Watt assuming +15V input to the reference IC's and +/- 15V power input to the amplifier IC's. Note that because of the small amount of area required, these circuits would probably be integrated onto the strain gauge board.

3.4.6 Laser/Photosensor System Option

Experiment Option A uses 2 lasers on the boom tip for precision pointing of the lasers at a photosensor array located on the spacecraft bus at the base of the boom. Three photosensor array options were identified and investigated for their applicability to the mission. Each option has to

cover enough of the base area on which the truss mounts onto the spacecraft so that the two lasers mounted on the end of the truss have enough photosensitive area to be easily located after initial deployment. The spacing of the photosensitive elements can be relatively coarse over the array area (~0.25 in.) except for a small 1 sq. in. area that will be used by the "pointer" laser. The spacing there is to be fine enough to detect subarcminute LOS errors of the pointing laser 20 ft away (this is a resolution on the order of 0.02 in.).The options identified are as follows:

> Option 1. This concept uses discrete, square photodetectors with center to center spacing of 0.25 in. along with a commercially available unit, the Hamamatsu S3805, having a resolution of 0.03 in. used for the "pointing" laser target. The problem with this option is that it requires about 50W or more of power and high data rates. The power problem may have a work-around solution, however, a reduction in the required data rates is not as easy.

> Option 2. This concept is based on large area position sensitive detectors (PSD's), like the Hamamatsu 45mm X 45mm device, that provides position accuracy much better than 0.02 in. These devices can be placed checkerboard fashion over the required detection area in a manner such that about 1/2 the area is filled with active photodetectors. About 40 such photodetector elements are required. The data rate for this system may also overload the system, however, de-activating certain unnecessary elements can greatly reduce the data rate such that this won't be a problem. The power required is about 300mW per detector.

> Option 3. This concept consists of commercial CCD cameras, one or two per laser, with lenses appropriate to the required resolution. For a 180mm lens the corresponding resolution is 0.02 in. Analog electronics determine the CCD pixel being illuminated. Power required is about 5W.

All options are approximately the same weight, volume and cost. Option 2 seems the most viable at the present time and is selected for the system.

The 3mW laser used in this study requires input power of 1.85V at 0.25A of constant current. The laser power is to be modulated on/off at 2kHz to provide for synchronous detection with position sensitive detectors (PSD's). (This allows laser spot detection even with high background noise.) The unipolar laser drive circuit consists of a servo-type amplifier with a transistor output stage for current boost. Because this circuit is projected to be electrically noisy, a clock circuit was planned to be dedicated to the laser modulation circuit. The clock circuit sizing is as follows;

- 1 ea. 8 pin DIP (16MHz Oscillator)
- 3 ea. 20 pin DIPs (Octal Drivers)

- 2 ea. 14 pin DIPs (4-stage binary counters)

The laser driver circuitry itself is planned as follows;

- 1 ea. 8 pin DIP (Voltage Reference for constant current source)
- 1 ea. 14 pin DIP (SPDT CMOS analog switch e.g. Harris HI-301/883)
- 2 ea. 18 pin DIPs (Instrumentation amplifiers e.g. PMI AMP-05)
- 2 ea. NPN transistors
- 8 ea. resistors
- 6 ea. capacitors
- Together these result in an approximate board area of 10 sq in

The power required for the laser electronics would be approximately 8 Watts, which includes the power to drive the two lasers.

The position sensitive detectors (PSDs) required for use with the lasers would be placed on the bus surface facing the boom. The detectors would need to be modulated synchronously with the lasers to reject background noise. Each PSD would be built as a custom hybrid and would include the equivalent of 13 op amps to condition the X-Y signals. The PSDs are based upon a commercial 45mm x 45mm PSD manufactured by Hamamatsu. The PSDs require very little current in dark or standby mode, if the PSDs were operated at 28V the drain current would be 2 micro amps. When illuminated, the PSD requires 0.6 amps/watt of illumination, which for a 3mW laser results in 0.2 Watts for 2 PSDs at 28V. The 30 ea. op amps (for 2 ea. PSDs) are estimated as 15V x 50 micro amps = 0.02W which is negligible for these calculations (This op amp power is based upon a low power device e.g. the PMI OP-220). The two PSDs would output 4 data lines which must be sampled at 2kHz by analog to digital converter(s) on a Ball SFI card. The bus processor would be responsible for computing position from the proportional X-Y signals from each PSD. Each PSD hybrid is estimated to weigh 130gm based upon a size of 71mm x 71mm x 10mm.

3.4.7 Sun Sensor System Option

Option B considers a sun sensor system instead of the laser/photosensor system of option A. This option was considered because the laser/photosensor concept was more complicated and heavier than originally envisioned. The Adcole two-axis Digital Fine Sun Sensor (DFSS), which has been used on TOPEX and Radarsat, was selected for Option B. The DFSS consists of an optical sensor head assembly and an electronics unit. Figure 3-9 shows a photograph of these components. The sensor head contains the optical elements for sensing sun angle about two orthogonal axes over a ±32° square field of view. The electronics unit processes the sensor head signals and for each measurement axis of the sensor, outputs a 14 bit serial binary word that is used in the sensor transfer function to solve for the sun angle. The average angular resolution is 0.004° (0.24 arcmin). In addition to the sun angle measurement data, the electronics outputs a bit
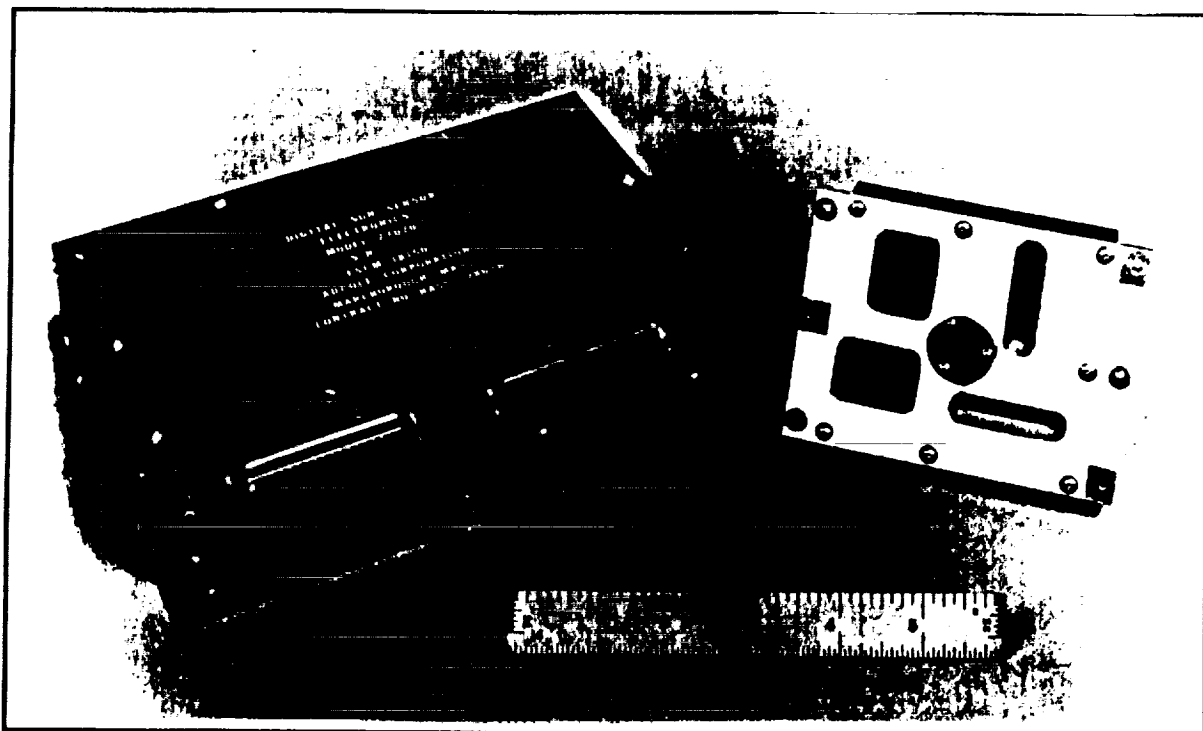
Figure 3-9. Off-the-Shelf Precision Solar Sensors can be Used for CSI-Star Pointing Payloads.

to identify the externally selected sensor head and sun presence bit to indicate whether or not the sun is in the field of view of that sensor. The cost is estimated at $250K.

3.4.8 Gimbals

The gimbal drive motors (used as disturbance source and to point lasers or sun sensors) and associated electronics will be supplied by Ball as an integrated assembly that includes the motors, resolver, caging mechanism, shaft and housing. The basic requirements for the gimbals are to be able to oscillate a 2 lb pointing payload ±30° at 1 Hz about an axis 2 inches from the pointing payload c.g., with position reporting in the sub-arcminute range. The pointing payload is fastened to a titanium shaft with a motor on one end and a precision resolver on the other. The shaft is split in the center for assembly and is supported on a duplex bearing on the resolver side and an angular contact bearing in the titanium diaphragm on the motor side. A drawing is shown in Figure 3-10. The main hardware components are as follows;

- Sierracin/Magnedyne 3 phase brushless DC motor with Hall cell commutation with 40 oz-in peak torque
- Vernitron VRP20-2 Resolver, with accuracy of 20 arcsec over ±6° and 28 arcsec over 360° accounting for A/D error
- Ball Caging mechanism with redundant solenoids

The resolver is mounted in a titanium housing bolted to the baseplate on a pair of duplex pair of precision bearings as required for maximum accuracy. The titanium resolver shaft and housing

minimize stresses on the punchings as temperature changes, which is also necessary for maximum accuracy. Because the payload c.g. will probably be off the drive centerline, it must be caged for launch. A Ball pin-puller caging mechanism that was designed and qualified for a previous program. This unit uses two solenoids redundantly. It is positioned so that caging is at the payload c.g. to minimize lateral loads on the pin. The caging mechanism can withstand more than 100 g along the axis of the solenoids without releasing. A few items not shown on the drawing that will be required are: soft stops at the ends of the ±30° travel range; flexing leads to the resolver rotor; wiring for the motor and solenoids; and an electrical connector. It is assumed that the payload leads would be on a flexible tape going around the outside of the assembly. The total drive assembly weighs 2lbs without the payload attached. The motor control electronics (also provided by Ball) performs the following functions;

- Interface the main processor bus and control lines
- Contain position control electronics including resolver input to form a closed control loop
- Contain motor driver circuits designed around discrete driver parts e.g. power MOSFETs

The motor control could be handled by the main processor at a 100Hz control and read-back data rate. If a constant slew rate is desired (versus a simple repositioning of the motor) a DMA channel in the Ball Modular Spacecraft Processor can be dedicated to each motor. The DMA
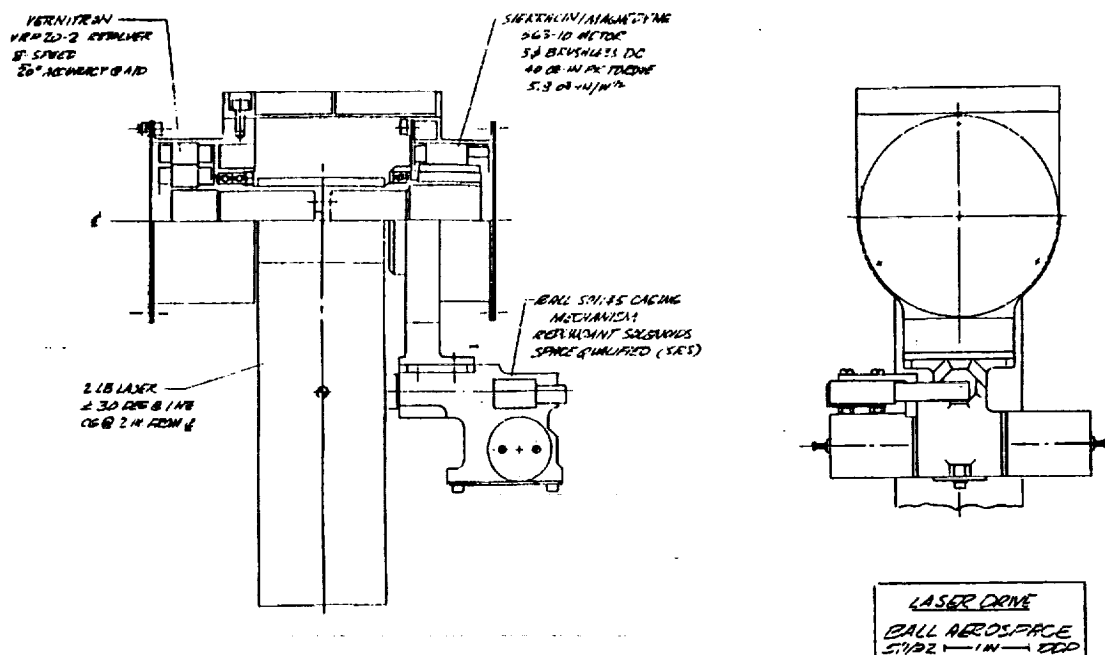

Figure 3-10. Ball Gimbal Design Drawing for CSI-Star Laser/Sun Sensor Payload.

channel together with a circular buffer could handle repetitive motor control without interrupting the main processor.

3.4.9 Proof Mass Actuators

A SATCON RMA2-10 reaction mass actuator (or Proof Mass Actuator) was studied for experiment integration. The actuator requires a 0-5V peak 1-100Hz sine wave input with up to 2.5W peak power. The actuator current-voltage behavior is approximately linear when providing a constant force output. The PMA electronics must be designed to provide a digitally programmed sine wave oscillator with variable amplitude and frequency in the range of interest. In addition the electronics will have the following characteristics;

- Oscillator based upon quad DAC and quad low-noise op amp ICs, with the DACs providing the programmable frequency function
- The main processor will "set and forget" frequency and amplitude of output to actuator

The output power amplifier will have a programmable voltage gain obtained by varying the gain resistance (e.g. with a PMI AMP-05). The PMA controller electronics were sized as follows;

- 1 ea. 28 pin DIP (Quad DAC, 0.6 in wide)
- 1 ea. 16 pin DIP (Quad Op Amp)
- 5 ea. diodes
- 31 ea. resistors (oscillator 11 ea. + 20 ea./amplifier)
- 1 ea. power MOSFET
- 16 ea. capacitors (oscillator 8 ea. + 8 ea./amplifier)
- 1 ea. 16 pin DIP (8 bit latch)
- 2 ea. 16 pin DIPs (Quad comparators)
- 4 ea. 16 pin DIPs (Quad switching FETs)
- 1 ea. 18 pin DIP (Instrumentation Amplifier)
- 2 ea. BJT power transistors (0.5 x 0.5 in ea.)
- Results in an approximate board area of 20 sq in

The electronics power is approximately 1.5W plus 2.5W for the PMA for a total of 4W peak.

3.4.10 Active Members

The active members have been sized based on attenuating a sinusoidal unit moment disturbance (at 1 Hz) at the truss tip so that a pointing instrument also at the truss tip achieves an order of magnitude reduction in LOS error in closed loop (LAC) response compared to open loop response. Twelve active struts used as 6 actuator pairs must output about 0.6 lb force maximum with a corresponding 23 volts max. This is shown in Figure 3-11. Active struts can be fabricated as shown in the photograph in Figure 3-12. There are three other similar active struts
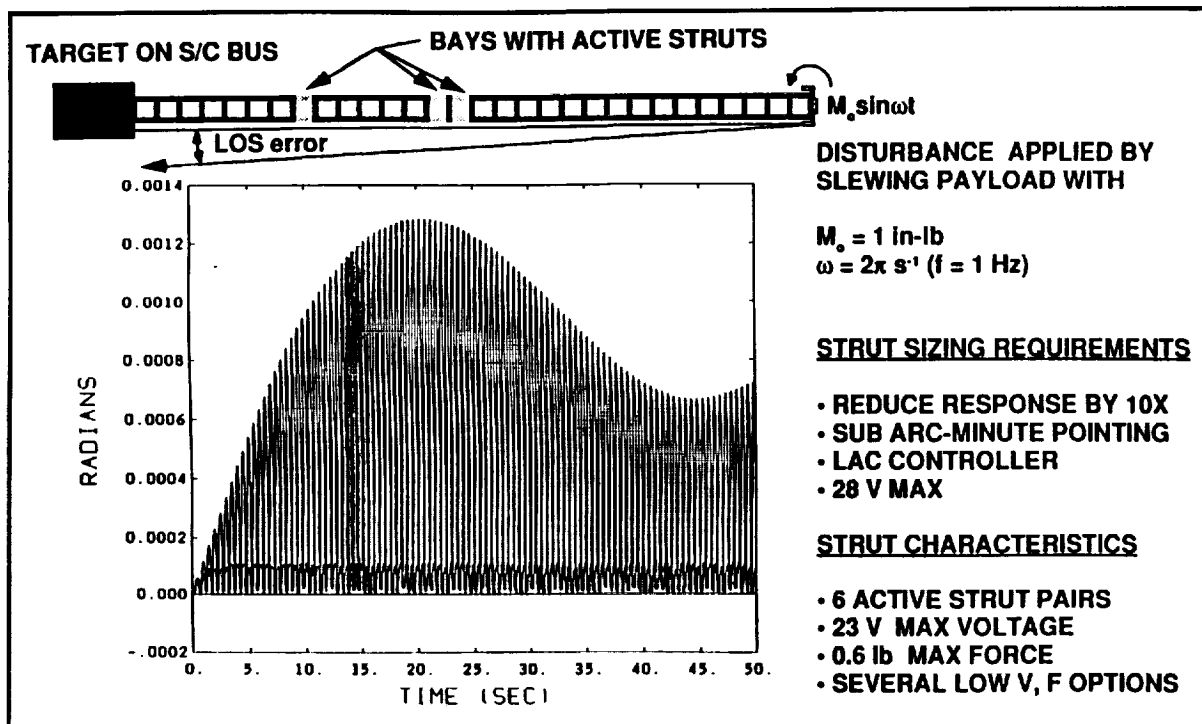
TARGET ON S/C BUS

BAYS WITH ACTIVE STRUTS

LOS error

$M_o \sin \omega t$

DISTURBANCE APPLIED BY SLEWING PAYLOAD WITH

$M_o = 1$ in-lb
$\omega = 2\pi$ s⁻¹ (f = 1 Hz)

STRUT SIZING REQUIREMENTS

- REDUCE RESPONSE BY 10X
- SUB ARC-MINUTE POINTING
- LAC CONTROLLER
- 28 V MAX

STRUT CHARACTERISTICS

- 6 ACTIVE STRUT PAIRS
- 23 V MAX VOLTAGE
- 0.6 lb MAX FORCE
- SEVERAL LOW V, F OPTIONS

Figure 3-11. Control Simulation Used to Determine Baseline Number and Location of CSI-Star Active Strut Members.
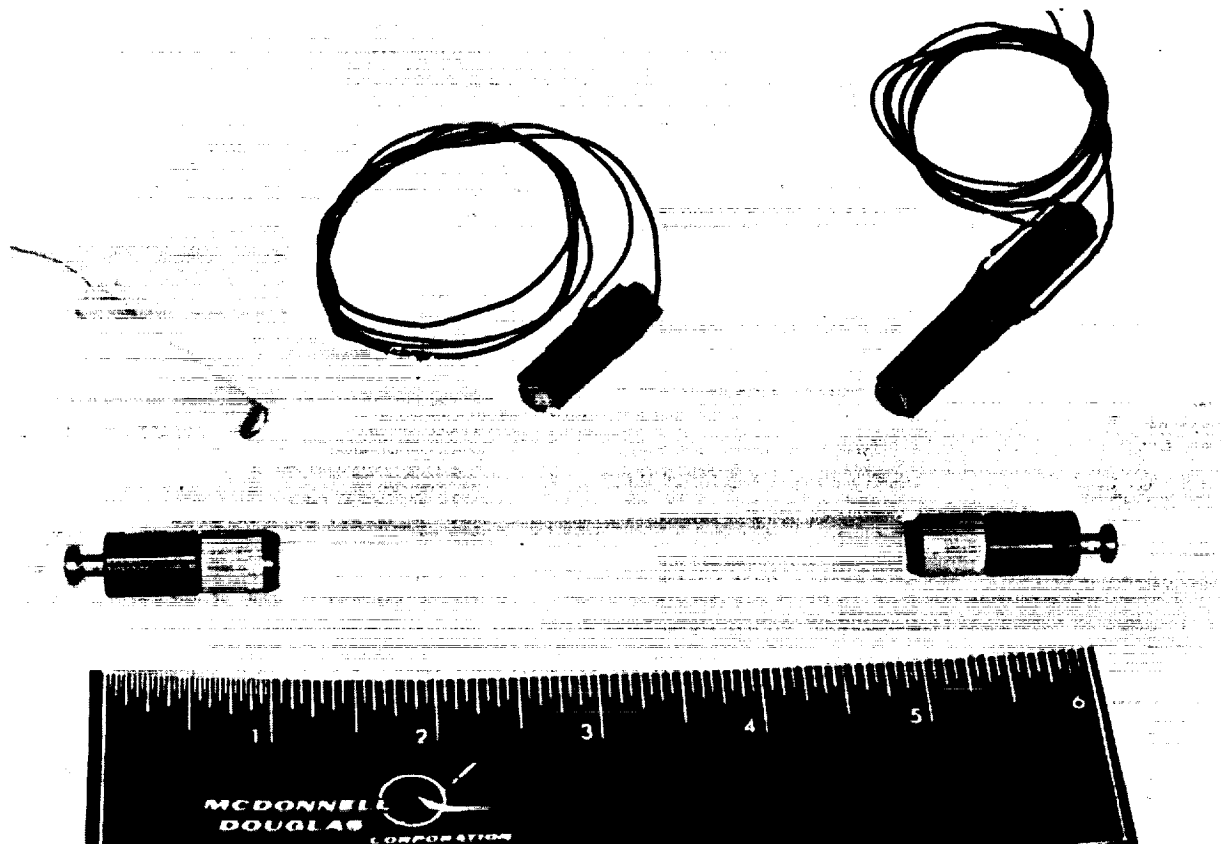

Figure 3-12. Active Members can be Based on Cylindrical or Stacked-Wafer Piezoelectric Designs.

used in the isolation tripod attached to one of the gimbaled payloads. The strut electronics sizing estimates were obtained by simply using the electronics requirements for strut control on other similar space-based experiments, e.g., ACTEX, INFLEX, and AMASS. The active strut electronics were thus estimated to be on a 8 x 11 in circuit card assembly. It was assumed that the control for the 12 struts could be placed on 50 sq in of board space resulting in a 1.8 lb circuit card. Power for this electronics function was estimated at 3 W.

3.4.11 Video Camera

The video camera studied for experiment integration is a Xybion model ISS-255. This is a CCD based camera using the EIA RS-170 525 line format with a resolution of 768h x 493v pixels. This camera has a volume of 56 cubic in, weighs 2.75lbs, and requires 5W of power at 15Vdc. The camera interface electronics could be designed with a selective field-of-view to eliminate video data storage prior to downlink or he data will have to be compressed for storage and downlink. The main processor would be used to control parameters to select relevant windows within the camera field-of-view (FOV). This approach requires the main processor to setup parameters within the full frame video capture buffer to predict the section of FOV that contains the deploying boom. The video chip set must be manufactured as custom space hardened versions of existing commercial video chip designs. The video electronics board will include A/D, memory buffers, and FPGAs. The electronics would occupy a volume of approximately 27 cubic inches, weigh 4 lbs, and consume 4W - 5W. The options studied are given in Table 3-1.

Table 3-1. Video Electronics Trade Study

Requirement	Driver
768 h x 493v CCD Sensor Video I/F	378,624 Samples Per 1/30 of a second
11.4 Mbytes/sec Camera Data Rate	Write Timing to Memory Buffer
91 Mbits/sec	Write Timing to Memory Buffer
1 Mbits/sec	Read Timing from Memory Buffer to Downlink
5 Gbits of Data Storage	1 Minute of Live Video Capture (i.e., no data loss)
10 Gbits of Data Storage	2 Minutes of Live Video Capture

DESIGN APPROACH	POWER	TOTAL POWER	TOTAL VOLUME	TOTAL WEIGHT	TOTAL COST (with NRE & No 883C)
4 Mbit Dynamic Memory Chips	9 Watts (memory) + 15 Watts (A/D, control logic and memory drivers)	24 Watts	108 Cubic Inches	8 lbs	$ .5 M
16 Mbit Dynamic Memory Chips	4.5 Watts (memory + 10 Watts (A/D, control logic and memory drivers)	14.5 Watts	28 Cubic Inches	4 lbs	$ .5 M
4 Mbit Dynamic Memory Chips and 10:1 Data Compression	1 Watt (memory) + 18 Watts (A/D, control logic and memory drivers)	19 Watts	54 Cubic Inches	4 lbs	$ .4 M
16 Mbit Dynamic Memory Chips and 10:1 Data Compression	.5 Watts (memory + 13 Watts (A/D, control logic and memory drivers)	13.5 Watts	27 Cubic Inches	4 lbs	$ .4 M
90:1 Data Compression	5 Watts (A/D, control logic and compression chipset)	5 Watts	27 Cubic Inches	4 lbs	$ .25 M
Intellegent (Selective) Capture of Relavent Video Data	4 Watts (A/D, Memory Buffers, and Field Programmable Gate Arrays)	4 Watts	27 Cubic Inches	4 lbs	$ .25 M

3.4.12 Hardware Summary

Summary data of experiment hardware weights and power are given in Tables 3-2 and 3-3. Note that the miscellaneous and miscellaneous structures categories consist of mounting brackets, ties, bolts, etc. required to mount components to each other and to the STA. These are estimated using established design factors for spacecraft.

Table 3-2a. Configuration A Experiment Payload Weight

Item	Unit Mass (lb)	25% margin (lb)	Quantity	Total Mass (lb)	Total Mass + 25% margin (lb)
1-axis gimbal	1.5	0.4	1	1.5	1.9
2-axis gimbal	3.0	0.7	1	3.0	3.7
able mast (aluminum)*	5.3	N/A	1	5.3	5.3
accelerometer*	0.0	N/A	20	0.2	0.2
active strut	0.2	0.1	12	2.4	3.0
camera electronics*	1.0	N/A	1	1.0	1.0
camera lens (75 mm)*	1.0	N/A	1	1.0	1.0
camera*	2.8	N/A	1	2.8	2.8
disturbance payload	1.6	0.4	1	1.6	2.0
gimbal electronics	1.6	0.4	1	1.6	2.0
laser 1	1.7	0.4	1	1.7	2.1
laser 2	1.7	0.4	1	1.7	2.1
laser electronics	0.4	0.1	1	0.4	0.5
load cell	0.1	0.0	2	0.2	0.2
mast cannister*	12.0	N/A	1	12.0	12.0
mast motor*	5.5	N/A	1	5.5	5.5
misc.	0.3	0.1	1	0.3	0.4
misc. structure	0.7	0.2	1	0.7	0.9
MLI	0.1#/ft^2	0.0#/ft^2	3.75 ft^2	0.3	0.3
photo sensor	0.1	0.0	10	1.4	1.8
PMA	2.4	0.6	2	4.8	6.0
PMA electronics	0.4	0.1	2	0.8	1.0
sensor electronics	0.2	0.0	9	1.4	1.8
strain gage	0.0	0.0	20	0.2	0.2
strut electronics	1.8	0.5	1	1.8	2.3
temperature sensors	0.0	0.0	6	0.2	0.3
tripod, active laser	0.8	0.2	1	0.8	1.0
wire harness	1.1#/ft	0.3#/ft	4450 ft	5.0	6.2
Payload Total (lb)				59.4	67.4

*Exact mass via vendor

Table 3-2b. Configuration B Experiment Payload Weight

Item	Unit Mass (lb)	25% margin (lb)	Quantity	Total Mass (lb)	Total Mass + 25% margin (lb)
1-axis gimbal	1.5	0.4	1	1.5	1.9
2-axis gimbal	3.0	0.7	1	3.0	3.7
able mast (aluminum)*	5.3	N/A	1	5.3	5.3
accelerometer*	0.0	N/A	20	0.2	0.2
active strut	0.2	0.1	12	2.4	3.0
camera electronics*	1.0	N/A	1	1.0	1.0
camera lens (75 mm)*	1.0	N/A	1	1.0	1.0
camera*	2.8	N/A	1	2.8	2.8
disturbance payload	1.6	0.4	1	1.6	2.0
gimbal electronics	1.6	0.4	1	1.6	2.0
load cell	0.1	0.0	2	0.2	0.2
mast cannister*	12.0	N/A	1	12.0	12.0
mast motor*	5.5	N/A	1	5.5	5.5
misc.	0.3	0.1	1	0.3	0.4
misc. structure	0.7	0.2	1	0.7	0.9
MLI	0.1#/ft^2	0.0#/ft^2	3.75 ft^2	0.3	0.3
PMA	2.4	0.6	2	4.8	6.0
PMA electronics	0.4	0.1	2	0.8	1.0
strain gage	0.0	0.0	20	0.2	0.2
strut electronics	1.8	0.5	1	1.8	2.3
sun sensor 1*	3.0	N/A	1	3.0	3.0
sun sensor 2*	3.0	N/A	1	3.0	3.0
sun sensor electronics*	0.5	N/A	1	0.5	0.5
temp sensors	0.0	0.0	6	0.2	0.3
tripod for sun sensor 1	0.8	0.2	1	0.8	1.0
wire harness	1.1#/ft	0.3#/ft	4450 ft	5.0	6.2
Payload Total (lb)				59.3	65.6

*Exact mass via vendor

Table 3-3. Experiment Payload Component Power

ITEM	ITEM POWER (W)	QUANTITY	TOTAL POWER (W)
accelerometer	0.06	20.00	1.12
active strut (incl. tripod struts)	0.16	15.00	2.40
active strut electronics	0.25	12.00	3.00
gimbal drive electronics	2.00	3.00	6.00
gimbal drive motor	2.00	3.00	6.00
instrument heating	10.00	1.00	10.00
laser electronics (2A)	3.00	1.00	3.00
laser power (2A)	0.90	2.00	1.80
load cell	0.90	2.00	1.80
mast motor	14.00	1.00	14.00
photo sensor (2A)	0.03	20.00	0.50
photo sensor electronics (2A)	0.00+	9.00	0.01
proof mass actuator	5.50	2.00	11.00
proof mass electronics	0.08	1.00	0.08
strain gages	0.13	20.00	2.50
sun sensor electronics (2B)	3.00	2.00	6.00
temp sensors	0.00+	6.00	0.01
video camera	5.00	1.00	5.00
video electronics	15.00	1.00	15.00

3.5 SPACECRAFT BUS

The QuickStar design is a derivative of the U. S. Government funded prototype spacecraft, LOSAT-X. Figure 3-14 is a photograph of LOSAT-X in the clean room at Ball just prior to shipment to Cape Canaveral Air Force Station Delta Launch Complex 17. LOSAT-X was the result of a government push to develop, test, launch, and operate small spacecraft and complementary sensor technologies. Designed by Ball Aerospace, the LOSAT-X spacecraft included an integrated avionics suite built around two 80C86 processors, a 0.25 Gbit mass memory, Ball-developed reaction wheels, and a new wide field-of-view (WFOV) star camera. Design drivers dictated that this complicated spacecraft fit within a very small envelope on a McDonnell Douglas Delta II rocket as a secondary payload and still be sophisticated enough to accomplish mission science objectives.

3.5.1 Spacecraft System

QuickStar is a free-flyer. Design life is one year with a goal of up to three years. QuickStar is a small highly-capable, low-cost, light-weight satellite system utilizing modern design techniques. The QuickStar spacecraft is a 3-axis stabilized vehicle that utilizes three reaction
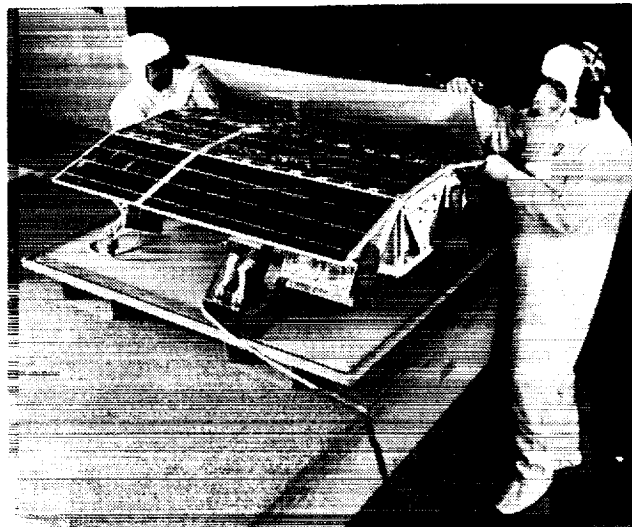
Figure 3-14 The LOSAT-X Spacecraft

wheel assemblies, three magnetic torque rods, two sun sensors, a 3-axis magnetometer, and two 2-axis gyro packages to maintain attitude control and determination. Figure 3-15 is a system concept summary and illustration of the QuickStar spacecraft.

A functional block diagram of the QuickStar flight system shown in Figure 3-16 illustrates the extent that the spacecraft is under software control. Through the use of an integrated central processor, as compared to most satellite systems that are a combination of dedicated hardware control units and software processors, QuickStar improves reliability by replacing hardware with software at the same time reducing volume, power, and weight requirements. In addition, with the integrated central processor, extensive testing of all spacecraft systems and control modes is possible on the ground giving confidence that it will function the same way on orbit.

Spacecraft subsystem components are mounted internal to the spacecraft or attached to the exterior structure within the envelope provided. Equipment attached to the spacecraft exterior include two avionics modules, three solar array panels, reaction wheels, torque rods, two patch antenna sets, trickle charge and test connectors, and a separation fitting/connector. Internal equipment include a communication transponder, gyros, battery, and the payload. A small propulsion unit can be added if needed for a particular mission. Figure 3-17 gives plan views showing the standard QuickStar bus component general arrangements. Figure 3-18 shows the available payload volume, both internal and external to the bus.

The power summary in Table 3-4 shows the bus consumption as a best estimate by subsystem. The integrated avionics includes power for attitude actuator electronic drivers. RF
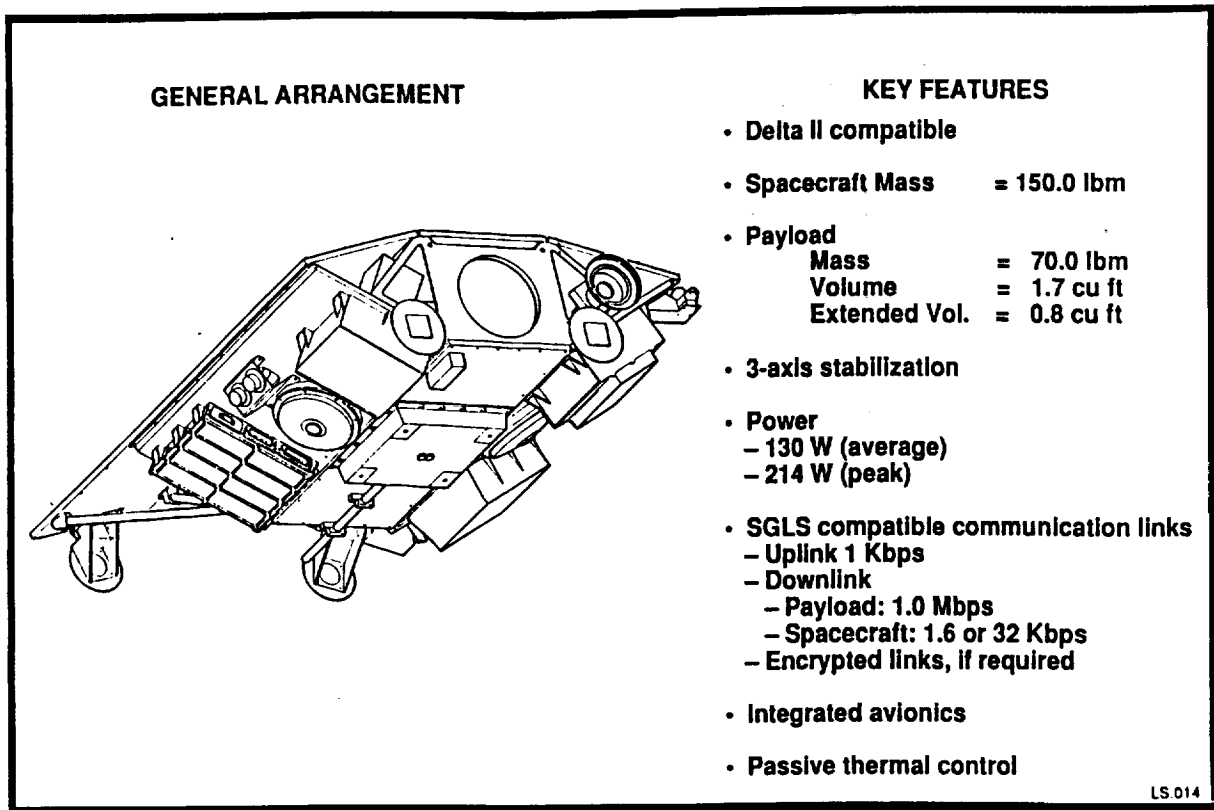
GENERAL ARRANGEMENT

KEY FEATURES

- Delta II compatible

- Spacecraft Mass $\approx$ 150.0 lbm

- Payload
  - Mass = 70.0 lbm
  - Volume = 1.7 cu ft
  - Extended Vol. = 0.8 cu ft

- 3-axis stabilization

- Power
  - 130 W (average)
  - 214 W (peak)

- SGLS compatible communication links
  - Uplink 1 Kbps
  - Downlink
    - Payload: 1.0 Mbps
    - Spacecraft: 1.6 or 32 Kbps
  - Encrypted links, if required

- Integrated avionics

- Passive thermal control

LS.014

Figure 3-15. QuickStar Spacecraft System General Arrangement
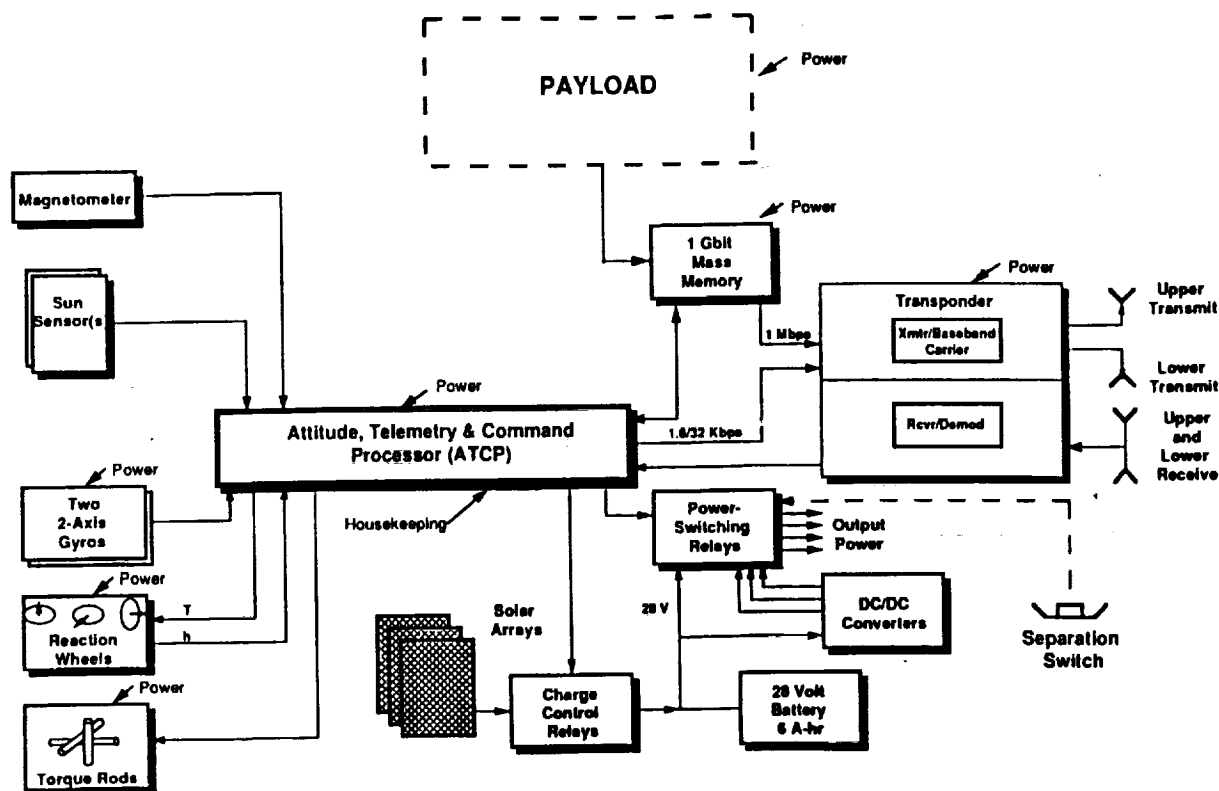
Figure 3-16. QuickStar Spacecraft Functional Description

- 31 -
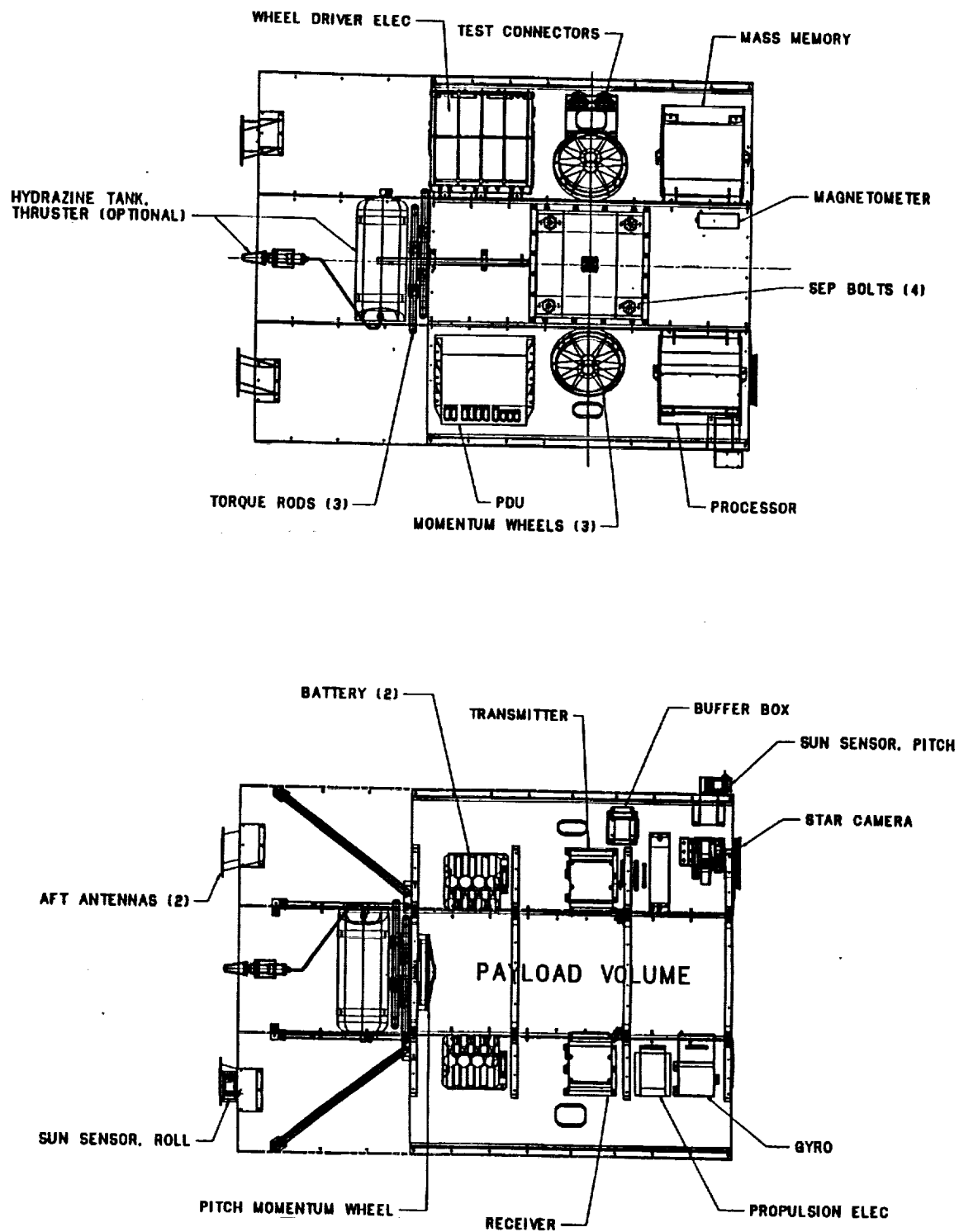
Figure 3-17. Standard QuickStar Component General Arrangement

Bulkhead
(3 Places)

Figure 3-18. QuickStar Internal and External Payload Volume
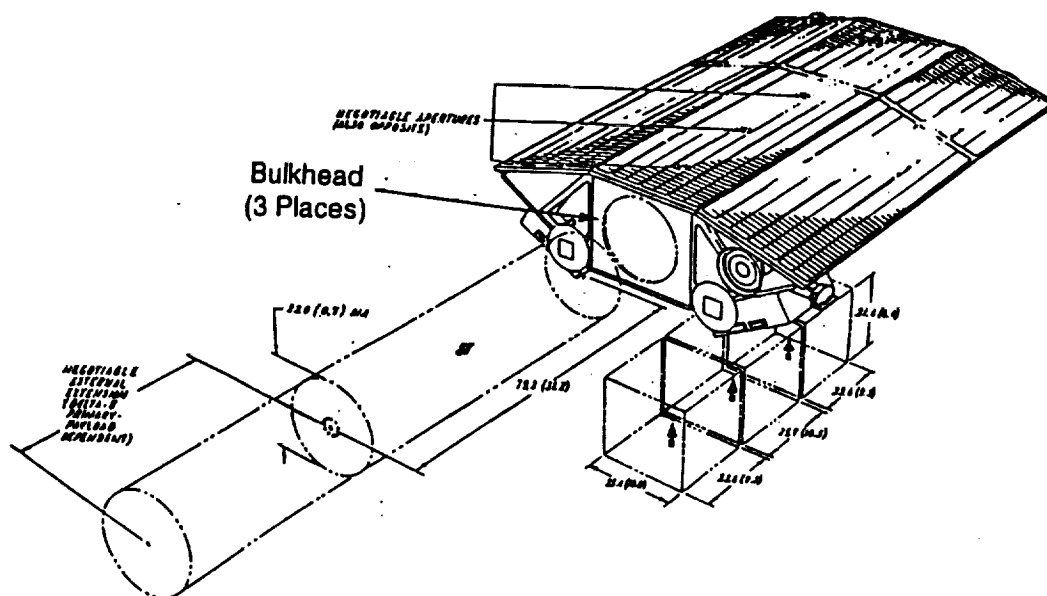
Table 3-4. QuickStar Power Budget Breakdown

Subsystem/Component	Peak Pwr (watts)	Duty Cycle (percent)	Orbital Ave. Power (watts)	Subsystem Ave. Power (watts)
Avionics				36.2
S/C Control Unit	18.8	100	18.8	
Data Storage Unit	17.4	100	17.4	
Attitude Determination & Control				27.7
Reaction Wheels	17.7	100	17.7	
Gyro	10.0	100	10.0	
Sun Sensors	-		-	
RF				
Transponder				8.20
RCVR Standby	1.68	100	1.68	
RCVR Operate	4.30	20	0.86	
Transmit	28.3	20	5.66	
Electrical Power				9.84
PDU	3.17	100	3.17	
Distrib. Loss	1.34	100	1.34	
Battery Loss	5.33	100	5.33	

Total Bus Power	81.9
5% Contingency	+4.1
TOTAL ORBITAL AVE	86.0

- 33 -

power is orbital average, assuming infrequent (<1 per orbit) transmissions from the satellite. A 5% contingency is retained to cover uncertainty in the power budget. The solar array generates >130 W (10 % margin) average in low earth orbit after 1 year. 86 W are nominally required by the bus, thus 44 W are left as a budget for payload (Table 3-5). Based on a 1.5 hour orbit, 66 W-hr of energy is available to the payload. As an example, assuming 75 W of peak power are required for 10 minutes, than 40 Watts average is available to the payload over the rest of orbit.

3.5.2 Structure/Mechanisms Subsystem

The QuickStar spacecraft structure is approximately 49 inches long by 36 inches wide and 12 inches deep. The upper deck doubles as solar panel substrates and is covered with solar cells providing approximately 12 square feet of solar array area on three panels. The lower deck assembly provides mounting surfaces for all electronics boxes and spacecraft components. The upper and lower decks are connected by four yoke assemblies forming the spacecraft bus enclosure containing the CSI-Star payload (Figure 3-17).

The spacecraft structural subsystem is made up of primary and secondary structure. The aluminum primary structure consists of an interface adapter, four milled yokes, three half-inch honeycomb (with 20 mil face sheets) decks, three half-inch honeycomb solar panel substrates, solar panel doublers and braces, fasteners and a separation fitting. The secondary structure consists of individual brackets and fasteners used to support wiring harnesses, antennas, sun sensors, and other components aboard the spacecraft.

Table 3-5. QuickStar Payload Power Budget

	Peak (watts)	Orbital Ave. Power (watts)
QuickStar Solar Array Output	213	145
10% Margin		-15
		130
Spacecraft Bus Power Budget		-86
Payload Power Budget		44

Payload Peak Power Computation:

44 watts x 1.5 hours = 66 watt-hours per orbit

Assuming 75 watts of peak power required by the payload for 10 minutes:

75 watts x 10/60 hours = 12.5 watt-hours of peak power

66 watt-hours - 12.5 watt-hours = 53.5 watt-hours

53.5 watt-hours x 60/80 = 40.13 watts of orbital average power available to payload for the rest of orbit

A separation attach fitting is externally mounted on the lower deck (Figure 3-17). The attach fitting mates with the launch vehicle separation mechanism mounted on the side of the Delta second stage guidance section. Separation mechanism and ordnance consisting of a 9 inch clamp-band adapter using two explosive bolt assemblies to initiate spacecraft separation are provided on the launch vehicle side of the separation interface. Total allowable CSI-Star satellite weight mounted to the launch vehicle separation mechanism is baselined at 220 pounds.

3.5.3 Thermal Subsystem

The thermal subsystem provides the capability to maintain all spacecraft components to within prescribed temperature limits. Thermal control is accomplished by passive means using high emissivity/low absorptivity finishes, and thermal isolating hardware. The spacecraft bus design does not require the use of multi-layer insulation blankets, louvers and/or active heaters. Although, after further study, the CSI-Star payload requirements may dictate the use of blankets to maintain thermal balance, e.g., on the active struts. Telemetry provides temperature measurements from thermistors located near or on various key components and payload equipment.

3.5.4 Electrical Power Subsystem

The electrical power subsystem provides electrical bus power to energize spacecraft loads in all phases of the orbit. It provides regulated power to the payload, power switching for non-essential components, and undervoltage and overcurrent protection for the spacecraft bus. The QuickStar spacecraft utilizes a GaAs solar array for power collection and a battery for energy storage. The electrical power subsystem consists of three solar panels, a 6 Amp-hour NiCd battery (or an optional 12 Amp-hour battery), dc/dc converters, charge control and power switching relays. The power subsystem operates at a nominal 28 volt dc. The system is designed to provide an average of 130 watts to the spacecraft system including a 15 watt reserve. Forty-four watts of orbital average power (or 66 watt-hours of energy) is available to the payload.

Bus undervoltage levels ("yellow" and "red") are ground selectable. When bus voltage drops below the "yellow", non-essential components are switched off including the payload, mass memory, and spacecraft transmitter. The receiver, flight processor, gyros, PDU, reaction wheels and drivers are maintained on the essential bus. In the event of a "red" undervoltage, only the spacecraft flight processor, power distribution unit, and receiver are left powered. This configuration is sufficient to safe the spacecraft until a plan is generated by the satellite operations crews to analyze the anomaly and command disconnected equipment back on. Protection is also provided should an overcurrent condition occur. Components on the non-essential bus are switched off similarly to the bus undervoltage situation.

3.5.5 Avionics

The concept of an integrated avionics suite is borrowed from current developments for fighter aircraft where all the monitoring, control, housekeeping, and processing functions are integrated together, not only for the synergistic effect, but also to reduce cost and improve reliability and maintainability.

In keeping with the concept of integrated avionics, QuickStar has replaced the separate boxes for each major on-board function (i.e., command and data handling, attitude determination and control, and telemetry, track, and control) each typically with its own power supply, packaging, connectors, and cable harness with a 80386 central processor, memory, and architecture technologies.

The spacecraft control unit (SCU) provides for 64 analog inputs and 8 outputs, 64 parallel inputs and 64 outputs, 8 serial inputs and 8 outputs, and 64 relay driver outputs. The special functions interface contains a serial I/O DMA controller, torque rod drivers, sun sensor preamplifiers, momentum wheel tachometers, transponder interface, and real-time clock circuits. The memory devices, built with CMOS technology, are packaged using state-of-the-art memory module manufacturing techniques, mounted to four printed circuit wiring boards using surface mount technologies, and architected into the avionics suite with error detection and correction circuitry. The result is a processor box that can recover from single event upsets (SEUs), is latchup free, and can tolerate a 100 krad total dose of radiation.

The 80386 in the data storage unit (DSU) is essentially dedicated to the payload. It performs memory management and maintenance that requires very little throughput leaving essentially the entire throughput of the 80386 to control of the payload. The throughput is rated at 2 MIPS or 0.4 MFLOPS at the current processor clock speed of 8 MHz.

The I/O available in the SCU is also available in the DSU but is an upper limit that could be provided to the payload by the payload-dedicated DSU. Mass memory for the payload is installed in the DSU on a whole-card basis. At some point, mass-memory cards begin replacing I/O cards, depending on the density of the memory chips used. The actual I/O available to the payload, therefore, will be the result of a tradeoff against the payload mass-memory requirements, with consideration for the density of the memory chips in use at the time. It is also possible that there may be some unused I/O capability available from the SCU.

3.5.6 Command, Telemetry, and Ranging (C,T&R) Subsystem

The CT&R subsystem provides for the communication between the spacecraft and the ground based stations in addition to providing an interface with all spacecraft subsystems.

Omnidirectional uplink capability is provided by the fore and aft L-band patch antenna sets, a communications transponder, and the spacecraft control unit (SCU). The command uplink rate is 1-2 Kbps. Downlink capability is provided by the SCU, data memory assembly (DMA), transponder, and fore and aft S-band patch antennas. Downlink rates include 1 Mbps for the payload data and real time 1.6/32 Kbps for spacecraft health and status.

A hardware command buffer in the SCU holds up to 512 commands which are either executed immediately upon arrival from the receiver or stored for delayed execution in command stored memory (CSM). Pseudo random noise (PRN) ranging data is also sent to the receiver via the antenna and is filtered and routed to the transmitter for turnaround transmission to the ground station (used for range determination). The receiver portion of the transponder is always powered-on from the spacecraft essential bus.

3.5.7 Attitude, Determination and Control Subsystem (ADACS)

The ADACS provides attitude determination and control for the QuickStar satellite. The ADACS consists of two 2-axis rate gyro packages, two coarse one-axis sun sensors, a 3-axis magnetometer, three 1.0 Nms reaction wheel assemblies and drive electronics, and three 30 Amp-m^2 control electromagnets (torque rods).

Attitude determination is accomplished using inputs from the two sun sensors and the magnetometer when in the inertial pointing mode and from the gyro package during maneuver operations. Using sensed Earth field line and sun directions, spacecraft body-axis attitude solutions with accuracies on the order of 1 to 2 degrees are available. Attitude control is achieved using the reaction wheels while magnetic torquing is used to dump stored momentum in the wheels. During normal operations, QuickStar is maintained in a Sun Point Mode in which the solar panels are positioned normal to the sun-line for optimum power output.

Onboard attitude estimates will be optimized by appropriate combining and filtering of sensor and gyro measurements. In the shadowed parts of orbits, the attitude will be propagated based on gyro measurements and partial attitude information from the magnetometers. Accuracies available with this sensor set will be enhanced by uploading refined sensor biases determined during early-mission ground processing of telemetered data.

Attitude control is effected by the set of reaction wheels which create torques to maneuver the satellite and vary their speeds to absorb external disturbance torques. The absorbed momentum is "dumped" using three control electromagnets ("torque rods") which create counter torques by interacting with the earth's magnetic field.

3.5.8 Satellite Control

The baseline satellite control system (two-axes) has a bandwidth of 0.05 Hz and an effective damping of 0.7. The proportional gain is 52.3 Nm/rad and the derivative gain is 233.1

Nm/rad/sec given a system inertia of 530 kg-m^2. Phase margin is 62 deg at 0.075 Hz. The system sampling frequency is 10 Hz with a total measurement/process delay of 20 msec. Actuation is obtained from a 0.042 Nm wheel which has 0.011 Nm of friction. Attitude and rate are obtained from a body-rate-integrating sensor which has 15 μrad resolution. During maneuvers, rate commands are limited to $\sqrt{2\theta_E \alpha_{max}}$ where θ_E is the attitude error and α_{max} is the maximum acceleration allowed (5.9e-5 rad/sec^2).

Pointing error due to wheel friction is 210 μrad or 0.012 deg (0.011/52.3). Reduction of pointing error from this source may be accomplished by adding integral compensation. Command torque jumps due to rate sensor quantization are 0.035 Nm (233.1(15e-6)/0.1). Reduction of command torque jumps from this source may be accomplished by effectively reducing the quantization level itself or by reducing the control system bandwidth.

3.5.9 Flight History

On July 3, 1991, the prototype to QuickStar was successfully launched into low earth orbit as a secondary payload aboard a McDonnell Douglas Delta II 7925 launch vehicle. The primary payload aboard the Delta II was the Air Force GPS-11 spacecraft. To minimize risk to the primary payload, the QuickStar prototype was completely inert (powered down) at liftoff, placed into orbit by the second stage and activated at separation, well after the GPS vehicle had been deployed.

At separation from the Delta, the QuickStar prototype powered-up all subsystems and payload, nulled body-axes rates, maneuvered to the required attitude, and approximately 34 minutes later performed a crucial element of the mission. Accomplishment of a mission event so soon after spacecraft separation represents atypical early orbit operation as most spacecraft require lengthy checkout periods before attempting any type of payload operations.

3.6 GROUND STATION

As part of the overall small satellite system architecture, a low-cost multi-purpose ground station to support production, test, launch, and orbit operations of QuickStar has been developed. Figure 3-19 shows the QuickStar ground station providing independent data acquisition and mission control for the CSI-Star missions. Figure 3-20 is a functional representation of the ground station showing the extensive use of existing commercial components. The versatility and transportability built into the ground station allows placement at any government installation, university or contractor facility. Command and control of the satellite and its payload can be as close as the desk in your office.

The QuickStar ground station and payload processing center provides support for CSI-Star mission planning, command generation/uplink, data acquisition, processing, and analysis.
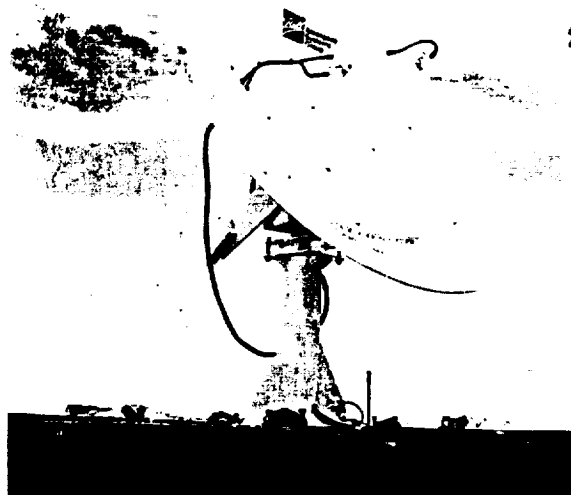
2-M Aperture Gimballed Antenna
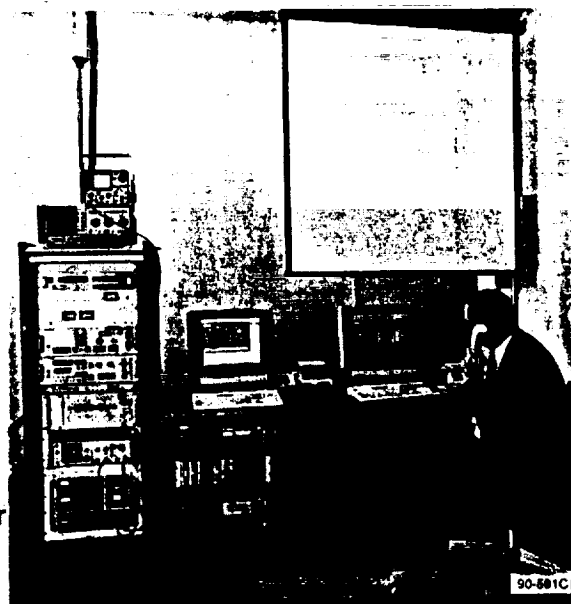
Operations Control Center

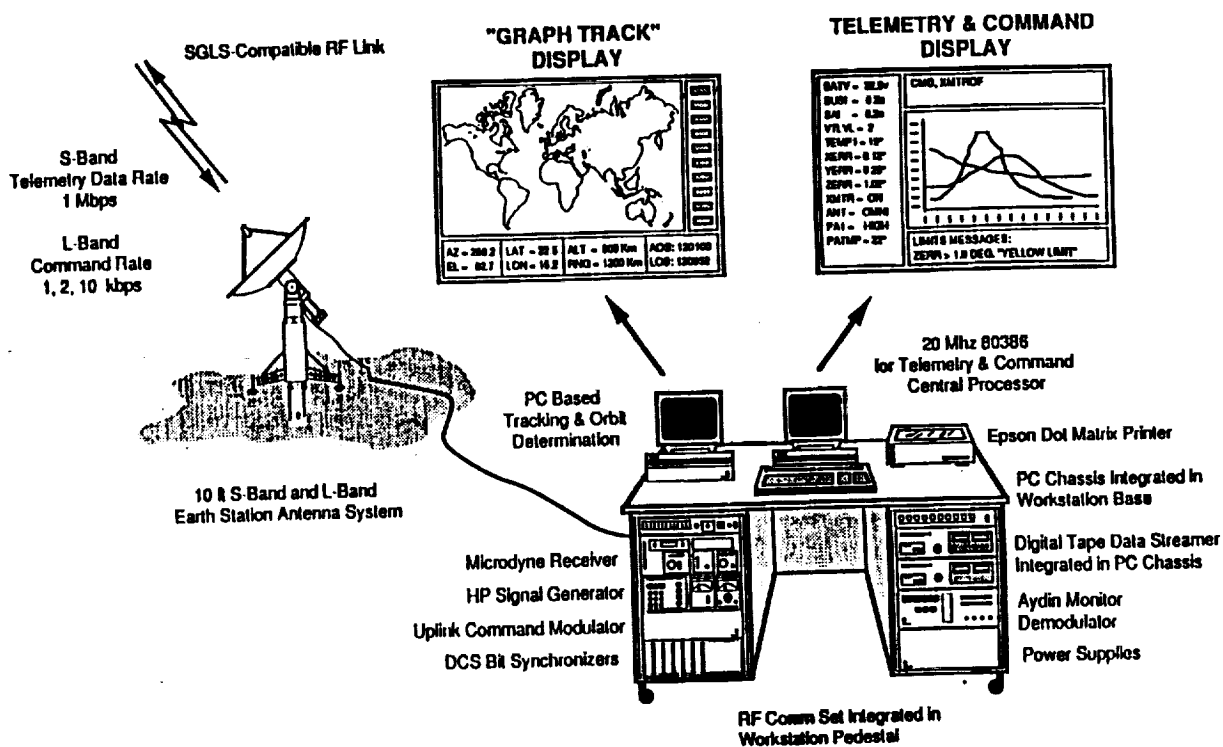**Figure 3-19. QuickStar Operational Ground Station**

SGLS-Compatible RF Link

"GRAPH TRACK" DISPLAY

TELEMETRY & COMMAND DISPLAY

S-Band Telemetry Data Rate 1 Mbps

L-Band Command Rate 1, 2, 10 kbps

10 ft S-Band and L-Band Earth Station Antenna System

PC Based Tracking & Orbit Determination

20 Mhz 80386 for Telemetry & Command Central Processor

Epson Dot Matrix Printer

PC Chassis Integrated in Workstation Base

Microdyne Receiver
HP Signal Generator
Uplink Command Modulator
DCS Bit Synchronizers

Digital Tape Data Streamer Integrated in PC Chassis

Aydin Monitor Demodulator

Power Supplies

RF Comm Set Integrated in Workstation Pedestal

Figure 3-20. Ground Station Functional Diagram Showing Extensive Use of Existing Commercial Components

The ground station consists of an RF rack housing a Global Positioning System (GPS) station clock, a digital ranging receiver, a telemetry demodulator, bit synchronizer, baseband assembly unit, signal generator, and 250 watt uplink power amplifier. A rack mount workstation style desk houses the baseband receiver, 1.0 Mbps demodulator/bit-synchronizer, antenna control unit, and two redundant 25 Mhz 80486 microprocessors. A roof mounted 2.9 meter antenna system includes the low noise preamplifier and RF downconverter. Both the 80486 processors are capable of real-time telemetry processing/display and/or command and equipment control.

The complete workstation incorporates additional 80486 microprocessors and off the shelf equipment in a distributed processing environment providing mission planning and orbit determination support, as well as off-line data processing and analysis. Ground station processors are networked via Ethernet links and are separately connected to the incoming telemetry data and command lines via RS-422 high speed serial interface boards. Each workstation is provided with a printer for local control of telemetry snaps, system messages, and status printouts. All incoming telemetry data are archived redundantly on digital 2.3 Gbyte 8 mm tape drives. Telemetry data is first buffered in ground processor memory and then subsequently stored off to either disk or tape.

As backup, the CSI-Star mission can be supported through NASA's Goddard Space Flight Center (GSFC) and its worldwide tracking and data network (GSTDN). This has the benefit of providing the CSI-Star mission with satellite command and data coverage at selected passes on a 24 hour per day basis. A 9600 bps modem interface provides CSI QuickStar ground station communication to/from the QuickStar mission unique equipment (MUE) in the GSFC environment and also remote telemetry display capability to other non-collocated PCs. The MUE and software are identical to the command and control system used in the CSI QuickStar ground station. The MUE receives all telemetry data from the GSTDN via an RS-422 serial interface. Di-bit commands are generated in the MUE for throughput to the network. Data from the spacecraft is serially routed through the GSTDN to the GSFC MUE where it is put on tape and routed to the CSI QuickStar ground station for processing and review.

Orbit determination is performed at the QuickStar ground station. At the ground station, digital ranging data (without range rate) is collected and a single site solution is generated using the Microcosm 80386 based orbit determination system.

The ground station and CSTC mission unique equipment operated as designed during the LOSAT-X mission. The Boulder site supported 5 passes per day in addition to all engineering data analysis, mission planning and command generation.

3.7 CSI PAYLOAD ACCOMMODATION ON QUICKSTAR

This section discusses the accommodation of the CSI experiment payload on the QuickStar smallsat bus based on the CSI-Star system concept described above.

3.7.1 Requirements/Capabilities Summary

Table 3-6 summarizes the QuickStar capabilities, the CSI experiment payload requirements, and the margins. The weight margins seem low, however, this is due to the extensive use of "off-the-shelf" hardware.

3.7.2 Layout and Mass Properties

The CAD system configuration layouts for the stowed CSI-Star Configuration A are shown in Figures 3-21 through 3-26. Figure 3-21 shows an exploded view of the CSI-Star. Figures 3-22 shows top view, Figure 3-23 shows the side view, Figure 3-24 shows the bottom view, Figure 3-25 shows the front and end views, while Figure 3-26 illustrates sectional views of Figure 3-22. The mass properties summary for the CSI-Star are provided in Table 3-6. QuickStar subsystem weights are derived from component weighings during the LOSAT-X program and are considered "actual".

3.7.3 Computation

The baseline processing configuration for CSI-Star includes two processors. The first processor is the spacecraft control unit (SCU) which handles the spacecraft bus processing and I/O needs (power, thermal, command and data handling, attitude determination and control, and

Table 3-6. CSI-Star Requirements are Satisfied by QuickStar Capabilities

Item	QuickStar Capability	CSI-Star Requirement	Margin
Payload weight			
Option A	70 lbs	59.4 lbs (67.4 lbs*)	18 % (4 %*)
Option B	70 lbs	58.5 lbs (64.6 lbs*)	20 % (8 %*)
Payload power			
Peak	140 W	69 W	51%
Orbit Average	44 W	16 W to 38 W	175 % to 16 %
Data Storage	1 to 2 Gbits	0.72 Gbit (orbit ave)	39 % to 178 %
Downlink Data Rate	1 Mbps	0.56 Mbps (orbit ave)	79 %
Onboard Processing	0.6 MFLOPS	0.44 MFLOPS (nom)	36 %

*When vendor-supplied component weights were not available, a 25% margin was added to that components weight.

telemetry, track, and control). The second processor is a data storage unit (DSU) which handles the processing, I/O and storage needs for the CSI-Star payload. The DSU not only contains the mass memory (1-2 Gbits), but it also includes the payload accommodation card, and a complete 80386 processor card.

The computational throughput available to the CSI-Star experiment payload is baselined at 0.6 MFLOPS. This is provided by the spacecraft CPU (in the SCU) and the mass storage CPU (in the DSU). Each has a 0.4 MFLOPS capability. The unused throughput capability of the SCU
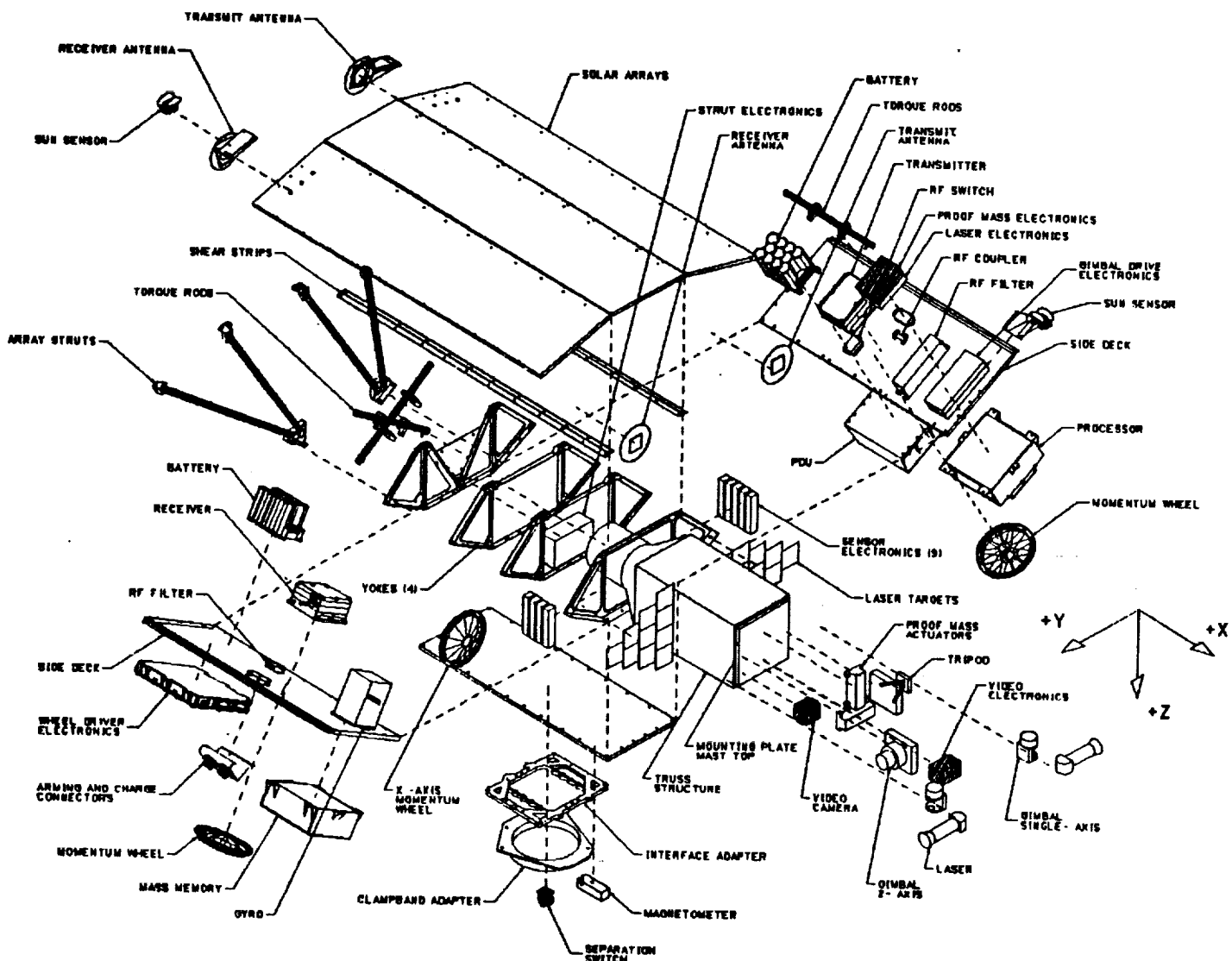
Figure 3-21. CSI-Star CAD Layout Drawing - Exploded View

can be used to help process payload algorithms. Conservatively speaking, there is probably as much as 0.2 MFLOPS of unused throughput capacity in the SCU based on the current CSI QuickStar satellite configuration. The disadvantage of this approach is it forces the payload software to be written in such a way that it can be distributed between both the SCU and the DSU. At this time it is felt this partitioning can be accomplished fairly easily. The mass storage CPU is not used heavily and thus about 0.4 MFLOPS are nominally available to the experiment payload.
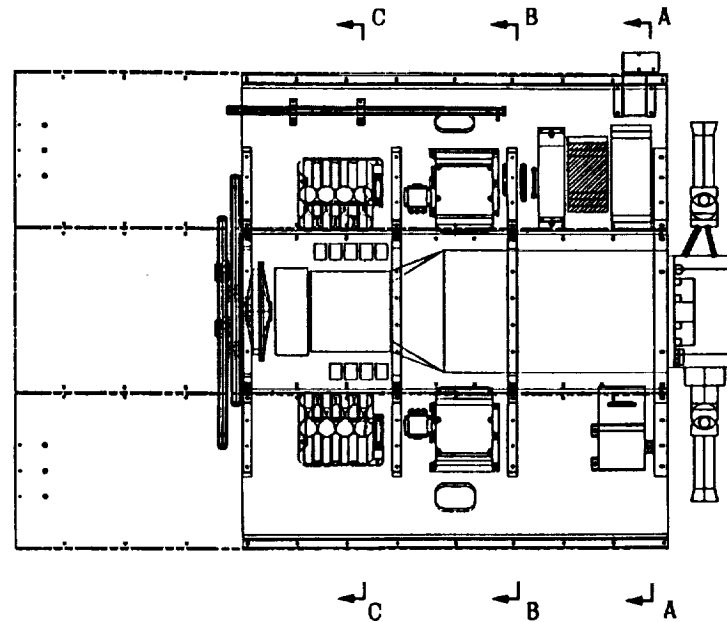
Figure 3-22. CSI-Star CAD Layout Drawing - Top View
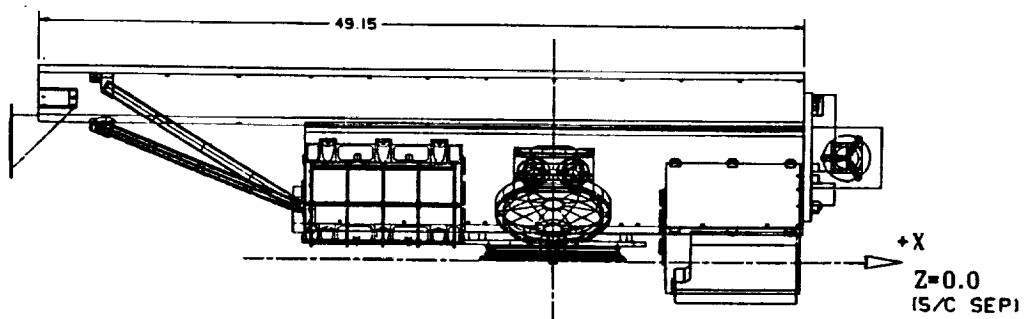
Figure 3-23. CSI-Star CAD Layout Drawing - Side View
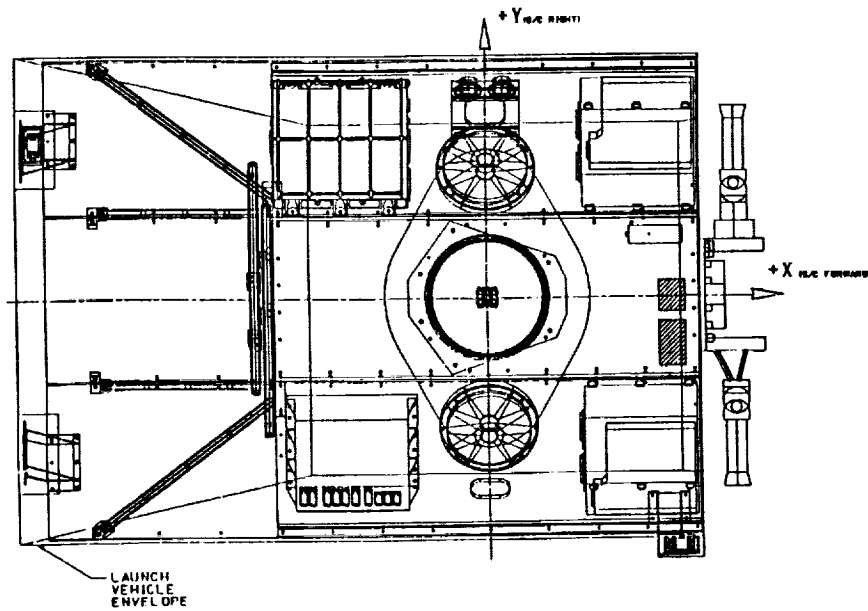
Figure 3-24. CSI-Star CAD Layout Drawing - Bottom View

Front View
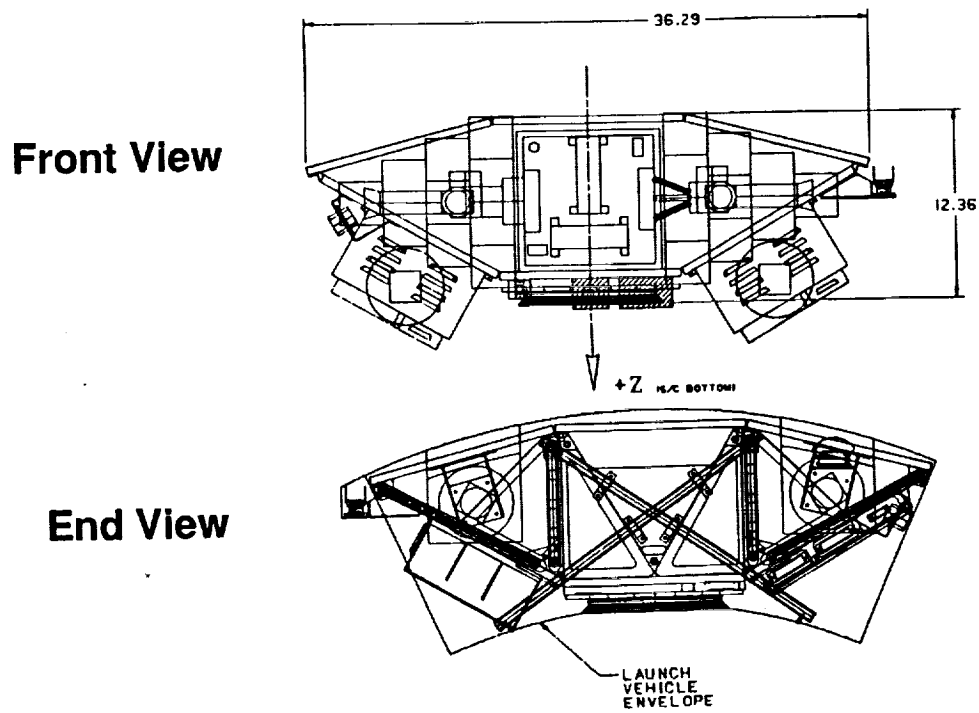
End View

Figure 3-25. CSI-Star CAD Layout Drawing - Front and End Views
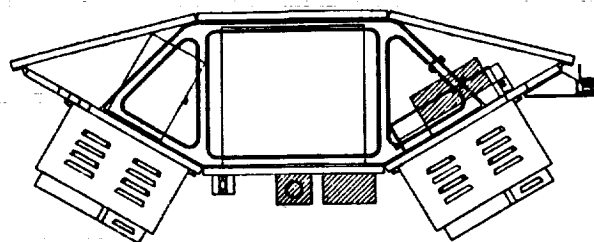
View A - A
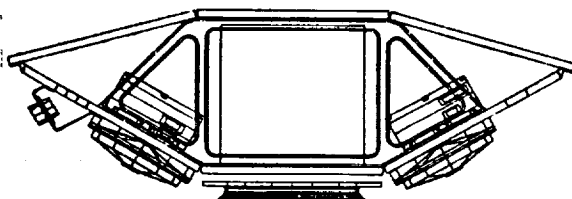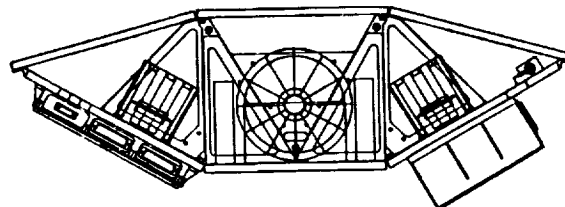
View B - B   **View C - C**

Figure 3-26. CSI-Star CAD Layout Drawing - Section Views From Figure 3-22

Table 3-6. CSI-Star Mass Properties

Subsystems	Weight (lbs)	X (in)	Y (in)	Z (in)
Mechanical structure	44.24	-4.256	-0.052	-6.868
Electrical power	46.97	-8.156	-2.311	-6.734
Avionics	28.00	7.280	0.080	-2.940
Attitude control	20.90	-3.322	1.484	-5.291
RF	11.08	1.353	-8.279	-5.886
Thermal	0.05	0.000	0.000	-4.250
QuickStar bus total	151.25	-2.790	-1.120	-5.809
CSI-Star satellite total:				
Payload option A	218.66	1.112	-0.996	-5.574
Payload option B	215.86	0.986	-0.971	-5.515

There was some concern that the baselined 0.6 MFLOPS may not be enough to meet some CSI payload processing requirements. Options have been looked at which would increase the throughput available to the payload. A recommended option is to increase one of the 80387 math co-processor clocks in the DSU from 8 MHz to 12 MHz. The 80387 employs two clocks: one for bus synchronization and the second for internal operations. In the present design, these two clocks are tied together, but can be separated. Increasing the speed of the 80387 internal operations clock will speed up floating point math operations. The heavy reliance on floating point in the CSI-Star payload algorithms will lead to a very effective increase in total throughput. This is a simple change to make, with the only real disadvantage being that the 80387 co-processor will dissipate more power, reducing its long-term reliability. Ball analyzed the impact of the reliability change and feels that the clock speed selected (12MHz) will yield a 0.2 MFLOP increase while maintaining an acceptable mission reliability.

Additional options that increase reliability and increase this throughput total are discussed in the section on reliability. The vibration control capability of this available throughput is discussed in Section 4 dealing with on-orbit operations.

3.7.4 Attitude Determination and Control

The baselined attitude control components for CSI-Star are based on analyses of disturbance torques and electromagnet torques estimated for a near-polar orbit at 550 km altitude. The major attitude disturbance for this mission will be the gravity-gradient torques created by the extended boom with its tip mass. These torques are proportional to the difference between boom-axis and transverse moments of inertia. The comparatively long boom configuration increases the difference in these moments of inertia, potentially inducing large gravity-gradient torques.

The system moment of inertia about an axis transverse to the axis of the boom is estimated in Figure 3-27, for boom lengths of 10 to 20 feet and tip masses of 20 to 30 lbm. It shows that the transverse moment of inertia would exceed 500 kg-m^2 for a nominal tip mass of 25 lbm and boom length of 20 ft. Numerical values supporting the inertia calculations for the nominal boom length and tip mass are given in Table 3-7.

A general result of gravity-gradient analyses is that this torque would be largest whenever the boom axis is 45 deg out of the orbital plane. For this 45 deg flight attitude, gravity-gradient torques could exceed the ability to control the CSI-Star configuration, as shown in Figure 3-28. (This figure also includes the effects of estimated aerodynamic drag torque.)

As Figure 3-28 shows, without momentum dumping using control magnets the torques would saturate the reaction wheels in about 30 minutes (less than one-half orbit). The torques could be controlled somewhat using QuickStar's nominal 10 Amp-m^2 electromagnets; however, wheel saturation still is reached after about 120 minutes. Ultimately, controlling in the presence
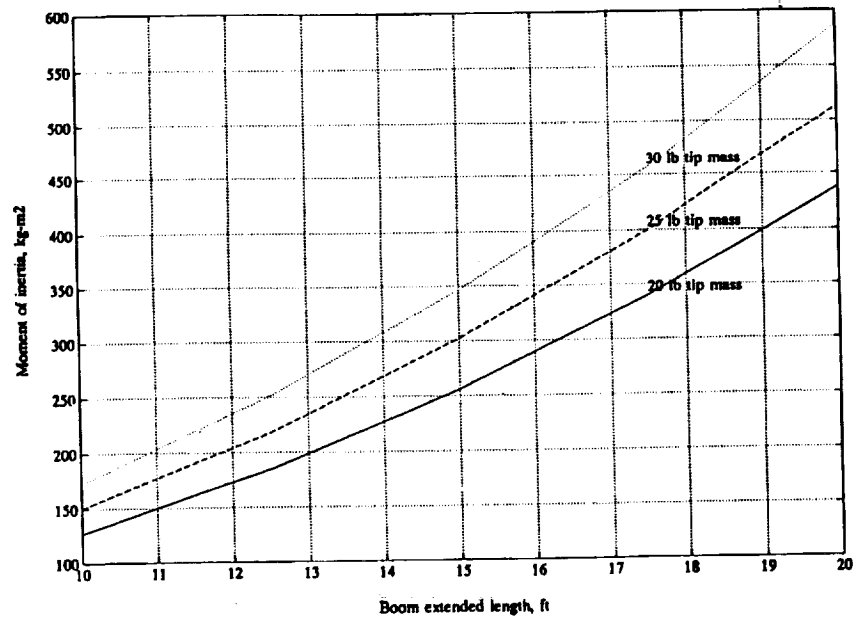
Figure 3-27. Moment of Inertia vs. STA Boom Length and Tip Mass

Table 3-7. CSI-Star System Moments of Inertia (Rigid Body)

Boom extension, ft: 20.0	X CM ft	X CM m	MASS kg	Ixx kg-m2	Iyy kg-m2	Izz kg-m2
	From system CM			About system CM		
QUICKSTAR BUS	-3.05	-0.93	86.36	5.08	81.99	86.03
EXTENDED BOOM	8.28	2.52	6.08	0.06	57.88	57.88
TIP MASS	18.78	5.73	11.34	0.18	371.89	371.89
Totals about sys CM				5.32	511.77	515.80
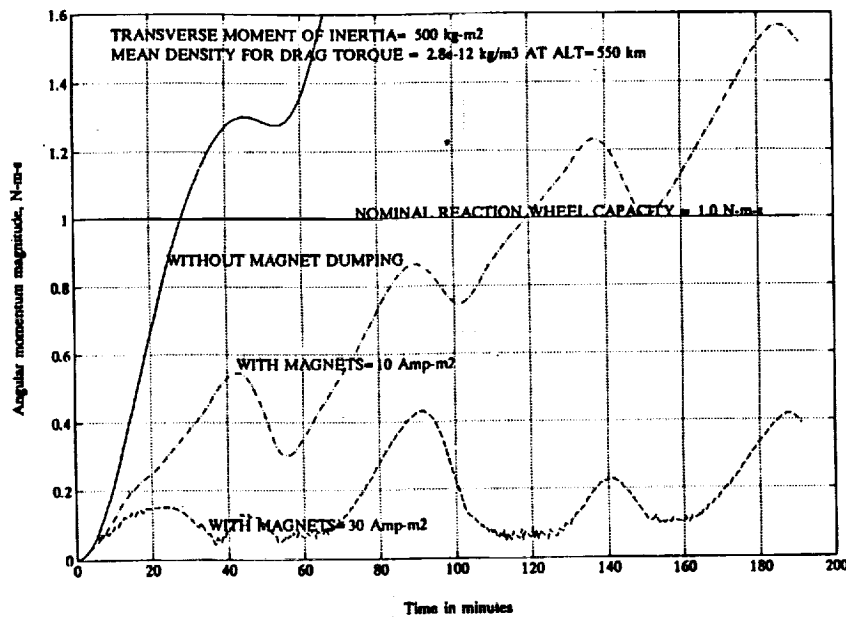
Figure 3-28. Angular Momentum Control with STA 45° Out of Orbit Plane.

of the modeled gravity-gradient and aerodynamic torques requires upgrading to 30 Amp-m^2 electromagnets as shown by the third curve in Figure 3-28. With these magnets, the disturbance torques at the worst-case attitude of 45 deg out of the orbit plane can be adequately controlled. This upgrading has insignificant weight impact on the CSI-Star. This means that if the CSI-Star facility is to have the capability to be placed into any orbit that the launch vehicle's primary mission puts it into, the 30 Amp-m^2 electromagnets are required. If only polar or near-polar orbits are selected, then the original 10 Amp-m^2 electromagnets are satisfactory. Therefore, the 30 Amp-m^2 electromagnets are baselined so that CSI-Star maintains the greatest flexibility in taking advantage of launch opportunities.

3.7.4.1 Recommended Operational Attitude. The attitude to be recommended keeps the extended boom in or near the orbital plane. The would reduce the environmental torques to the levels shown in Figure 3-29, where the secular component seen in Figure 3-28 no longer exists. The resulting cyclic momentum is potentially manageable with reduced control magnet capability, as in the case of some anomaly.

A second aspect of the recommended attitude is that the boom axis be oriented perpendicular to the sun line. This allows a simple roll control about the boom axis to maintain the solar panels

- 48 -

toward the sun at or near polar inclination orbits. The low system inertia about the boom axis allows rapid panel repointing.

With the boom axis in the orbital plane and oriented perpendicular to the sun line, one choice remains: the boom axis direction can meet these constraints equally well if yawed 180 deg about the sun line. The choice can be made based on which attitude provides a better communications geometry. The recommended attitude is summarized in Figure 3-30.

The time required to reorient the boom direction is limited by the momentum and torque capacities of the selected reaction wheels. General wheel relationships governing reorientation capabilities are shown in Figure 3-31 for a reorientation of 60 deg, for available torques of 0.01 to 0.05 Nm, and for momentum capacities of 1.0, 2.0, and 3.0 Nms. These relationships assume the boom is fully deployed, creating transverse inertias of 500 kg-m^2 as discussed above. Characteristics of specific reaction wheels are superimposed.

The baseline wheels for CSI-Star are of the LOSAT-X class. These would produce a 60 deg reorientation in about 10 minutes, based on Figure 3-31. This performance is deemed adequate for the requirements of this mission. Reorientation time could be reduced by using wheels of increased momentum capacity; Figure 3-31 indicates that motor torque is not the limiting characteristic.
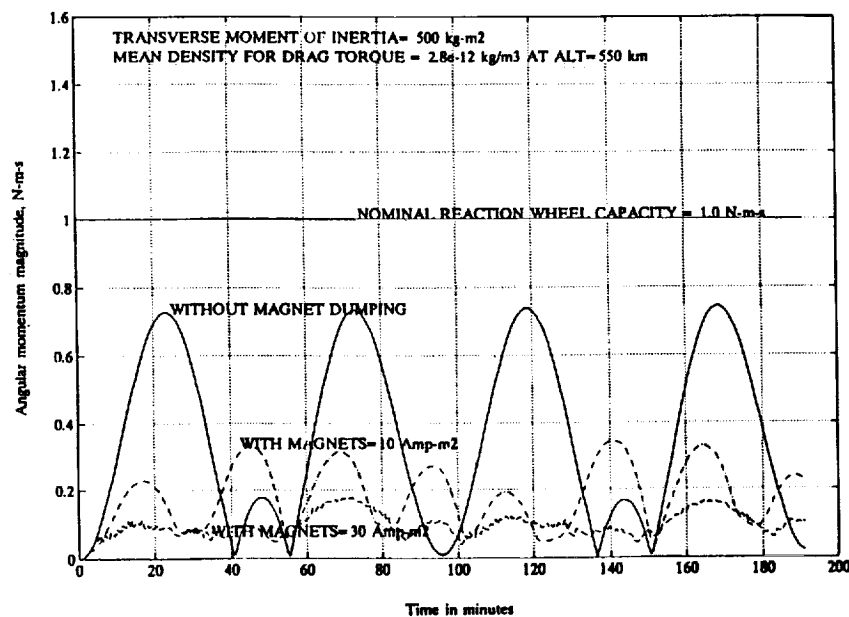
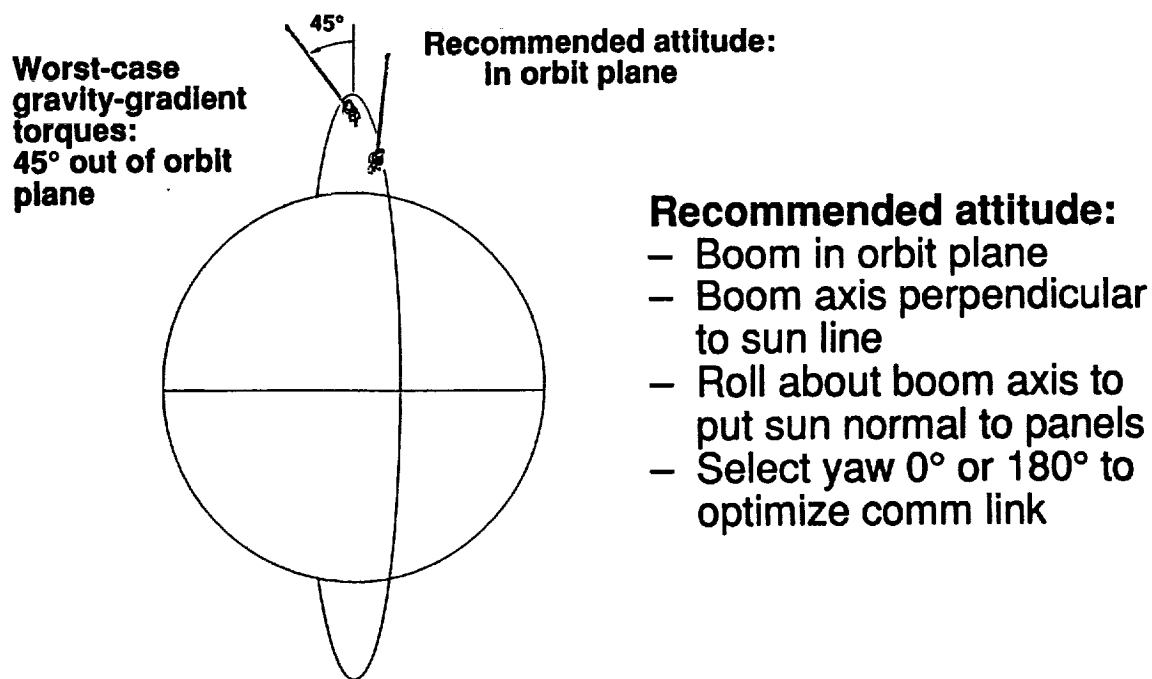**Figure 3-29. Angular Momentum Control with STA 0° Out of Orbit Plane.**

- 49 -

Worst-case gravity-gradient torques: 45° out of orbit plane

45°

Recommended attitude: in orbit plane

Recommended attitude:
— Boom in orbit plane
— Boom axis perpendicular to sun line
— Roll about boom axis to put sun normal to panels
— Select yaw 0° or 180° to optimize comm link

Figure 3-30. Recommended Attitude of CSI-Star is STA in Orbit Plane.

Figure 3-31 graph showing:
- Body moment of inertia = 500.0 kg-m2
- Max wheel momentum, Nms
- LOSAT-X (1.0)
- Bendix GPS
- Teldix, Ithaco A
- BAero
- Bendix INSAT
- Y-axis: Total turn time, minutes
- X-axis: Available wheel motor torque, N-m (0.01 to 0.05)
- Curve labels: 1.0, 2.0, 3.0
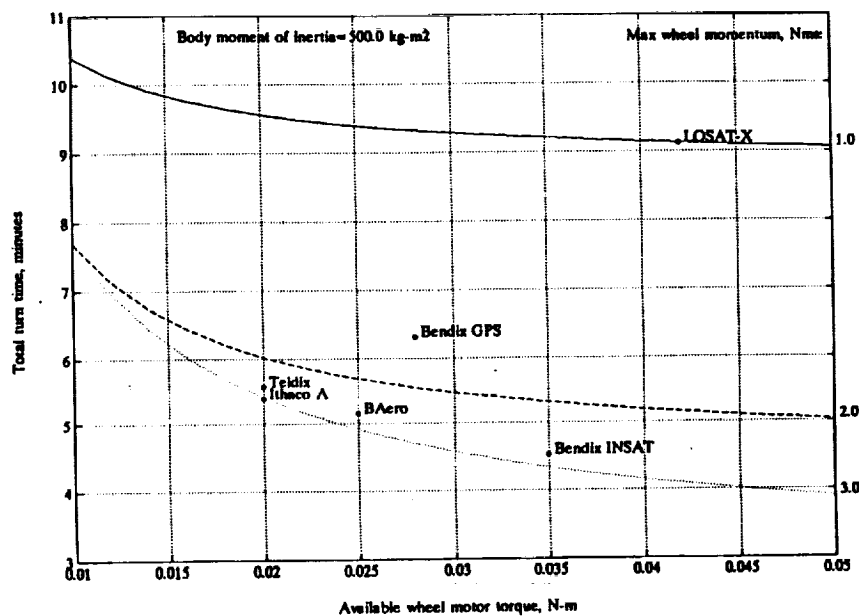
Figure 3-31. Time Required to turn 60° vs. Reaction Wheel Parameters.

A satellite with an attached boom is controllable, in the same way a satellite without a boom is controllable, by measuring only the states of the satellite and without directly measuring boom motion. A simple proportional-plus-derivative attitude control system, with reaction wheels for actuation and accurate rate sensors for monitoring satellite motion, provides stable satellite pointing and actively damps boom motion. The ability to accurately point the satellite in a given inertial frame requires the inclusion of an inertial reference sensor which provides rate sensor drift corrections. Torque rods and a magnetometer are used for momentum management.

To increase effective boom damping, the closed-loop bandwidth of the satellite pointing control system is made substantially less than the free-free satellite-boom system resonance and system time delays are minimized.

Boom state control, by the satellite reaction wheels, requires measurement or estimation of boom states and a satellite attitude control system bandwidth near or above the system resonance to obtain the desired boom responsiveness. This high bandwidth results in implementation problems given sensor noise and wheel torque limits. The concept of satellite boom control warrants further investigation and should be a topic for future studies.

Using the baselined spacecraft control system discussed in Section 3.5.8, Figure 3-32 shows the attitude and boom error response to an attitude step command of 0.01 rad or 0.6 deg. The first boom free-free mode in the system model is at 0.95 Hz with no damping. Figure 3-33 shows the difference between satellite and boom attitude. The difference stays less than 35 μrad or 0.002 deg. Notice that between two and seven seconds, while the wheel command is saturated and constant, relative motion remains constant amplitude indicating zero damping. Figure 3-34 shows torque delivered to the satellite from the wheel. At two seconds the wheel passed through zero speed and friction changed polarity. At about eight seconds the rate limit begins to reduce the torque command. A near steady-state condition exists after 30 seconds.

3.7.4.2 Satellite Dynamics. A two-body model is used to predict satellite and first-bending-mode boom dynamics. The satellite without the boom has an inertia component, I_s, of 90 kg-m^2, the boom has an inertia component, I_b, of 440 kg-m^2, the total system has an inertia, I_t, of 530 kg-m^2 $(I_s + I_b)$, and the effective system, used in determining the free-free resonant frequency, has an inertia, I_e, of 74.7 kg-m^2 $((I_s I_b)/(I_s + I_b))$. The torsional spring required for a free-free mode of 0.95 Hz is 2662 Nm/rad $(\omega^2 I_e)$. A constrained satellite results in a boom resonant frequency of 0.39 Hz ($\sqrt{2662 / I_b}$).

Figure 3-35 shows wheel-torque-to-satellite-attitude and wheel-torque-to-boom-attitude. The satellite attitude transfer function is:

$$\frac{\theta_s}{T_s} = \frac{0.011111s^2 + 0.067225}{s^4 + 35.629s^2} \frac{rad}{Nm}$$
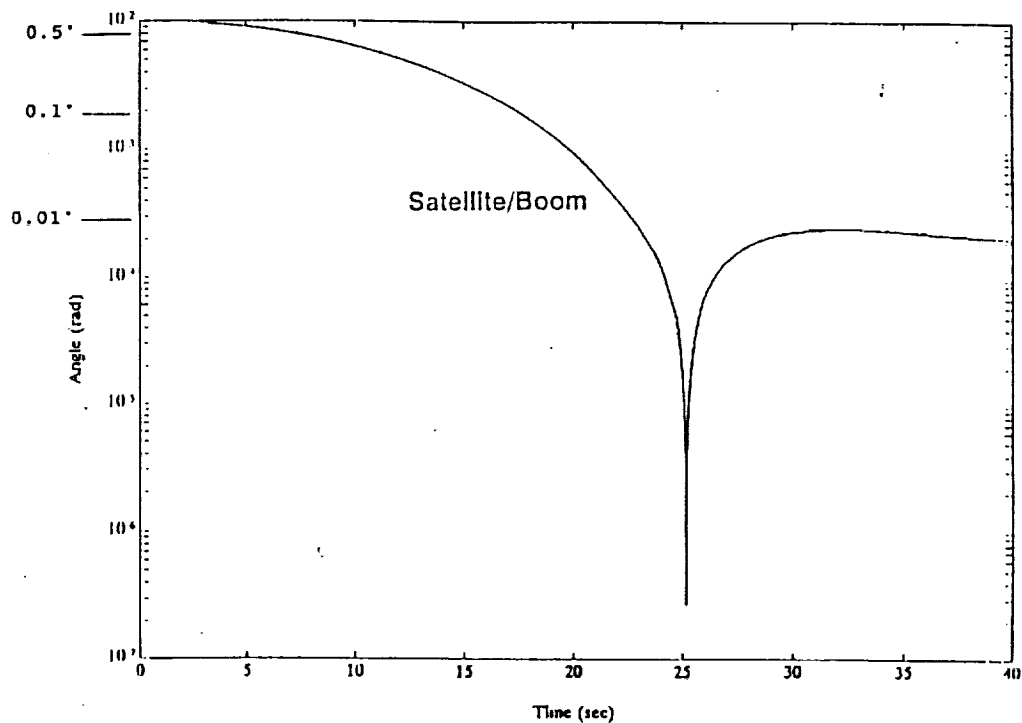
- 51 -

Figure 3-32. CSI-Star Response to 0.6° Step Input (System Position Error and Recovery).
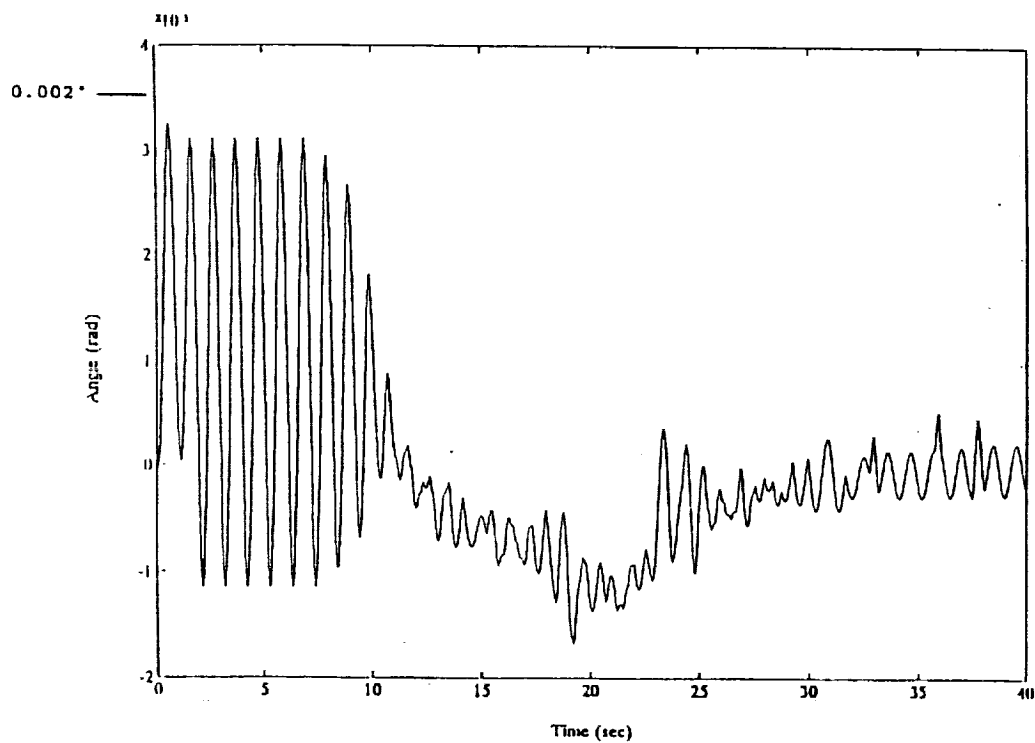

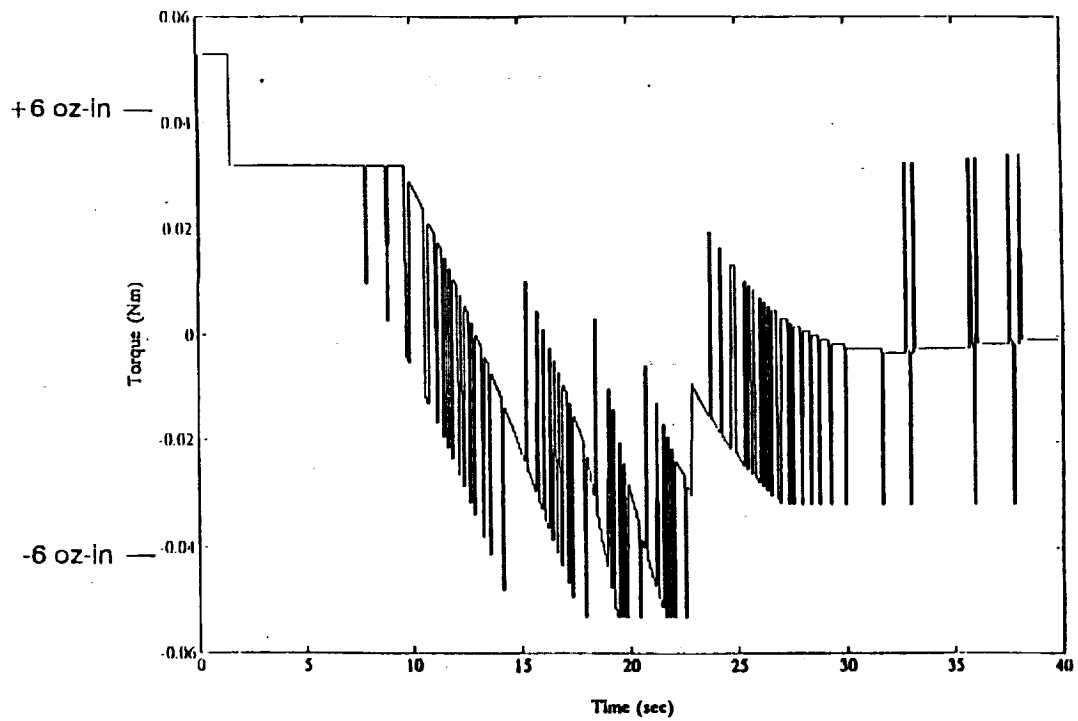**Figure 3-33.** Relative Motion During Step Response (Bus Minus STA Position).

- 52 -

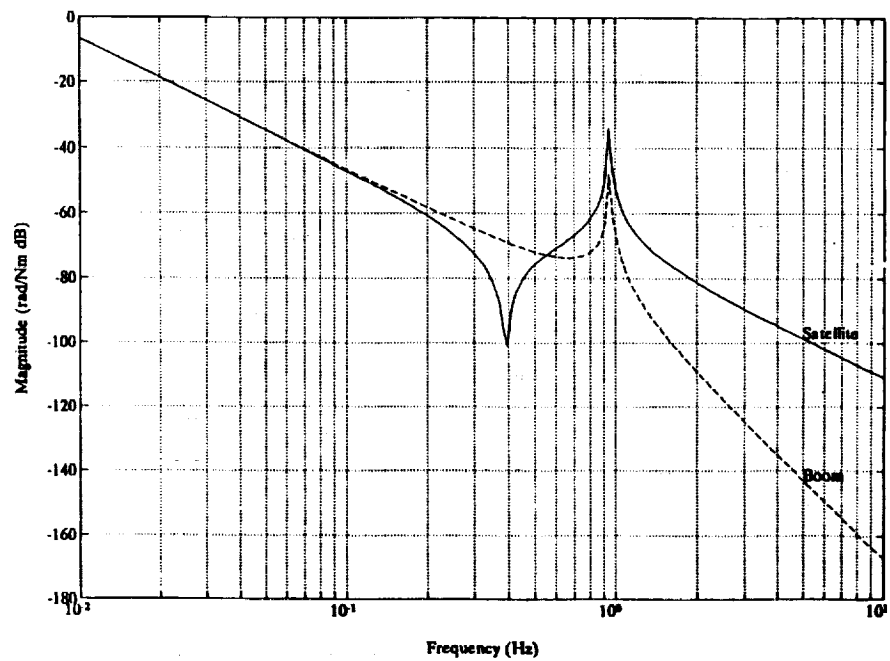**Figure 3-34. Reaction Wheel Torques During Step Response.**

Figure 3-35. Wheel Torque to Bus and STA Boom Position.

and the boom attitude transfer function is:

$$\frac{\theta_b}{T_a} = \frac{0.067225}{s^4 + 35.629s^2} \frac{rad}{Nm}$$

3.7.4.3 Attitude Control System Stability.

System stability is graphically illustrated in Figures 3-36 through 3-41. Figure 3-36 shows the open-loop frequency response of the nominal attitude control system given no system delays. The phase margin at 0.075 and 1.15 Hz determine stability. Both are above 60 deg indicating a highly stable system. The frequency of the first 0 dB crossing of magnitude and the phase at that frequency are driven primarily by control system parameter selection to obtain desired satellite pointing accuracy and responsiveness. The characteristics of the second crossing are driven by the free-free resonant frequency of the system, the control system sampling frequency, delays in the system, and control system parameter selection.

Delays in attitude measurement signal processing affect the system stability by altering phase and gain margins and the effective damping. Figure 3-37 shows the effect of imposing a 0.1 sec delay in the control loop. The delay ($f(s)=e^{-0.1s}$) has only changed phase at higher frequencies. The phase margin of the first crossing remains almost unchanged at about 60 deg. The control system bandwidth is 0.05 Hz and a 0.1 sec delay has little effect. The phase margin of the second crossing, though, has dropped from over 60 deg to less than 30 deg. Boom oscillations do not damp down as fast with increased loop delay. The downward and upward cusps of these plots are also meaningful. The downward cusp occurs at the "cantilever" frequency of the overall system under control. This would be the resonant frequency of the STA if the spacecraft bus were held inertially stationary. The upward cusp (at about 0.95 Hz) is the free-free frequency of the STA and bus system in the absense of attitude control.

Figure 3-38 shows phase and gain margins versus loop delay for the nominal control system. Delays larger than 0.165 sec result in an unstable system. Figure 3-39 shows the effective boom damping versus loop delay. Delays less than 0.06 sec provide a reasonable degree of damping with an effective damping of greater than 0.15. Figures 3-40 and 3-41 show the exponential decay of the satellite relative boom rate (which can be extrapolated to attitude decay) given loop delays of 0 and 0.1 sec after a system disturbance impulse. In the QuickStar system, the delays can be confidently held to less than 0.1 sec by attention to the sequence and priority in which the innermost processor software loop samples the attitude sensors and executes the control algorithms.
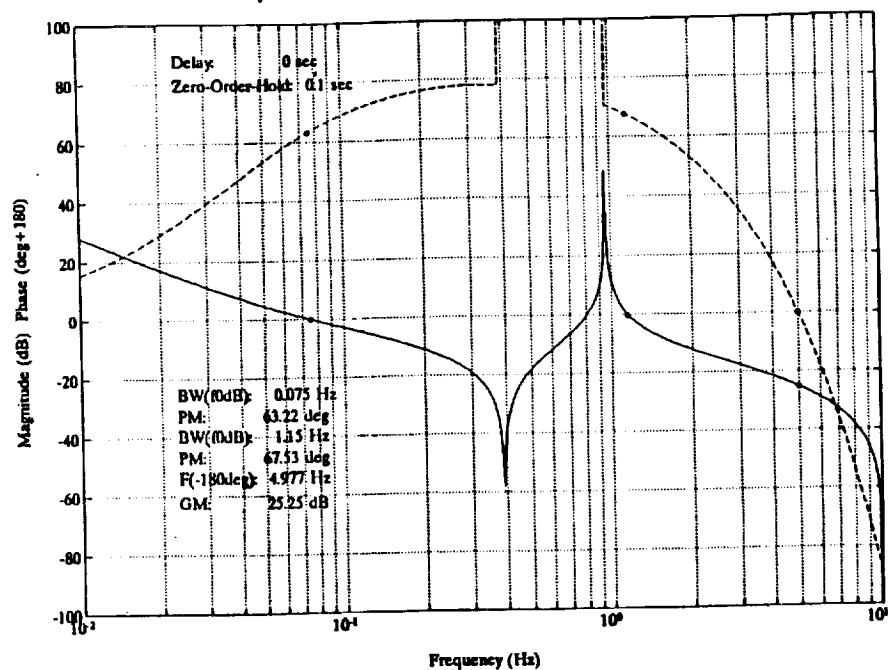
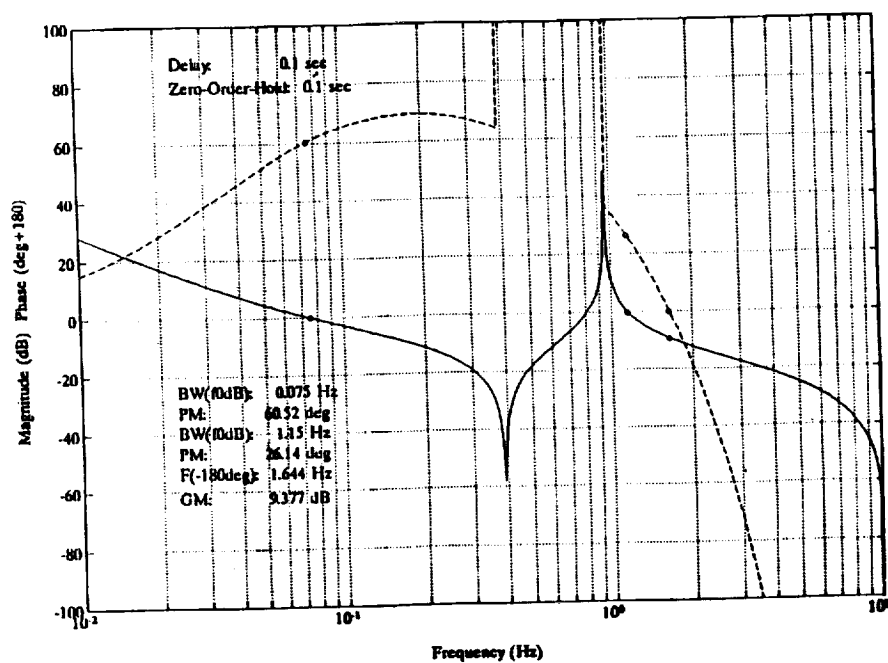**Figure 3-36. Open-Loop Frequency Response (No System Delay)**

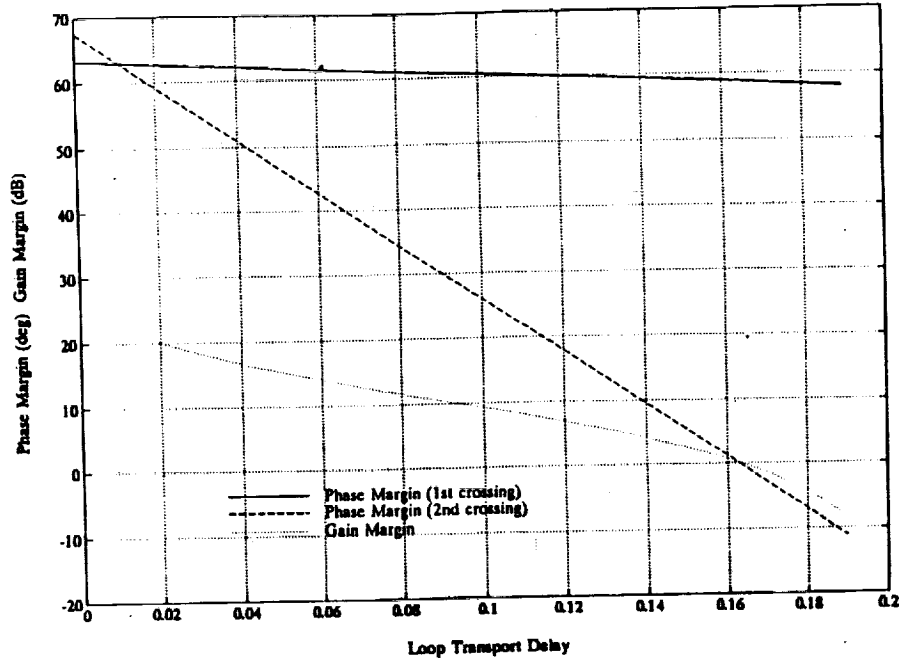**Figure 3-37. Open-Loop Frequency Response (System Delay = 0.1 sec)**

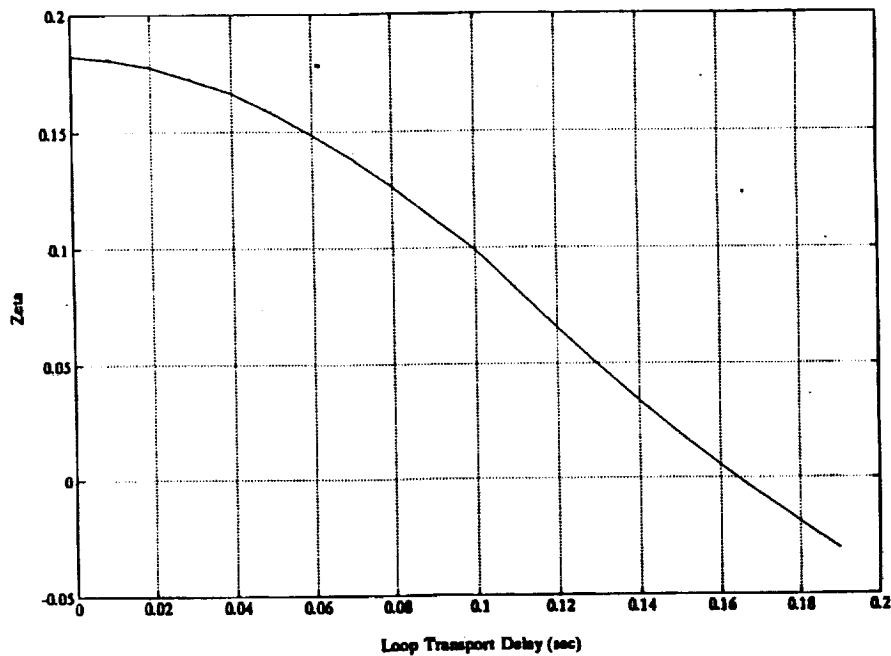**Figure 3-38. CSI-Star Phase and Gain Margins (0.05 Hz Control) vs. Loop Delay**

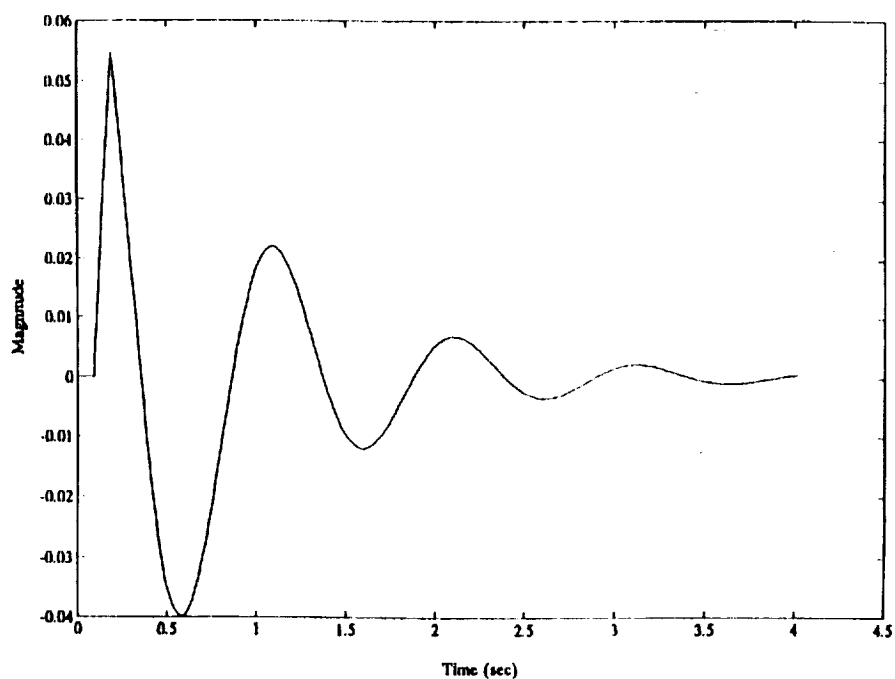**Figure 3-39. Effective Bus/STA Damping (0.05 Hz Control) vs. Loop Delay**

Figure 3-40. CSI-Star Relative STA Boom Rate (rad/sec) After Impulse (No System Delay)
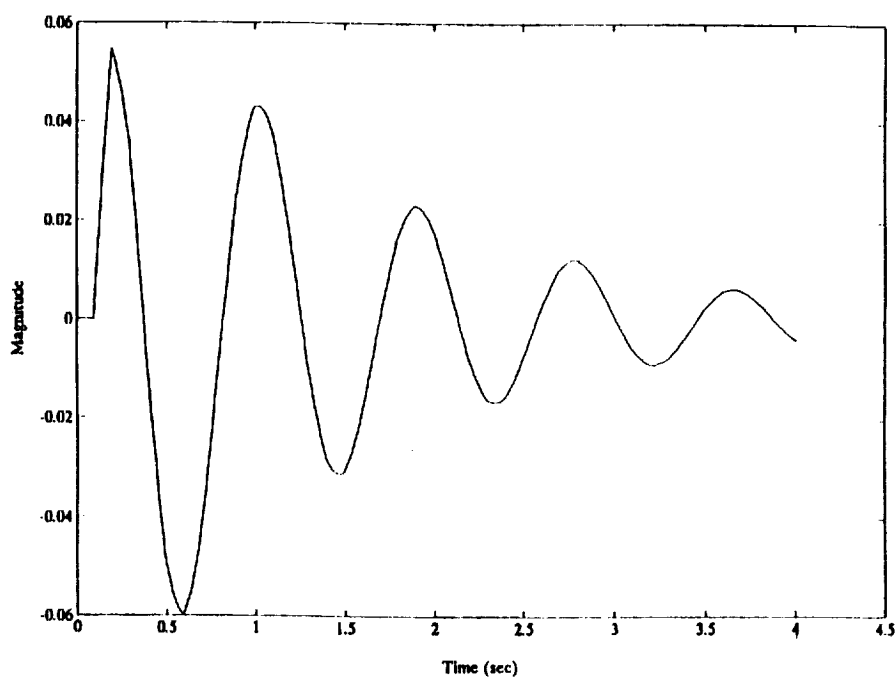

Figure 3-41. CSI-Star Relative STA Boom Rate (rad/sec) After Impulse (System Delay = 0.1 sec)

- 57 -

3.7.5 Spacecraft Bus Modifications

The experiment payload was designed to fit within the spacecraft bus volume, however, there will be some modifications to the bus that are required to accommodate clampband c.g. requirements and system controllability. The ACTP, mass memory and batteries had to be relocated to maintain system c.g. location. The standard 10 Amp-m^2 control magnets had to be replaced with 30 Amp-m^2 units to allow for control of aerodynamic disturbance torques at worst case CSI-Star attitude of 45° out of orbit plane.

4.0 ON-ORBIT OPERATIONS

This section describes the multi-task operations of the CSI-Star spacecraft during its lifetime. These operations include initial start-up and diagnostic testing of all hardware components. Several system identification procedures for the characterization of the spacecraft dynamics are described, including power, computation, and data storage requirements. Orbit selection based on data and command transmission requirements is presented, and end-of-life deorbit options are considered.

4.1 SEPARATION & START-UP

The QuickStar bus is unpowered during the initial launch phase and the primary payload/launch vehicle separation sequence. Once the Delta II second stage has circularized the spacecraft orbit, the spacecraft bus is separated from the second stage skirt. Within 30 seconds of separation, the bus is powered up, and ACS diagnostics begin. After ACS diagnostics are completed, each QuickStar bus subsystem will be tested for correct operation. If all bus subsystems are cleared as nominal, the payload STA is deployed, and the experiment hardware is tested. Table 4-1 summarizes the QuickStar start-up procedures. From this timeline, it is fairly apparent that conducting such operations on an STS mission would severely limit the amount of time allocated to the actual experiments, since at least half of a ten-day mission may be required to verify the experiment support equipment.

Table 4-1. QuickStar Post Second Stage Separation Sequence

Operation	Time After 2nd Stage Separation
QuickStar separation & start-up	0 to 30 sec
Null all body axis rates & hold	30 sec to 2 min
Detect & orient solar panels to sun	2 min to 4 min
Initial Checkout	Day 1
- dump attitude constants & verify	"
- determine clock drift rates	"
- validate EPS charge/discharge	"
- validate EPS V/T settings	"
- checksum verification of memories	"
Spacecraft subsystems checkout	Days 2 to 5
Payload checkout	Day 6+

Table 4-2. Baseline Experiment Procedures

EXPERIMENT	CONTROL ARCHITECTURE	DISTURB. SOURCE	CONTROL ACTUATORS	FEEDBACK
SYSTEM ID				
• Broadband Mode Detection (Burst)	N/A	PMA	N/A	Accel/Strain
• Fine Detection (S. Sweep/F. Decay)	N/A	Gimbal/Struts	N/A	Accel/Strain
ACTIVE CONTROL				
• Global Vibration Suppression Using Several Actuators	Global	PMA/Gimbal	PZT Struts	Accel/Strain
• μ-Amplitude Vibraton Suppression During Precision Payload Pointing	Local	PMA/Struts	Gimbals/tripod	Sun Sensor
• Global Vibration Suppression During Multiple Payload Pointing	Hierarchical	PMA/Gimbal	Struts/Gimbals	Accel/S. Sensor
• Global Vibration Suppression During Spacecraft Slewing	Global	ADCS	Struts	Accel/Strain

4.2 BASELINE EXPERIMENT PROCEDURES

Once the QuickStar spacecraft has completed its start-up and diagnostic tests of all bus and payload operations, the experiment payload can begin a "shake-down period" conducted by the contractors to characterize the open and closed-loop dynamic behavior of the spacecraft. As shown in Table 4-2, the baseline procedures of this period consist of system identification (SID) and active control tests. The system ID tests will provide the means to clearly discern the structural modes of the payload, and the active control tests will attempt to validate several control algorithms for suppressing modal vibration. While this agenda appears ambitious for a first set of tests, it is developed to provide a solid base of information for use by future guest investigators. In reality, however, local closed control loops will be implemented, followed by limited global and hierarchical testing.

4.2.1 System Identification Procedures

In order to successfully implement control algorithms for the suppression of vibration within the CSI-Star spacecraft, the on-orbit dynamic behavior of the spacecraft must first be quantified through system identification. System identification resolves the frequencies and associated damping levels for the modes of interest of the spacecraft through the measurement of a controlled disturbance via the on-board sensors. Several identification methods are available for the detection of resonant modes within the spacecraft, each with its own requirements, advantages and disadvantages in use.

The parameters which most directly affect the time required to implement SID methods are: structural damping, instrument power consumption, and data storage. Generally, tests conducted on a structure with low damping will require longer test periods, thereby increasing the number of orbits required for completion. Increased damping proportionately reduces the time of completion, and consequently the number of orbits. Instrument power consumption also dictates the number of tests per orbit. Because the spacecraft bus provides a fixed amount of energy to the payload per orbit, the number of experiments that can be conducted during one orbit is limited. Closed-loop tests generally consume more power, but have increased damping. Data storage is currently limited to approximately 1 Gbit. Most tests consume far less than this; however, if stored data cannot be downloaded immediately, the mass storage may fill up with several orbits' worth of data. This would then require the spacecraft to wait one or more orbits until the ground station is in sight for downlinking. Data rates do not pose a problem, as most of the 1 Gbit mass storage can be downlinked in one fly-over.

4.2.1.1 Burst Random.

The burst random test involves the input of a broadband disturbance in order to excite all modes simultaneously. To generate an accurate picture of the modes' relative strengths, the disturbance bandwidth must exceed that of the highest mode of interest. In addition, the sensor data must be sampled at least an order of magnitude above the highest mode frequency to avoid any aliasing problems. The sensor time response data collected is converted to a frequency response spectrum through a Fast Fourier Transform (FFT). The frequency resolution of the FFT is inversely proportional to the sample period; for example, to obtain 0.001 Hz resolution from the FFT, the time response must be sampled for at least 1000 seconds.

In general, the burst random method is an excellent means to determine the approximate positions of all critical modes simultaneously, usually requiring only one short time sample of 100 seconds. However, it is very costly in time, energy and data storage when used for fine modal resolution. Because the resolution of the FFT is a function only of time, increased damping in the system does not reduce the time or storage requirement for the closed-loop tests. In addition, a single test must be repeated, stored and averaged over several intervals to ensure confidence in the resulting FFT. Tests also need to be performed at multiple input amplitude levels to detect any non-linearities in the structural damping with increasing deflection. The completion of all these tests requires several orbits. A general guideline requires that ten identical tests be performed at three different amplitude levels for a total of 30 burst random tests.

4.2.1.2 Sine Sweep.

The sine sweep tests are performed by exciting the structure with a single disturbance source vibrating at a fixed frequency and amplitude. Once the structure has reached steady state, a single output response data point is collected. This process is repeated at small frequency intervals around a resonant mode.

The sine sweep test has the advantage of reduced storage requirements, because only one data point is collected per test. The sine sweep still suffers from long test periods, however, and does not provide the same resolution as the burst random tests, as the typical sine sweep interval is 0.01 Hz. The sine sweep test period is inversely proportional to the modal damping, and is very long for a mode with low frequency and/or damping. Assuming second order behavior for each structural mode, the time to reach steady state is:

$$t_{ss} \approx \frac{4}{2\pi\zeta f} \qquad \text{(seconds)} \qquad (4.1)$$

where ζ is the damping ratio and f is the mode frequency in Hz. For a 1 Hz mode with open-loop damping of only 0.2%, time to reach resonance is over 300 seconds (Fig. 4-1). Like the burst random test, this procedure must be repeated at different input amplitudes to detect non-linearities in damping and at each frequency interval around the resonant frequency. Therefore, complete sine sweep tests can be very time and energy-consuming. For example, to obtain 0.01 Hz resolution about a resonant mode, 100 sine sweep tests must be conducted about the mode. Also, at least three different input amplitudes must be used. Therefore, over 300 sine sweep tests must be performed to resolve one mode only. Because the time to resonance is inversely proportional to both frequency and damping, a significant increase in either variable will reduce the experiment times proportionately. Therefore, both closed-loop and higher frequency mode sine sweeps will be completed much more quickly and with far less energy consumption per orbit.

4.2.1.3 Free Decay.

The free decay test can be considered a hybrid between the burst random and sine sweep tests in its application and benefits. In general, the structure is excited with a single disturbance source operating at a regular sine wave frequency close to that of a resonant mode. The structure is excited until the desired response is acquired, at which point the disturbance is stopped, and the free decay response is recorded.

The free decay test has several advantages over the other two methods. First, because only the free decay response is needed for analysis, the recorded sample period is shorter, and the

sample rate need only be an order of magnitude above the single mode frequency. Therefore, the time and storage requirements are considerably less than that of the burst random test. Second, the free decay will "ring down" at the nearest resonant mode at a rate proportional to the damping ratio. If the damping ratio varies with amplitude, this can be detected in the decay "envelope" of the response as the amplitude falls. Therefore, both the resonant frequency and amplitude-dependent damping ratios can be determined from one free decay test, without the need for incremental frequency increases or multiple tests. As a rule, however, at least four identical tests are conducted to ensure confidence in the measurements.

As with the sine sweeps, the sample period varies inversely with both mode frequency and damping ratio (see Eq. 4.1). An increase in either will result in a proportional decrease in sample period, thereby reducing storage and energy requirements.

4.2.1.4 Line-of-Sight Error.

The line-of-sight test is not directly a system identification method, but rather a means to quantify the effects of vibration on a pointing instrument's operation. An instrument such as the laser or sun sensor is pointed at another sensor or object, and the structure is then shaken, either broadband or at a single frequency. The resulting jitter in the instrument pointing is then recorded and analyzed for frequency content and amplitude. The effects of an active controller on the jitter can also be measured, providing a direct means to quantify the improvement in
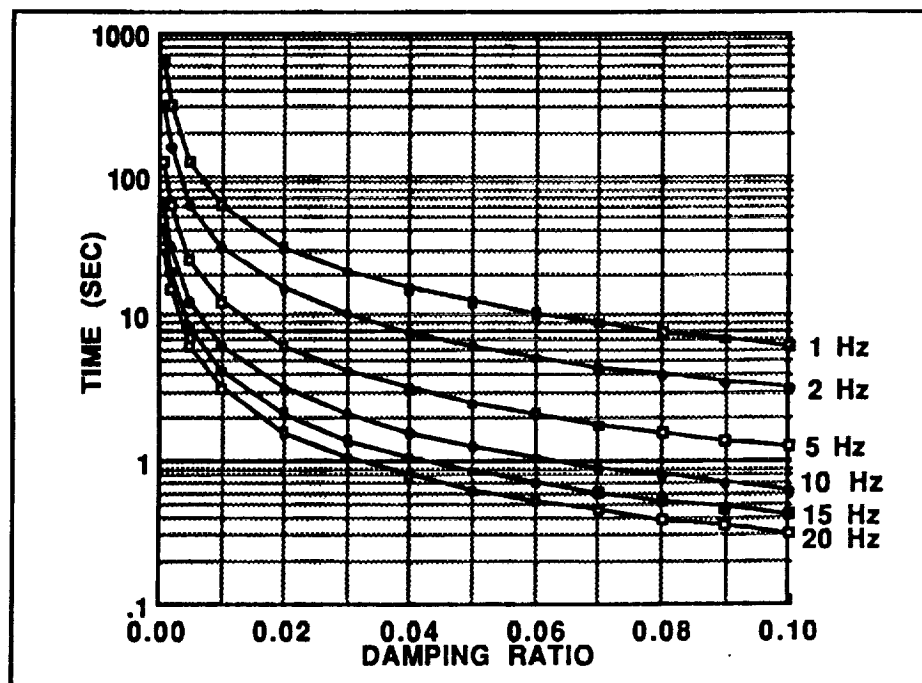

**Figure 4-1. Time to Reach Within 2% of Steady State Response
for Second Order System as a Function of Damping**

- 63 -

instrument pointing. As a rule, ten averages are performed to confidently measure the structural response.

Through the above system identification methods, both open and closed-loop baseline experiments can be performed. In both experiments, certain instruments, actuators and sensors must operate simultaneously during the testing period. Possible experiment timelines are now presented for both open and closed-loop tests, along with their power, storage and computation requirements.

4.2.2 Open-loop Experiment Requirements

Several variables must be addressed when developing experiment timelines using the available experiment equipment. First, a choice of active equipment must be made to determine the power consumption during various phases of the experiment. Second, the amount of available storage must be considered to ensure that all tests can be conducted without relying on a direct ground link during testing. Third, the capability for real time assimilation and computation of sensor data is critical for the successful detection and control of resonant modes. These variables are considered in both open and closed-loop tests.

Table 4-3 lists those experimental variables which most directly affect the number of orbits required to complete a particular experiment, which in turn affects the period of time required by a guest investigator to conduct his research.

Table 4-3. Effects of Experiment Variables on No. of Orbits Required for Testing

Variable	Impact on No. of Orbits
Time required per sample period	Directly increases by reducing no. of experiments per orbit
No. of averages and amplitudes required	Directly increases by increasinf no. of samples per experiment
Experiment power	Increases by reducing power budget margin per orbit
Data storage per sample period	Increases only if total data storage requirement exceeds that of hardware
Downlink period per orbit	Increased downlink period decreases no. of orbits by reducing orbits required for downloading of data

4.2.2.1 Power.

For open-loop tests, a set of active instruments were selected from those available. These are as follows:

2 proof-mass actuators (PMAs) - 11 Watts	2 load cells - 1.8 Watts
20 accelerometers - 1.12 Watts	20 strain & temperature gages - 2.5 Watts
1 video camera & electronics - 20 Watts	laser or sun sensor assemblies - 5 Watts
instrument heating - 10 Watts	

It is assumed that during the active phase of the experiment, when both PMAs are acting as the disturbance source, the total power consumption is approximately 55 Watts. During the stand-by phase, the PMAs and load cells are shut down, reducing the power requirement to approximately 42 Watts. Both estimates are highly conservative, because the video camera will not be used for most experiments. Once the experiment is completed, only the instrument heating will remain operating, requiring 10 Watts to 12 Watts of continuous power.

The current energy budget allocated by the QuickStar bus for the experiment payload defines an operating envelope of 44 watts average power consumption over an assumed 90 minute orbit. Therefore, the total energy consumption per orbit is 66 watt-hours, which can be used along any desirable timeline, the only restriction being that the instantaneous power consumption is not to exceed 140 watts. This would cause the power supply to exceed its current limited capabilities.

Figures 4-2 through 4-4 illustrate typical power timelines for open-loop burst random, sine
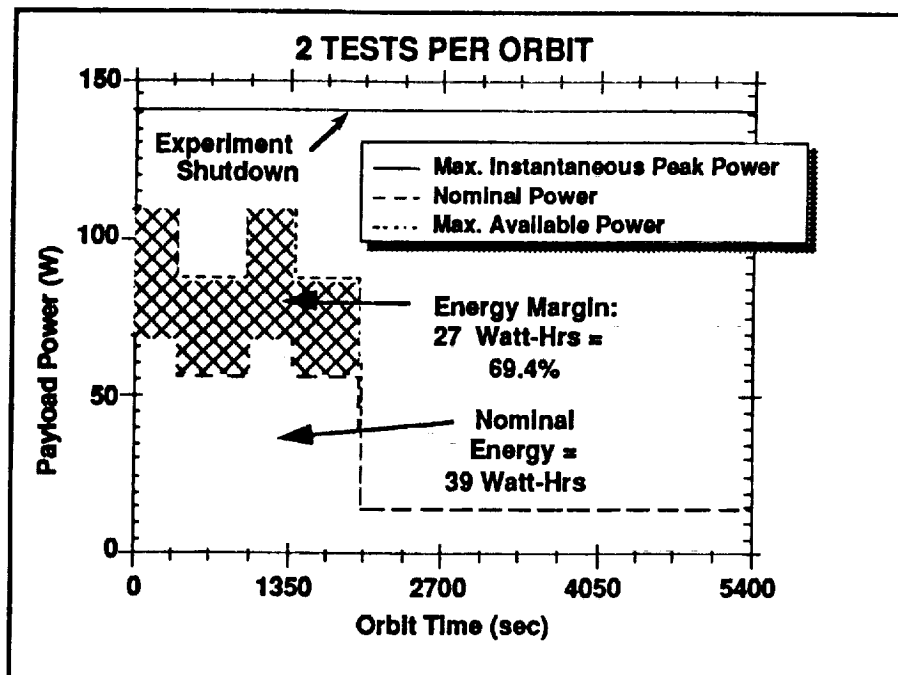

Figure 4-2. Burst Random Open-loop Power Timeline ($\zeta = 0.2\%$)

sweep and free decay tests, respectively. In Figure 4-2, two burst random tests are conducted per 90 minute orbit. The lower curve represents the nominal power consumption during the experiment period within an orbit. The active phase lasts for 400 seconds, followed by a stand-by phase of 600 seconds. The 400 second active period was selected to reach resonance in a 1 Hz mode with open-loop damping of 0.2%. The 600 second stand-by period was selected to fill out the sample period to 1000 seconds to obtain the 0.001 Hz FFT resolution.

The area under the lower curve, or energy consumed within the orbit, is nominally 39.0 watt-hrs, leaving a 27 watt-hrs or 69% energy margin during that orbit. The upper curve represents the increased level of power consumption allowable during the experiment phase of the orbit if required. The active and stand-by phase power requirements are increased to 111 watts and 85 watts, respectively. The shaded area represents the energy margin. Note that the energy margin can be altered by increasing or decreasing the number of tests conducted per orbit. In the case of Figure 4-2, up to four tests could be conducted within the same orbit. This, however, would leave only a 14% energy margin, increasing the maximum allowable active power to only 64 watts. In addition, four consecutive tests would require at least 4000 seconds to complete. This exceeds the period of daylight within any one orbit, and would introduce variations in the spacecraft dynamics as the structure's temperature changed.

A similar analysis can be conducted for the sine sweep and free decay profiles, as shown in Figures 4-3 and 4-4 respectively. The sine sweep timeline has only an active mode during which
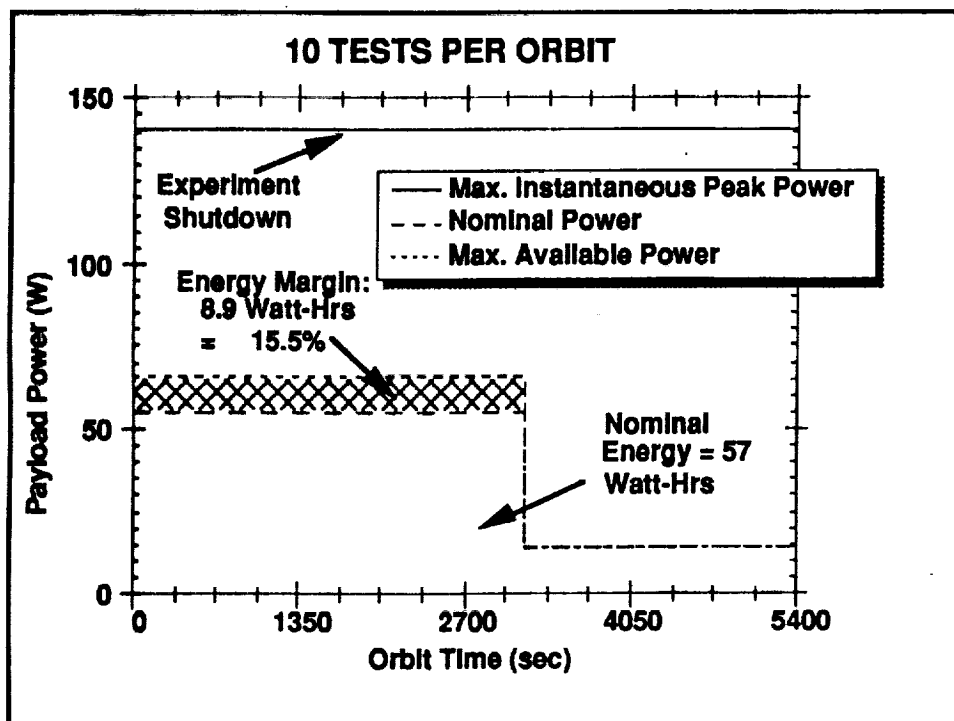

Figure 4-3. 1 Hz Sine Sweep Open-loop Power Timeline ($\zeta = 0.2\%$)

the frequency of the driving force is changed incrementally after equilibrium has been reached. The complete open-loop test during one orbit is 10 sequential periods of 320 seconds each for a mode near 1 Hz. This test consumes most of the allotted energy budget, leaving only a 15.5% margin. This allows a maximum peak power of 65 watts. The margin can be increased by reducing the number of test periods per orbit, but additional orbits are then required to complete the full identification of a mode. The analysis for the 1 Hz open-loop test is the most conservative, as increased damping and/or frequency would reduce the test period per orbit.

Figure 4-4 shows two free decay tests conducted during one orbit. Because the response time of the system falls inversely with increased mode frequency, higher frequency modes will have reduced response times. The figure illustrates the excitation of six modes, each having a resonant frequency twice that of the previous mode. Therefore, if 640 seconds are requirement to excite and observe the decay of the 1 Hz mode, all remaining critical modes can be excited and measured within an additional 640 seconds, assuming 0.2% damping in all modes. Two such tests consume 45 watts-hours per orbit, leaving a 46% margin. From this margin, the maximum allowable peak and stand-by phases are 88 watts and 67 watts, respectively. Because the free decay analysis requires only four tests, two orbits are sufficient to complete the analysis.
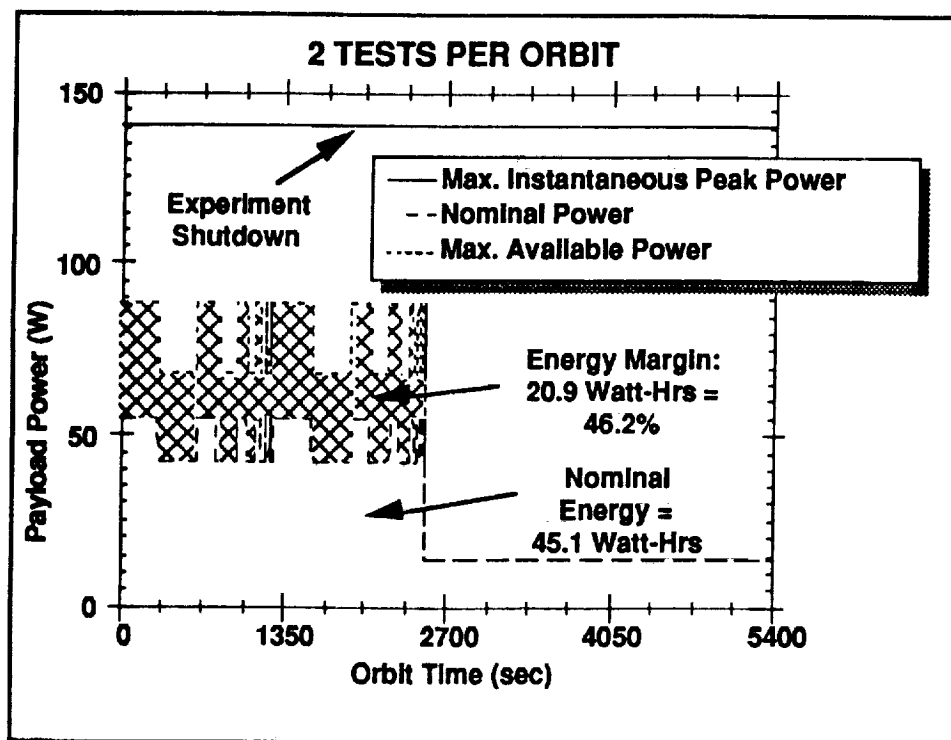

Figure 4-4. Free Decay Open-loop Power Timeline ($\zeta = 0.2\%$)

Table 4-4 summarizes the worst case power requirements for the open-loop system identification methods along with energy margins and number of orbits required to complete the tests.

4.2.2.2 Data Storage.

Data storage requirements vary considerably among the three described system identification methods. The amount of storage required can directly affect the speed with which these tests can be completed.

As stated earlier, the storage requirement for sine sweep test is very small because only one data point is collected per frequency interval. Therefore, if ten test intervals are performed in one orbit, only ten points are collected from each of 20 sensors, for 200 data points total. Assuming 12 bit data, only 2.4 kbits of storage are required per orbit. Because this is repeated over 30 orbits for the 1 Hz mode, a total of 72 kbits is stored. Even if up to 10 modes are sequentially analyzed, the total storage requirement will not exceed 1 Mbit, or 0.1% available capacity. Burst random and free decay tests, however, require considerably more storage.

Because extended data streams are collected during the burst random and free decay tests, data storage is dependent on the number of sensors used, sampling rate, period of sample and data bit size. The amount of data collected per test be determined as:

$$\text{\# bits} = (\text{\# sensors })(\text{samples/sec})(\text{sample time})(\text{bits/sample}) \qquad (4.2)$$

It is assumed that the data is 12 bit data, and the number of sensors operating is 20. For the burst random tests, both the sample rate and sample time are also fixed at 500 Hz and 1000 seconds, respectively. Therefore, each test period produces 120 Mbit of data for storage. Because the test periods are averaged sequentially, two sets of data from each sensor must be stored simultaneously, thereby doubling the storage to 240 Mbit. In addition, assuming that the time response data is converted to FFTs on-board, the FFT must also be stored. Because one test period contains 500,000 data points, a comparably sized FFT is also generated per sensor, adding approximately another 120 Mbit of data. Therefore, up to 360 Mbit of storage may be required for the burst random tests during any one orbit. Figure 4-5 illustrates the worst case storage

Table 4-4. Open-loop System Identification Power Requirements

Experiment	Peak Power (W)	Energy per Orbit (W-Hr)	Energy Margin (%)	No. Orbits Required
Burst Random (.001 Hz Res.)	55	39	69	15
1 Hz Sine Sweep (1 mode)	55	57	16	30
Free Decay	55	45	46	2

requirements for burst random testing, in which three series of 15 orbit tests for a total of 1.08 Gbits are stored before being downloaded over the course of several orbits. Each test series has two tests per orbit, which are averaged sequentially for 15 orbits for a total of 30 tests and 240 Mbits of data. This is then converted to FFTs, which adds an additional 120 Mbits of data to storage. This test series can be done three times before downloading is required.

The analysis for the free decay tests is similar. Data is collected only during the free decay period of the experiment, totaling 1280 seconds in the 1 Hz open-loop case. Again, the sample rate is assumed to be 500 Hz, although this is very conservative when sampling 1 Hz modes. Therefore, the amount of data collected per test period is 154 Mbits. For averaging purposes, two periods must be stored simultaneously, requiring 308 Mbits of storage. There is no further storage requirement, and the free decay tests are completed in two orbits. Therefore, data storage is not a difficulty for free decay tests. Table 4-5 summarizes the data storage requirements for open-loop tests.

Table 4-5. Open-loop System Identification Data Storage Requirements

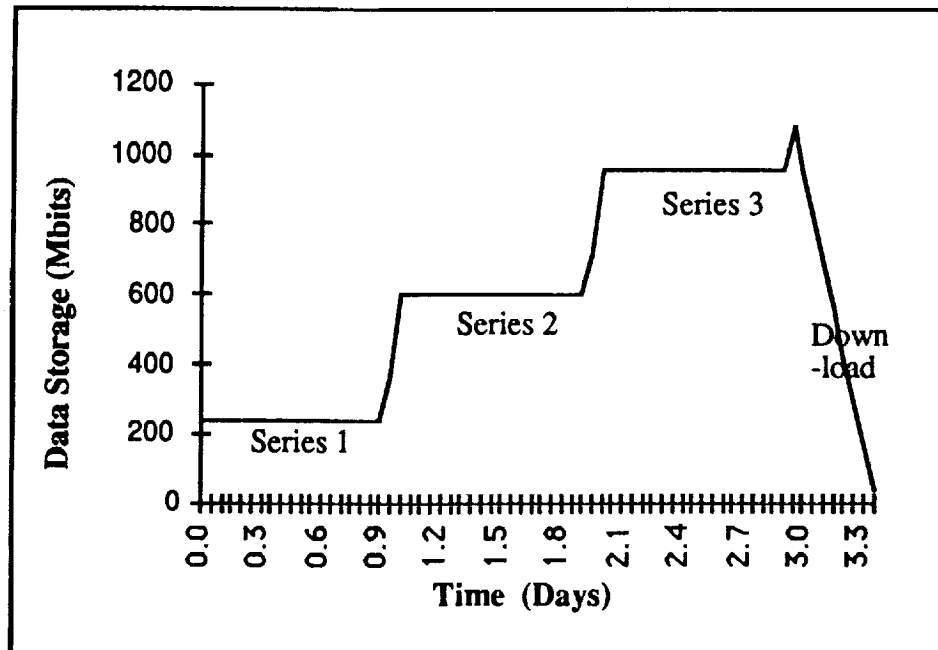| Experiment	Sample Period (sec)	Data Storage (Mbits/Orbit)	No. Orbits Required
Burst Random (.001 Hz Res.)	1000	360	15
1 Hz Sine Sweep (1 mode)	1	1	30
Free Decay	1280	308	2

Figure 4-5. Data Storage Timeline for Burst Random Tests

In all test cases, the operation of the video and the storage of video data is not considered. Currently, the operation of the video camera collecting one new image per second requires a data storage rate of 3 Mbit/sec. In every test case, this data rate would exceed the storage capacity of the on-board hard drive before the test was completed. Therefore, the camera is assumed to be used only for observation of mast deployment and for visual inspection when necessary.

4.2.2.3 Computation.

Because open-loop tests require only the collection and storage of response data, almost no real-time computational capability is needed. The only sensors requiring computation are the sun sensors which must calculate their position with respect to the Sun. Operating at 300 Hz, the sun sensors require only 0.006 MFLOPs to perform a real-time calculation, very minor compared to the processor capacity of 0.4 MFLOPs. The calculation of FFTs also requires computation, but is performed either after a completed test or on the ground, if necessary.

4.2.3 Closed-loop Experiment Requirements

4.2.3.1 Power.

For closed-loop tests, the set of active instruments described for open-loop operations remains the same, with the addition of two instruments:

   6 PZT active struts and electronics - 2 Watts

   2 gimbals - 12 Watts

It is assumed that during the active phase of the experiment, the PMAs are acting as the disturbance source, while the gimbals and struts act as the control actuators. The total active phase power consumption increases to approximately 69 Watts. During the stand-by phase, the PMAs and load cells are again shut down, reducing the power requirement to approximately 56 Watts. Once the experiment is completed, only the instrument heating will remain operating, requiring 10 Watts to 12 Watts of continuous power .

Figure 4-6 illustrates a typical power timeline for a closed-loop burst random test (sine sweep and free decay not shown). The active control has increased damping in all critical modes to 1.0%. In Figure 4-6, two burst random tests are conducted per 90 minute orbit. The lower curve represents the nominal power consumption during the experiment period within an orbit. The active phase lasts for 400 seconds, followed by a stand-by phase of 600 seconds. The 400 second active period is the same as that used in the open-loop test, although it could have been shortened to 80 seconds to account for the increase in damping. The 600 second stand-by period was selected to fill out the sample period to 1000 seconds to obtain the 0.001 Hz FFT resolution.

The area under the lower curve, or energy consumed within one orbit, is nominally 47 watt-hrs, leaving a 19 watt-hrs or 41% energy margin during that orbit. The upper curve represents the increased level of power consumption allowable during the experiment phase of the orbit if required. The active and stand-by phase power requirements are increased to 108 watts and 88 watts, respectively. The shaded area represents the energy margin. Note that the energy margin can be altered by increasing or decreasing the number of tests conducted per orbit. In the case of Figure 4-6, a third test could be conducted within the same orbit. This, however, would leave only a 10% energy margin, increasing the maximum allowable active power to only 77 watts.

A similar analysis can be conducted for the sine sweep and free decay profiles. The sine sweep timeline has only an active mode during which the frequency of the driving force is changed incrementally after steady state has been reached. Therefore, the complete closed-loop test during one orbit is 10 sequential periods of 64 seconds each for a mode near 1 Hz. Because the test period has been reduced by a factor of five from the open-loop case, the closed-loop test uses only 30 watt-hrs per orbit, with a 119% margin remaining. This margin is large enough to support operation of the test even at the current limited power maximum of 140 watts (although this is highly inadvisable). An alternate use of the margin is the increase of number of frequency increments to 40 per orbit, for a total active test period of 2560 seconds. This would leave a 10.5% energy margin. As stated earlier, the analysis for the 1 Hz open-loop test is the most conservative, as further increases in damping and/or frequency would reduce the test period per orbit.
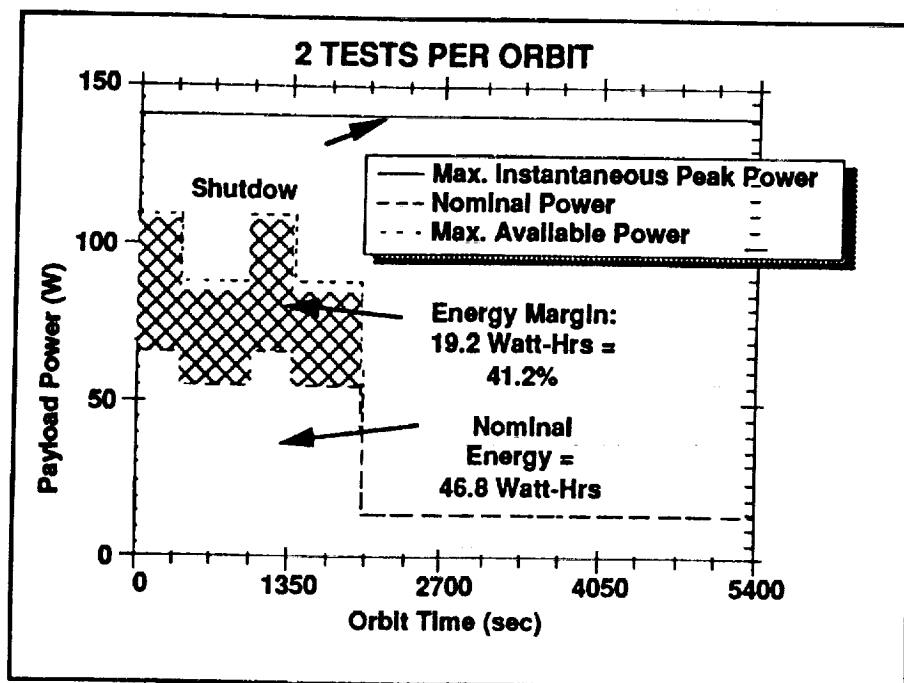

Figure 4-6. Burst Random Closed-loop Power Timeline ($\zeta = 1.0\%$)

Table 4-6. Closed-loop System Identification Power Requirements

Experiment	Damping Ratio (%)	Energy per Orbit (W-Hr)	Energy Margin (%)	No. Orbits Required
Burst Random (.001 Hz Res.)	1.0	32	41	15
"	5.0	32	41	15
1 Hz Sine Sweep (1 mode)	1.0	30	119	30
"	5.0	22	197	30
Free Decay	1.0	27	142	2
"	5.0	22	205	2

Because the response time of the system falls inversely to increased mode frequency, all the critical modes can be excited and measured in a free decay test within 256 seconds, assuming 1.0% damping. Two such tests consume 27 watts-hours per orbit, leaving a 142% margin. With such a large margin, all four required free decay tests can be performed in one orbit, with a 93% energy margin still remaining. In either case, all tests per orbit can be operated up to the current limited power maximum of 140 watts.

Table 4-6 summarizes the worst case power requirements for the closed-loop system identification methods along with energy margins and number of orbits required to complete the tests. It is apparent that from these figures that the energy requirements for the closed-loop tests are well within the resources of the QuickStar bus.

4.2.3.2 Data Storage.

The analysis for closed-loop data storage requirements is identical to that of the open-loop case. The principal difference is in the reduced sampling periods of the sine sweep and free decay tests. In the case of the sine sweep tests, however, there is no change in the already minimal storage requirements, because only one data point is collected per test. The storage requirement for the free decay tests is reduced by a factor corresponding to the increased damping in the modes. Therefore, an increase in damping from 0.2% to 1.0% reduces the original 1280 second test to 256 seconds. This translates into a total storage reduction from 308 Mbits to 61 Mbits (Table 4-7). As before, however, the storage requirements for burst random tests remain high. Again, the operation of the video camera and the storage of video data is not considered due to the extremely high bit rate involved and non-critical usage of the camera.

4.2.3.3 Computation.

When active control algorithms are implemented on the experiment payload, the energy and data storage requirements are not very critical. The primary resource in short supply becomes computation power. A first order analysis of the computation requirements for active control is now presented.

A generic controller architecture for a centralized multi-input/multi-output (MIMO) system is represented by the equations:

$$x_k = Ax_{k-1} + By_k$$
$$u_k = Cx_k + Dy_k \tag{4.3}$$

This requires approximately $2(n+m)^2$ floating point operations (FLOPs) per sample interval, where m is the number of states controlled, and n is the number of collocated sensor/actuator (S/A) pairs used. If the highest mode to be controlled has a resonant frequency f, then, assuming that the sample rate is 20 times greater than the highest mode frequency, the FLOP rate for a global controller is:

$$FLOPs = 40 f_{mode} (n+m)^2 \tag{4.4}$$

where f is the frequency of the highest controllable mode. This can also be used to approximate a local controller by isolating the number of S/A pairs and states directly affected by the controller. Figure 4-7 illustrates the quadratic nature of the controller throughput as a function of the number of S/A pairs (I/O channels) used.

Table 4-7. Closed-Loop ($\zeta = 1.0\%$) System Identification Data Storage Req's

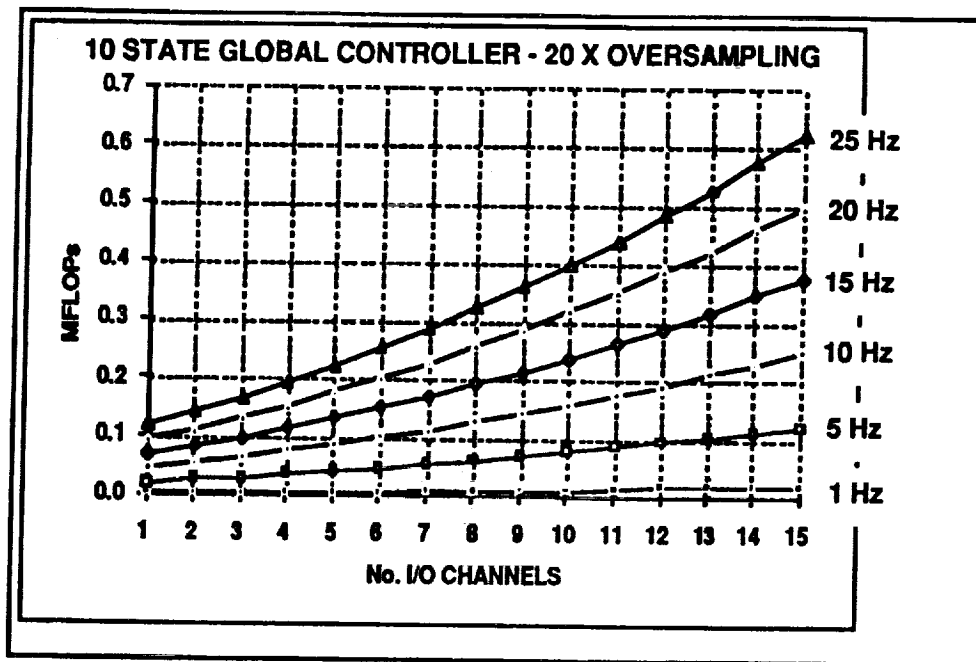| Experiment	Sample Period (sec)	Data Storage (Mbits/Orbit)	No. Orbits Required
Burst Random (.001 Hz Res.)	1000	360	15
1 Hz Sine Sweep (1 mode)	1	1	30
Free Decay	256	61	1

Figure 4-7. Computation Throughput Required to Operate a 10 State Controller with Each Curve Representing the Highest Mode Controlled

This analysis is based on two primary modeling assumptions. The first, commonly used in ground-based controllers, is that the controller gain rolls off rapidly at low and high frequencies. This is done to (1) eliminate the need to estimate the dynamics, or states, of modes beyond the observability of the controller, and (2) minimize the amplification of any instabilities within these unmodeled modes. The second assumption is that every actuator is colocated with at least one sensor. This is done to minimize the complexity of calculating I/O requirements from various sources. Also, for a baseline controller, 2 states must be observed and controlled for every mode controlled. The baseline global controller selected controls 10 states in 5 flexible body modes up to 15 Hz with 10 S/A pairs. Based on Eq. 4.4, this requires 0.24 MFLOPs to operate at a sampling rate of 300 Hz. A local gimbal controller, one which controls up to 8 rigid body states of the gimbals up to 50 Hz with 2 S/A pairs, requires 0.2 MFLOPs for operation at 1000 Hz. The total throughput for the baseline controller then is 0.44 MFLOPs.

The baseline throughput budget allowed by the QuickStar bus for experiment payload operations is 0.6 MFLOPs, and can accommodate more sophisticated estimators in the controller. Figure 4-8 illustrates a "performance envelope" between the number of S/A pairs used in a controller and the number of controllable states given a 0.6 MFLOP throughput capability. The curves define the maximum number of states controllable below the indicated frequency when operating n S/A pairs. The number of S/A pairs is extended to 16, the greatest number available using the CSI-Star experiment payload in its present configuration. This includes 12 piezo

actuators, two PMAs and two gimbals. There are excess sensors, such as accelerometers, for use in open-loop system identification. It can be seen that for modes up to 15 Hz, 16 states can be controlled when all S/A pairs are used. Normally, 16 S/A pairs are not used to control between 5 and 7 modes below 15 Hz at one time. However, to provide guest investigators flexibility in controller design, the experiment payload can support several combinations of fewer pairs and the three active struts of the isolation tripod.

4.3 DATA/COMMAND TRANSMISSION CAPABILITIES

Because there is only one ground station planned for communication with the CSI-Star spacecraft, data downlink and command uplink time may be somewhat limited, thereby restricting when and how often experiments can be performed. In order to understand these restrictions, an orbital analysis was performed to determine how often and for how long the spacecraft will be in contact with the single ground station.

4.3.1 Orbital Analysis

This orbital analysis is based on simple orbital geometry, assuming that the Earth is a perfect sphere and the orbit of the spacecraft is perfectly circular, with no variations in orbital velocity. In addition, it is assumed that the single ground station is located along the equator of the Earth. Although this may not be realistic, it provides for a conservative estimate of downlink time, because the rotation rate of the station is greatest at the equator. The only variables considered are orbital altitude and inclination.
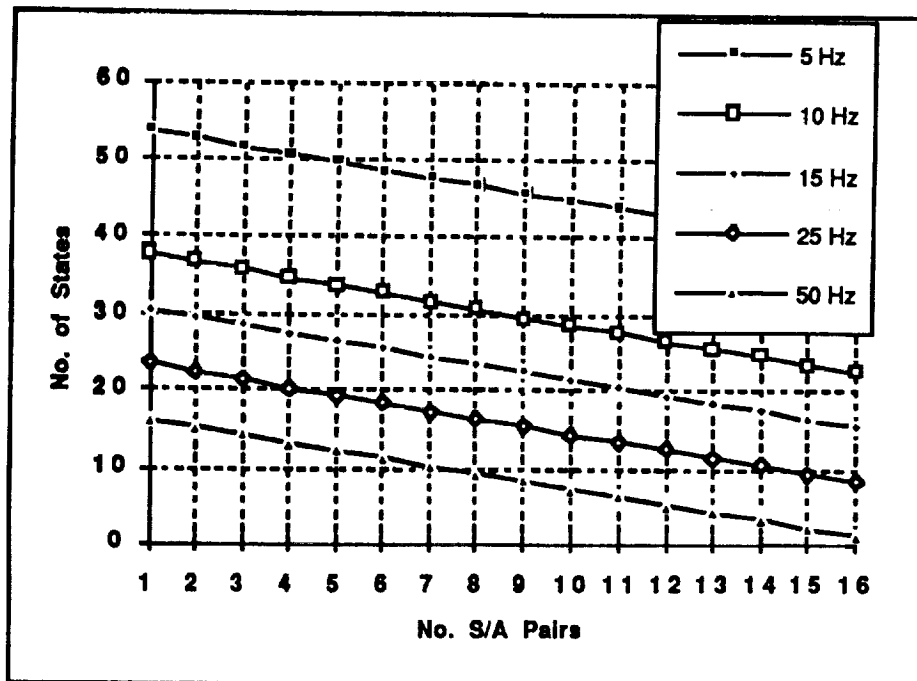

Figure 4-8. Controller States vs. S/A Pairs for 0.6 MFLOP Throughput

Assuming a circular orbit, a spacecraft utilizing an omni-directional antenna in orbit at an altitude h above the Earth's surface can "see" a circular cross-section of the Earth's surface defined by the half cone angle θ:

$$\theta = \cos^{-1}(\frac{R}{R+h}) \qquad (4.5)$$

where R is the Earth's radius. As the spacecraft circles the Earth, it maps out a flight swath in inertial space with width 2θ (Fig. 4-9). If a point on the Earth's surface enters the circle which the spacecraft can see midway across the circle's width, and assuming that the Earth's rotation rate is small compared to the orbital velocity ($\approx$ 1/17 orbital veloc.), the object will pass out of the spacecraft after the spacecraft has traveled 2θ radians, or the fraction (θ/π), of the total orbit. The orbital period is defined by:

$$P \approx \frac{5060}{\cos^{3/2}\theta} \qquad \text{(seconds)} \qquad (4.6)$$

The product of Eq. 4.6 and (θ/π) then defines the maximum downlink time in one fly-over of the ground station. Note that in this model, downlink time is a function of altitude only. To account for the fact that the spacecraft does not always fly directly over the ground station, thereby reducing the downlink time, an average downlink time was determined by calculating the average height of a semicircle, equal to π/4. Therefore, the average downlink time per fly-over is:

$$T_{DL} \approx \frac{1265\theta}{\cos^{3/2}\theta} \qquad \text{(seconds)} \qquad (4.7)$$

The number and frequency of fly-overs is now calculated. As shown in Figure 4-10, as the spacecraft orbits the Earth in an inertial plane at an inclination i with respect to the equator, the ground station at the equator rotates beneath. Twice per day, the ground station rotates beneath the flight swath of the spacecraft of width 2θ. The effective time which the ground station spends beneath the flight swath, however, is a function of the orbit inclination:

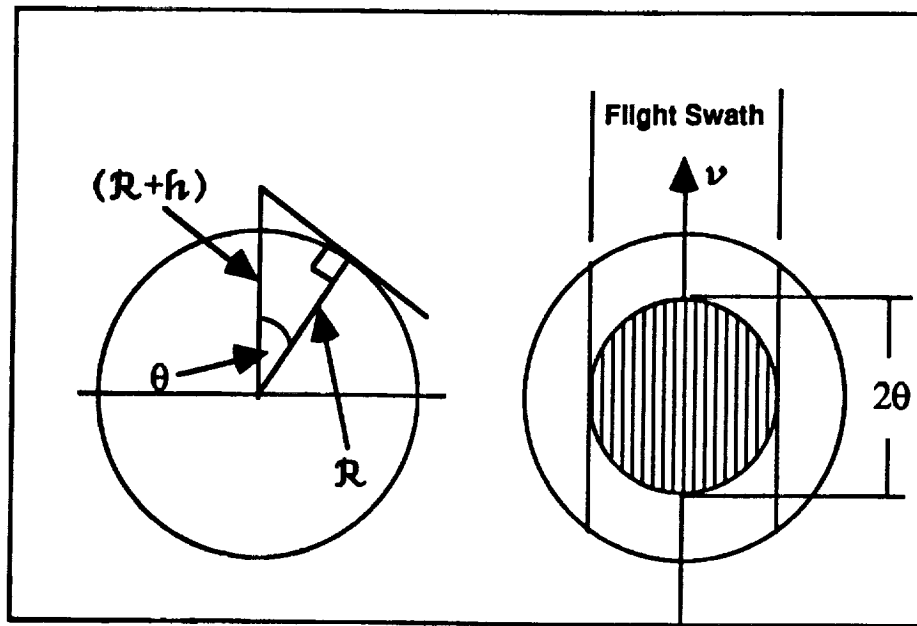$$T_{GS} = \frac{2\theta}{\sin i} \frac{1}{\omega_{earth}} \qquad (4.8)$$

Figure 4-9. Determination of Spacecraft Coverage Area

where ω_{earth} is the rotation rate of the Earth at its equator. The number of sequential orbits of the spacecraft during which the ground station is beneath the flight swath is just the quotient of Eq. 4.8 and Eq. 4.6. The total downlink time per day is estimated as the product of the total number of fly-over orbits and the average downlink time. Table 4-8 summarizes the analysis results. The shaded values in the final columns indicate most probable downlink times for CSI-Star depending on the orbital inclination.

4.3.2 Effects on Experiment Procedures

Higher orbits have longer viewing periods per fly-over, although the number of fly-over orbits per day flattens out beyond an altitude of 1200 km. Highly inclined orbits, such as sun-synchronous orbits, however, have fewer fly-over periods per day for a given altitude. These orbits follow paths nearly perpendicular to the Earth's rotation, and project a narrower flight swath with respect to the ground station. As shown in Table 4-8, the orbits of the two candidate primary missions provide significantly different transmission opportunities. The ACE mission, in a 28.5° near equatorial orbit, provides more fly-over orbits, 8 altogether, although each fly-over averages 10 minutes . The ATMOS mission has fly-over periods averaging 15 minutes, but sees the ground station only 4 times per day. In either case, however, the total daily transmission period is sufficiently long to allow a complete downlink of a one gigabit mass storage unit,

which requires 17 minutes. However, certain identification tests must be properly scheduled in order not to exceed the QuickStar storage capabilities before a fly-over occurs.
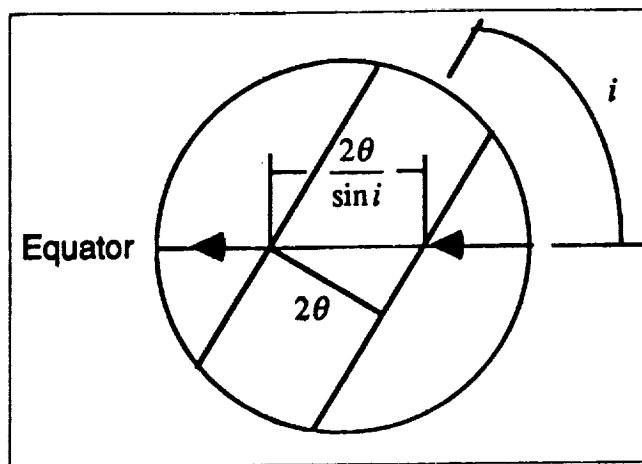

Figure 4-10. Determination of Ground Station Track Across Flight Swath

4.4 END OF LIFE DEORBIT

As with all current spacecraft, CSI-Star, once its operation life is completed, will become orbital debris, adding to the already growing problem of excessive space debris and uncontrolled reentry. In future, however, NASA may adopt a policy, either unilaterally or as part of a multi-national agreement, requiring controlled deorbit of all spacecraft to ensure safe reentry into international waters. If such a policy is adopted, and if analysis cannot ensure complete destruction of the CSI-Star spacecraft during reentry, a deorbit control system will be included. The weight of the propulsion components of this system is conservatively estimated at 5% to 8% of the spacecraft weight, approximately 10 lbs to 16 lbs. Assuming that an equivalent mass would be reduced from the payload capacity, the experiment mass total would be reduced to 54 lbs, thereby severely reducing the experiment capabilities.

Table 4-8. Calculated Orbital Parameters for Downlink Times

Orbital Altitude (km)	Field of View (rad)	Orbital Period (sec)	Max. Orbit Downlink Time (min)	Avg. Orbit Downlink Time (min)
0	0.00	5080	0.00	0.0
100	0.35	5200	4.85	3.8
200	0.49	5321	6.98	5.5
300	0.60	5443	8.69	6.8
500	0.77	5689	11.58	9.1
700	0.90	5939	14.13	11.1
800	0.95	6065	15.34	12.0
1000	1.05	6321	17.66	13.9
1200	1.14	6579	19.91	15.6
1500	1.25	6974	23.21	18.2

Orbital Altitude (km)	No. of Seq'ntial Orbits (i=98.5°)	No. of Seq'ntial Orbits (i=28.5°)	Average Daily Downlink Time (i=98.5°) (min)	Average Daily Downlink Time (i=28.5°) (min)
0	0	0	0.0	0.0
100	2	4	7.2	14.9
200	2	6	14.2	29.4
300	4	6	21.0	43.5
500	4	8	34.1	78.7
700	4	8	46.6	96.6
800	4	10	52.7	109.1
1000	4	10	64.3	133.3
1200	4	10	75.4	156.4
1500	6	10	91.2	189.1

5.0 COST, RISK, AND SCHEDULE ASSESSMENTS

5.1 COST ASSESSMENT

Preliminary cost estimates were developed for the Quickstar bus and the experiment payload independent of one another. The elements of each are described below, and total program costs are then presented.

5.1.1 Quickstar Bus

A rough order of magnitude (ROM) cost estimate for the Quickstar bus is provided as a lump sum by Ball Aerospace. This estimate is based LOSAT-X experience and on current Ball Aerospace man-hour labor rates, hardware costs (both subcontracted and fabricated), company overhead (burdened wrap rates), and current understanding of the CSI-Star mission and payload requirements. This estimate includes all design, development, testing and evaluation costs for the bus, including the modifications for accommodation of the experiment payload as described in Section 3.7, but does not include launch integration or operations costs. A lump sum estimate is also provided for the purchase, operation and maintenance of a single ground station.

5.1.2 Experiment Payload

5.1.2.1 Component Level Costs

The CSI-Star cost estimates were performed on both component and program levels. On the component level, cost estimates were generated for the hardware components of both the laser (option A) and sun sensor (option B) configurations. In most cases, vendor prices were available for development and recurring costs, and those which were not were priced using cost estimating relationships (CERs) and the GE PRICE cost model. Space qualification estimates were also generally available, but have been included as part of the programmatic costs. Table 5-1 lists each hardware item, and compares the two experiment configuration costs. Those components which do not have vendor estimates are:

Structure   MLI
Wire Harness   Miscellaneous
Component Electronics (Strut, Photo Sensor, Sun Sensor and PMA)
Disturbance payload

Table 5-1. Experiment Payload Component Cost Breakdown

Item	QTY	Develop. Cost ($K)	Recurring Unit Cost ($K)	Total Cost ($K)	Option A Cost ($K)	Option B Cost ($K)
1-axis gimbal	1	200	50	250	250	250
2-axis gimbal	1	400	100	500	500	500
accelerometers	20	0	1	20	20	20
active struts	12	200	3.33	240	240	240
camera w/75 mm lens	1	0	15	15	15	15
component electronics (A)*	1	415	50	465	465	N/A
component electronics (B)*	1	370	38	408	N/A	408
deployable mast	1	0	900	900	900	900
disturbance payload*	1	25	25	50	50	50
lasers	2	10	2	14	14	N/A
load cell	2	0	1	2	2	2
mast motor/cannister	1	0	100	100	100	100
misc.*	1	6.5	6.5	13	13	13
MLI*	1	2	5	7	7	7
photo sensors	10	40	1.2	52	52	N/A
PMA	2	100	10	120	120	120
strain/temp sensors	20	0	0.065	1.3	1.3	1.3
structure*	1	8	2	10	10	10
sun sensors	2	200	100	400	N/A	400
tripod, active laser	1	50	15	65	65	N/A
wire harness*	1	9	3	12	12	12
Payload H/W Total					2836.3	3048.3
* CER estimate						

The higher cost estimate for option B reflects the high cost for the sun sensor relative to the laser costs.

5.1.2.2 Program Level Cost Estimates

For the sake of comparison, two independent cost models were used to estimate the program level costs for the option A (laser) configuration. The first is a composite model used to derive high and low cost estimate boundaries based on the Space Station *Freedom* model and the Unmanned Spacecraft Cost Model (USCM) Version 5.

The second model is a Revised USCM model with standard deviation ranges for each variable in the model. Because the total payload hardware cost has been estimated, including

both development and recurring costs, the second model estimates the program cost using a theoretical first unit (TFU) model.

5.1.2.2.1 Model Definitions.

The program level model estimates are subdivided into eight groups: experiment payload hardware, experiment software development, experiment assembly and integration, experiment launch operations, experiment programmatic costs, ground station operations, spacecraft bus DDT&E, and launch vehicle integration. These are each defined in Table 5-2. The ground station and bus DDT&E costs are estimated directly from Ball's previous experience with the spacecraft. The remaining costs are estimated using either cost model.

The USCM part of the composite model is based on 30 different DoD satellites. This model calculates the payload cost, and the program level costs are considered a percentage of the payload costs. The non-recurring program level cost is calculated as (0.464 x payload cost) with

Table 5-2. Program Level Cost Model Definition of Terms

Experiment Hardware:	DDT&E and first unit cost
Software Development:	Conceptual and detailed designs, implementation, integration, and testing of preliminary system identification and controller algorithms
Experiment Assembly and Integration:	Hardware (including ground support equipment) and labor required for assembly and testing of payload subsystems and integration into spacecraft
Experiment Launch Operations:	Planning and operations to launch and perform on-orbit check-out
Experiment Programmatic:	Management, systems engineering, system testing and evaluation, reliability and quality assurance
Ground Station:	Leasing and labor costs associated with operation of ground station by contractor during mission
Spacecraft bus DDT&E:	Defined earlier
Launch Vehicle Integration:	Integration of entire spacecraft into LV

a validity range of $3.53M to $85.33M FY79. The recurring program level cost is calculated as (0.457 x payload first unit cost) with validity range of $.763M to $18.99M FY79. The Assembly and Integration cost is calculated as (0.06 x total payload cost). The launch operations and support costs are estimated at (0.19 x non-recurring payload cost). These estimates set a lower bound for the payload program costs.

The SSF part of the composite model is based on NASA programs, and includes both manned and unmanned systems. This model breaks down the costs into a greater number of categories than the USCM V5 model. These categories, their estimation relations, and ranges of validity are defined in Table 5-3. For easier comparison with the other models, these categories were grouped into the three primary areas of programmatic costs, launch operations and assembly and integration. The composite model is evaluated by calculating the mean value of each model term, and using the difference between the high and low estimates as a range of uncertainty.

The second model is a revised USCM model with deviation ranges assigned to each entry in the model. Because this model uses TFU estimates, only the recurring cost is evaluated. This model estimates costs for software development, spacecraft/launch vehicle integration, and spacecraft launch operations, whereas the composite model does not. The assembly & integration cost is calculated as (0.11 x total experiment payload cost), with a validity range of $23M to $285M and a standard deviation of $4.5M. The software development cost is calculated as ($345 x # lines of code in Ada), with no designated validity range and a standard deviation of (0.07 x software cost). Launch operations costs are calculated to be $2.96K per kilogram, with validity range of 200 kg to 1350 kg and a standard deviation of $371K. The programmatic cost is estimated at (0.33 x total hardware cost) with validity range of $2.5M to $94.5M and a

Table 5-3. Space Station Model Cost Estimation Relations

System Test & Evaluation (STE):	0.984 x Hardware $$^1.132
	Range = $4M to $30M FY78
Integration, Ass'y & Checkout (IA&C):	0.553 x STE^0.574
	Range = $6M to $80M FY78
Ground Support Equipment (GSE):	0.162 x (Dev $$ + IA&C + STE)^1.012
	Range = $20M to $200M FY78
System Engineering & Integ (SEI):	0.247 x (Dev $$ + IA&C + STE + GSE)^0.876
	Range = $40M to $5000M FY78
Program Management (PM):	0.380 x (Dev $$ + IA&C + STE + GSE + SEI)^0.731
	Range = $40M to $6000M FY78

standard deviation of $3.42M. The programmatic, launch vehicle integration and operations estimates were also applied to the spacecraft bus. The total program cost is the sum of the individual costs, and the total uncertainty is the root sum of the squares of the individual uncertainties. It should be noted that in both models, the values for the CSI-Star spacecraft fall considerably below the validity range of some of the cost estimates, making the estimates even more uncertain. We believe, however, that the estimates are conservative because the QuickStar bus and launch costs are based on actual costs from the LOSAT-X program. If the program approach used on the LOSAT-X project, i.e., a fast-trach, low-cost approach, is used for CSI-Star, we believe that the above estimates are reasonable.

5.1.3 CSI-Star Program Estimate Comparison.

Table 5-4 lists the results of both models for option A (laser) and the results of the Revised USCM model for option B (sun sensor). In the cases where the composite model did not provide estimates for some items, such as software development, the estimates of the Revised USCM model were substituted for an even comparison.

Table 5-4 CSI-Star Program Level Cost Estimates

| Item	OPTION A		OPTION B
	COMPOSITE (FY92 $K)	Revised USCM (FY92 $K)	Revised USCM (FY92 $K)
Experiment Payload Hardware	2836.0	2836.0	3048.0
Software Development	1035*	1035.0	1035.0
Assembly & Integration	1095.5	312.0	335.3
Launch Operations	435.5	90.6	86.8
Programmatic Cost	2942 §	936 §	1006 §
Ground Station Cost	1750**	1750**	1750**
S/C Bus RDT&E	10000**	10000**	10000**
Orbital Operations	203.3*	203.3	203.3
LV Integration	1100*	1100	1100
Contractual Fee (10%)	2139.7	1826.3	1856.5
Mean Program Cost	23537.0	20089.5	20421.1
Cost Uncertainty	2497.5	5759.4	5761.6
Max Program Cost	26034.5	25848.9	26182.7
* Not originally in model			
** Ball Aerospace Estimate			
§ Includes space qualification costs			

For option A, the mean program costs between the two models differ by $3.5M, due primarily to the larger programmatic cost in the composite model. However, the cost uncertainty in the revised USCM model is larger by $3.3M, bringing the two maximum program costs to within $200K at approximately $26M. Option B shows a somewhat higher maximum program cost, reflecting the $300K difference in experiment hardware costs. The cost uncertainty, however, is nearly identical to that of the Revised USCM model for option A. In each model, the total program cost contributed by the Quickstar bus is $14.35M, or 61% to 72% total cost. It should be noted that a total program cost estimate based on previous NASA experience yielded a significantly higher cost of about $40M.

5.2 RISK ASSESSMENT

5.2.1 Definitions & Assumptions

Item Reliability: The probability that a single piece of hardware will operate nominally during the hardware's lifetime. This value, ranging between 0 and 1, is usually determined as an exponential function of the measured failure rate of many identical pieces of hardware, λ, which is the inverse of the Mean Time Between Failures (MTBF). However, in the case of the payload hardware, no MTBF values are currently available. Therefore, manufacturer estimates were used where available. The remaining estimates were generated by MDA from literature searches and engineering judgment.

Net Reliability: The probability that several pieces of hardware, configured into a unit, will operate nominally during the mission lifetime. This is very dependent on the configuration of the hardware within the unit. A unit of components in series, such as the subsystems of the Quickstar bus, has a net reliability equal to the product of the component reliabilities. This occurs because the failure of one component is equivalent to the failure of all.
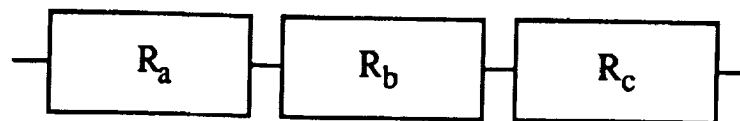

$$R_{net} = \prod_i R_i \tag{5.1}$$

Figure 5-1. Net Reliability of Components in Series

In series configuration, the net reliability is always lower than that of a single component. Components in parallel, however, provide much better net reliability. As shown in Figure 5-2, n

parallel components provide n independent paths through which an operation can be performed. Therefore, the net reliability is one (1) minus the product of the component failure probabilities.
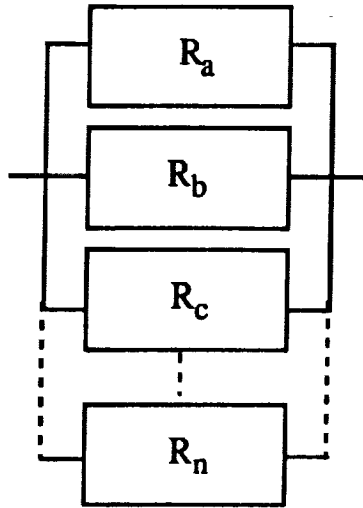
$$R_{net} = 1 - (1 - R_a)(1 - R_b)(1 - R_c)...(1 - R_n) \qquad (5.2)$$

Figure 5-2. Net Reliability of Components in Parallel

Effectiveness: The probability that mission objectives can be met after a single component failure. This is a rough measure of what can be accomplished in an experiment after a component fails. Effectiveness is quantified by an effectiveness factor (W), ranging from 0 to 1, which quantifies the impact of a single component failure on the remaining components. An effectiveness factor of zero (W=0) means that the component failure has no impact on the function of the system, whereas W = 1 is equivalent to a single point failure. For example, if three components operate independently, yet all are required for the total completion of an experiment, they are modeled as if they are in series. However, if one component fails, the other two can still operate, albeit less successfully. Therefore, an effectiveness factor W of 1/3, or 0.333, is assigned to this unit. The effectiveness of the unit is:

$$E_{net} = 1 - (1 - R_i^3)W \qquad (5.3)$$

where the term in parentheses is the failure probability of the three components in series. Therefore, the effectiveness of the three components is higher than the strict series reliability.

5.2.2 Quickstar Bus Reliability Assessment

The CSI-Star mission lifetime goal has been given as at least 1 year. Associated probabilities were not defined. Options for selected redundancy were analyzed considering mass, power, and

cost impacts. The baseline CSI QuickStar is a single string system. Incorporating MIL-STD 975 Grade 2 parts and/or screening to selected portions of MIL-STD 883 Class B allows a system reliability at the end of 1 year of 0.9056 (Table 5-6). No mission limiting aspects of the QuickStar design prohibit a longer mission lifetime.

5.2.3 Experiment Payload Reliability Assessment

The risk and reliability assessment of the experiment payload is more complex than that of the Quickstar bus, because the hardware components of the payload do not necessarily operate in series as do most in the spacecraft bus. There exist several identical components of some types of hardware such as accelerometers within the experiment payload, some of which can perform identical tasks, thereby acting in parallel. Also, several pieces of independently acting hardware are utilized during an experiment, where the failure of one piece does not necessarily prevent the completion of the experiment. In such a case, an effective reliability must be determined to measure the relative success of the mission after a partial failure. These issues in estimating the component and subsystem reliabilities of the experimental payload are now discussed.

The experiment payload is now divided into major subsystems, each of which consists of one or more components. The subsystem architecture for each is described, after which the net reliability and effectiveness of each are tabulated.

5.2.3.1 *Experiment Subsystem Reliability Architectures*.

The experiment subsystem groups to be addressed are:

accelerometers, strain and temperature gages	active struts and electronics
deployable mast and mast motor	gimbal drives, electronics, sun sensors or lasers
instrument heating	PMAs, electronics and load cells
video camera and electronics	

accelerometers: there are 20 accelerometers and/or 20 strain gages and 6 temperature gages within the experiment payload. The temperature gages are passive, and are assumed to have a reliability of 1.000. Because 5 modes of the boom structure are being actively controlled, it is assumed that at least 5 accelerometers and strain gages, evenly distributed, are required for sufficient observability. Assuming that all sensors are evenly distributed, they can be divided into 4 parallel strings of 5 accelerometers and 5 strain gages. In addition, within each string, an effectiveness factor of 0.2 is used to simulate the loss of one out of five required sensors.
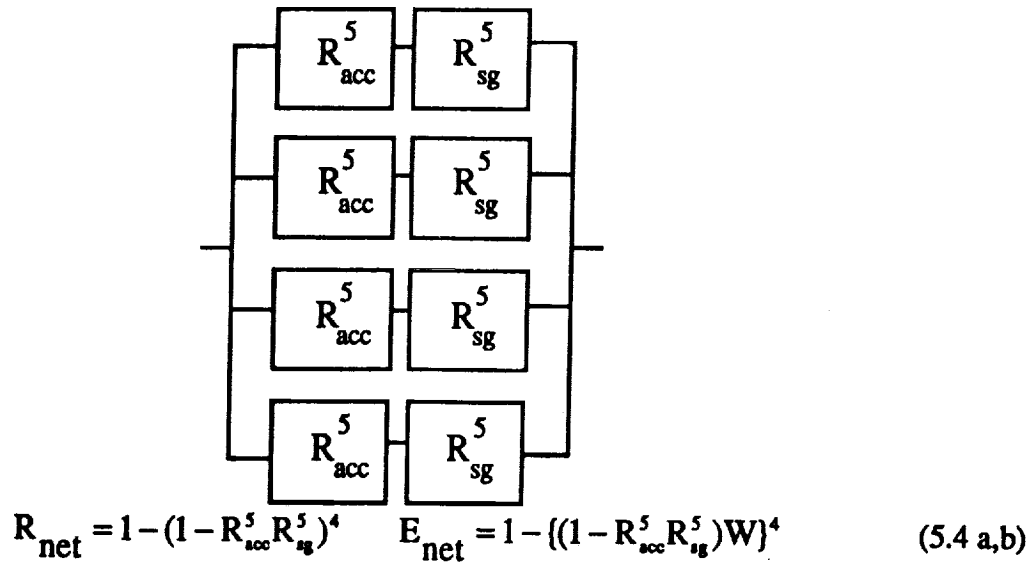
$$R_{net} = 1 - (1 - R_{acc}^5 R_{sg}^5)^4 \qquad E_{net} = 1 - \{(1 - R_{acc}^5 R_{sg}^5)W\}^4 \qquad (5.4\ a,b)$$

Figure 5-3. Subsystem Architecture for Accelerometers and Strain Gages

active struts: there are a total of 12 active struts in the mast structure of the payload. They are located in 3 bays of the mast: bays 15 and 16, and bay 24. Each bay has 4 active struts, acting as the 4 longerons within the bay. It is assumed that the struts in one bay can perform the same task as those of either of the other two bays; i.e., the 3 bays operate in parallel. All 4 struts must be operating for maximum performance, however. Also, the strut electronics, including the amplifier to drive the struts, are considered a component common to each bay of four struts. Therefore, the active strut subsystem is configured as 3 parallel strings of 4 struts in series with an electronics package. Each string has an effectiveness factor of 0.25.
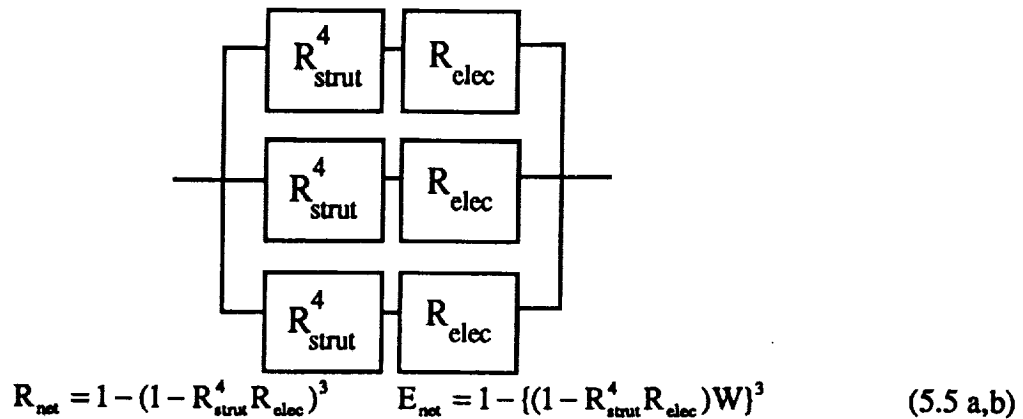

$$R_{net} = 1 - (1 - R_{strut}^4 R_{elec})^3 \qquad E_{net} = 1 - \{(1 - R_{strut}^4 R_{elec})W\}^3 \qquad (5.5\ a,b)$$

Figure 5-4. Subsystem Architecture for Active Struts and Related Electronics

deployable mast: the deployable mast assembly is a single string structure, with no redundancies. The single stepper motor deploys the 20 foot mast from its aluminum canister at

two inches per second. Probably the most critical pieces of experiment hardware, both the deployment motor and mast locking mechanisms are extremely reliable, according to the manufacturer. These same masts are developed to be used for deployment of Space Station's solar arrays. The mast and deployment motor are modeled in series.

$$R_{net} = E_{net} = R_{mast}R_{motor} \quad (W = 1) \tag{5.6}$$

gimbal motor/sun sensor/laser: The are two gimbaled payload assemblies on the mast structure, both located at the free end of the mast. Although one gimbal operates in one axis, while the other operates along two axes, both assemblies were assumed to perform the same tasks, and so are modeled as operating in parallel. The components of each assembly, the gimbal motor, gimbal electronics, and the sun sensor or laser, are modeled in series. If either motor or associated electronics fails, the assembly is inoperable. However, if the sensor or laser fails, the assembly can still be used as a disturbance source. Therefore, an effectiveness factor of 0.5 is assumed for the gimbals.
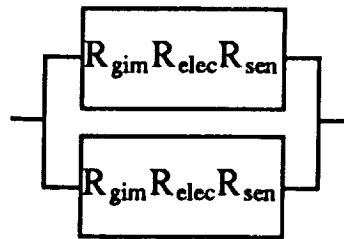
$$R_{net} = 1 - (1 - R_{gim}R_{elec}R_{sen})^2 \qquad E_{net} = 1 - \{(1 - R_{gim}R_{elec}R_{sen})W\}^2 \tag{5.7 a,b}$$

Figure 5-5. Subsystem Architecture for Gimbal Assemblies

instrument heating: The instrument heating units, although currently undefined, are assumed to be simple resistive heating coils. Modeled as simple wires, these units are assumed to have unity reliability.

PMAs, electronics and load cells: There are two proof-mass actuator / load cell assemblies on the mast structure. Within each assembly, the components are modeled in series, each with an effectiveness factor of one (1). Although the axes of motion of the two assemblies are aligned perpendicular to one another, and therefore cannot produce exactly the same disturbance, the assemblies are modeled as parallel units. This is then equivalent to the architecture seen in Figure 5-5 and Equations 5.7 (a,b).

C-2

video camera and electronics: The video camera, while important in observing the deployment of the mast and other experiment operations, is not critical to the success of the mission. Therefore, the camera and its electronics are modeled as a single string series unit with an effectiveness factor of 0.1.
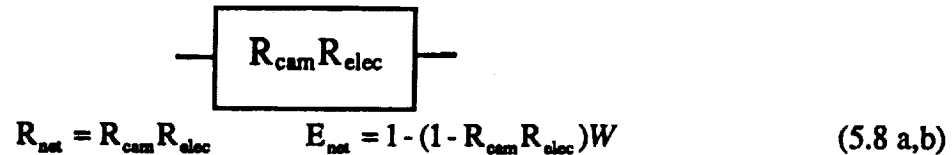
$$R_{net} = R_{cam}R_{elec} \qquad E_{net} = 1 - (1 - R_{cam}R_{elec})W \qquad (5.8 \text{ a,b})$$

Figure 5-6. Subsystem Architecture for Video Camera

5.2.3.2 Calculated Experiment Subsystem Reliabilities

Table 5-5 illustrates the reliabilities of each experiment payload subsystem based on estimated component reliabilities and the subsystem architectures defined in the previous section. The majority of the item reliability estimates were received directly from the manufacturers; those estimates that were not (labeled "MDSSC") were derived from previous experiences with similar hardware.

From Table 5-5, it is apparent that the least reliable subsystem of the experiment payload is the video camera, with a net reliability of 0.9627. As stated earlier, the camera is not critical to the operation of the spacecraft or experiment, and realistically should not be factored into the reliability calculation, which would raised the experiment payload total reliability to 0.9825. However, as a conservative estimate, the camera reliability is considered. The remaining payload subsystems have relatively high reliability estimates, either through parallel architecture or robust design and testing. The only questionable reliability estimates are those of the active struts and associated electronics. Little MTBF data has been collected for piezoelectric active struts, and piezo reliability is a strong function of the operating voltage. High voltage piezo struts (≥ 1000 V) have shown poor reliability near 0.50, due primarily to arcing. Low-voltage piezo struts required for CSI-Star will operate at the 28 V Bus voltage, and have a much lower chance of failure due to arcing.

The total payload effectiveness is very high at 0.9946, indicating that the large number of fairly independent components in the payload lessens the importance of a single component. Most probably, the experiment objectives of CSI-Star can be met even with the failure of a sensor or actuator.

The weakest link in the mission reliability for CSI-Star is the Quickstar bus itself. In its baseline configuration, the spacecraft bus operates its subsystems in a single string architecture, and is therefore very susceptible to single point failure. The total baseline CSI-Star mission

reliability is now evaluated along with several redundancy upgrade options within the Quickstar bus. For each option, the impacts on cost, power and spacecraft mass are evaluated.

Table 5-5. Experiment Payload Subsystem Reliability Estimates

Item	Item Reliab.	Redundancy	Net Reliab.	Effectiveness Factor (W)	Net Effectiveness	Estimate Source
accelerometer (20)	0.9500	5 in series	0.7738			MDSSC
strain gages (20)	0.9990	5 in series	0.9950			MDSSC
temperature gages	1.0000	none	1.0000			MDSSC
Sensors Total		4 parallel strings	0.9972	0.2000	1.0000	
active struts (12)	0.9500	4 in series	0.8145			Polytec
strut electronics	0.9500	none	0.9500			Polytec
Strut Total		3 parallel strings	0.9884	0.2500	0.9998	
mast	1.0000	none	1.0000			Able
mast drive motor	0.9990	none	0.9990			Able
Mast Total			0.9990	1.0000	0.9990	
gimbal drive motor (2)	0.9800	none	0.9800			Ball
gimbal drive electronics	0.9950	none	0.9950			Ball
sun sensor (2)	0.9900	none	0.9900			Adcole
Gimbal Ass'y Total		2 parallel strings	0.9988	0.5000	0.9997	
instrument heating	1.0000	none	1.0000			MDSSC
Heating Total			1.0000	1.0000	1.0000	
load cell (2)	0.9900	none	0.9900			MDSSC
PMA (2)	0.9900	none	0.9900			SatCon
PMA electronics	0.9900	none	0.9900			SatCon
PMA Total		2 parallel strings	0.9991	0.5000	0.9998	
video camera	0.9675	none	0.9675			Xybion
video electronics	0.9950	none	0.9950			Xybion
Camera Total			0.9627	0.1000	0.9963	
Payload Total			0.9459		0.9946	

5.2.4 CSI-Star Reliability and Quickstar Redundancy Upgrade Options

5.2.4.1 CSI-Star Baseline Reliability

As shown in Figure 5-7, the subsystems of the Quickstar bus are modeled as operating in series with those of the experiment payload. Therefore, the CSI-Star mission reliability is the product of the bus and payload reliabilities, equal to 0.8567. Because the bus operates in series, its effectiveness is equal to its reliability, 0.9056, for a CSI-Star system effectiveness of 0.9007. These reliabilities are summarized in Table 5-6. As discussed earlier, the bus subsystems with the lowest reliabilities are the spacecraft control and data storage units. Several options to improve the overall system reliability exist in the increase of redundancy within these two units.

5.2.4.2 Quickstar Reliability Upgrade Options.

Six upgrade options were considered for the avionics subsystem. Table 5-7 lists the six options. Option 1 involves the standby internal redundancy of both spacecraft control and mass storage units. This is done by removing four of eight mass memory ROM cards and replacing them with redundant s/c control and mass storage CPUs. Although the removal of the ROM cards normally would reduce the mass storage by 50%, recently introduced ROM cards have storage capacities roughly 400% greater than their predecessors, thereby doubling the original mass storage capacity to two gigabits. During nominal operation, the secondary s/c control and
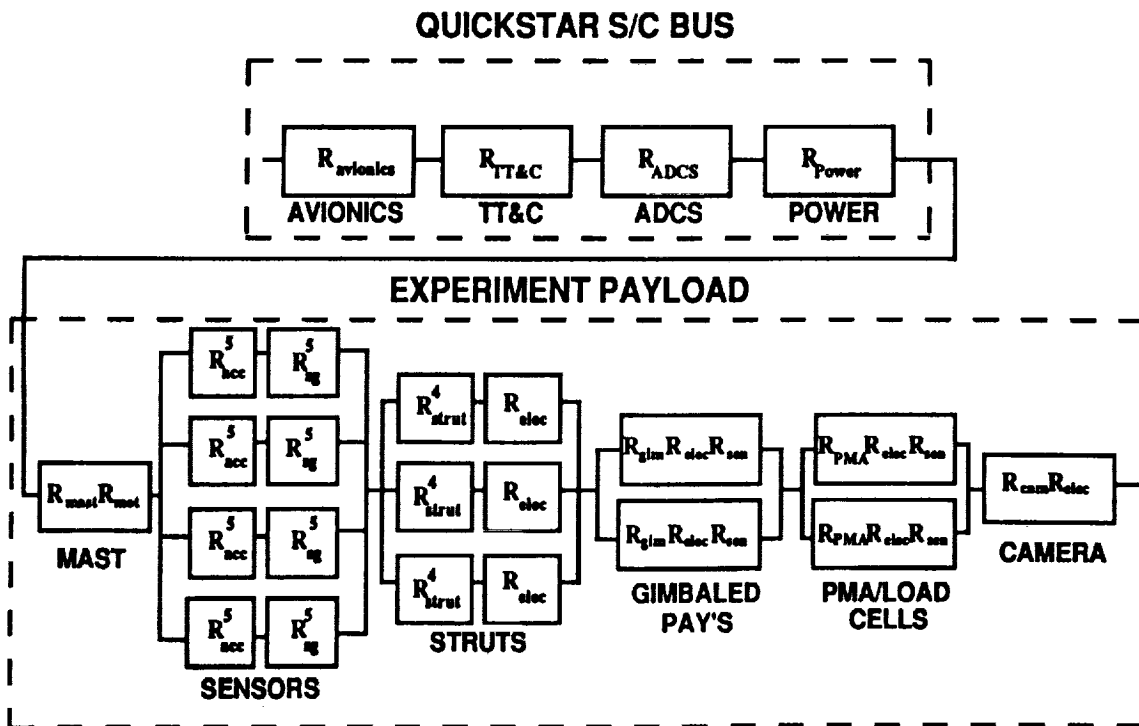

Figure 5-7. CSI-Star Subsystem Reliability Schematic

mass storage units are not powered, and their computational capabilities of 0.2 and 0.4 MFLOPs, respectively, cannot be accessed unless their primary counterparts fail. In addition, a single power supply powers both primary and secondary units.

Table 5-6 . CSI-Star Reliability Summary

	Subsystem	Subsystem Reliability	Redundancy	Effectiveness*
Quickstar Bus	Avionics	0.9662	none	0.9662
	Data Storage	0.9727	none	0.9727
	TT&C	0.9822	none	0.9822
	ADCS	0.9856	none	0.9856
	Power	0.9955	11 of 12 batt's	0.9955
	S/C Bus	0.9056		0.9056
Experiment Payload	Sensors	0.9972	4 strings of 5	1.0000
	Active Struts	0.9884	3 strings of 4	0.9998
	Deployable Mast	0.9990	none	0.9990
	Gimbaled Units	0.9988	2 in parallel	0.9997
	Instrument Heating	1.0000	none	1.0000
	Proof Mass Actuators	0.9991	2 in parallel	0.9998
	Video Camera	0.9627	none	0.9963
	Payload	0.9459		0.9946
CSI Star 1 Year Mission	Total	0.8567		0.9007

Table 5-7. Quickstar Bus Redundancy Upgrade Options

#	Description
1.	Standby internal redundancy in both spacecraft and mass storage control units
2.	Active internal redundancy in both spacecraft and mass storage control units
3.	Mass storage control remains actively redundant, secondary spacecraft control unit is dedicated to payload operations, only. Secondary s/c unit can be re-programmed via command uplink.
4.	Same as 3, except no option to re-program secondary s/c control CPU.
5.	Standby internal redundancy in both spacecraft and mass storage control units, additional externally redundant control unit dedicated to payload operations, only.
6.	Externally redundant CDU and transponder, actively redundant PDU.

Option 2 allows for the active operation of the secondary units along with the primary units, essentially placing the processors in parallel operation. Option 3 keeps both secondary units active, but converts the second s/c unit to a dedicated payload processor with the option to re-program the secondary unit via command uplink in the event of primary failure. Option 4 is identical to option 3, except that there is no option for re-programming. Option 5 is the same as option 1, with the addition of a new external processor identical to the s/c control unit, but is dedicated to payload operations. Option 6 is a secondary upgrade option, adding an externally redundant communication distribution unit (CDU) and transponder, and an actively redundant power distribution unit (PDU). Table 5-8 compares the impacts of each upgrade option.

Table 5-8. Impacts of Quickstar Bus Redundancy Upgrade Options

UPGRADE	CSI-Star RELIABILITY	CSI-Star EFFECTIVENESS	IMPACT		
			MASS (LB)	POWER (W)	COST ($K)
None	0.8566	0.9007	None	None	None
#1	0.9049	0.9514	None	None	None
#2	0.9046	0.9511	None	<1	None
#3	0.8779	0.9231	None	<1	None
#4	0.8505	0.8942	None	<1	None
#5	0.9012	0.9481	14	20	600
#6	(+)2.22%	(+)2.22%	18.7	3.1	720
UPGRADE	COMPUTATION (MFLOPS)	STORAGE (GBITS)	LOSS OF S/C CONTROL SDP	LOSS OF MASS STORAGE SDP	ORDER OF RECOMM.
None	0.6	1	Loss of S/C	Loss of S/C	N/A
#1	0.6	2	None	None	1
#2	1.2	2	(-)0.2 MFLOPs	(-) 0.4 MFLOPs	1
#3	1.4	2	(-)0.4 MFLOPs*	(-) 0.4 MFLOPs	3
#4	1.4	2	Loss of S/C	(-) 0.4 MFLOPs	4
#5	1	2	None	None	5
#6	no change	no change	no change	no change	6

5.2.4.3 Quickstar Reliability Upgrade Impacts.

From Table 5-8, it is apparent that option 1 provides the greatest improvement in system reliability and overall effectiveness with no impact to any operating parameters aside from an increase in mass storage. Option 2 offers a slightly smaller improvement in reliability, but offers twice the baseline computing capability at 1.2 MFLOPs. The active secondary CPUs incur an insignificant power penalty with no mass impact, because the secondary CPU cards are identical in mass to the original ROM cards. The only significant operational impact is in the loss of either s/c control or mass storage standard dedicated processor (SDP) within the control units. Failure of either SDP in the primary control units would cause the entire unit to shut down, and

- 94 -

its computing capability would be lost. This would reduce the versatility of CSI-Star in running higher order controllers, but would not endanger the operation of the spacecraft.

Option 3 and 4 offer the advantage of increased computing capability, but do not improve the system reliability significantly, and even reduce it in the case of option 4. The increased capability comes from the secondary s/c control unit which now dedicates its 0.4 MFLOPs to payload functions only. There is no power or mass impact, but because there is only one processor capable of performing s/c control functions, there is no longer internal redundancy. In option 3, if the primary spacecraft SDP fails, the spacecraft can be placed into a "safe" mode in which it turns its solar arrays toward the Sun, and waits for further instructions. At this point, the secondary SDP previously dedicated to payload operations can be re-programmed via ground uplink of the control software. Because this software is very extensive, the task of re-programming is difficult, and the software is too large to be stored on-board. If the re-programming is successful, the spacecraft can continue to operate, but the computation capability has been reduced by 0.4 MFLOPs. This option provides for "internal" redundancy for the SDP only, however. If the standard dedicated I/O card (STDIO) of the primary s/c control unit fails, the STDIO of the payload control unit cannot be re-programmed, resulting in a single-point failure.

In option 4, the payload control unit SDP cannot be re-programmed, either because the task of software development is too great, or for other reasons, and the spacecraft control unit is single string. If this unit fails, the mission fails. In both options, the loss of a mass storage unit would reduce the computation capability by 0.4 MFLOPs.

Option 5 introduces a new piece of hardware to the spacecraft, incurring significant mass, power and cost penalties without giving the best reliability nor the most computing power. The externally redundant control unit is identical to the s/c control unit, with its own standby internal redundancy, but is dedicated to payload processes only. It therefore operates in series with the other QuickStar subsystems, lowering the overall reliability gained though option 1. In addition, the mass penalty of 14 pounds exceeds the mass limits of the launch vehicle clampband, requiring an extensive and costly spacecraft and launch vehicle ACS redesign.

Option 6 improves reliability by introducing redundancy into the communication subsystem. This additional redundancy can be combined with any of the previous options, and increases the existing reliability by 2.22%. As in option 5, however, the significant mass impact would incur a large cost in redesign.

5.3 SCHEDULE

Two Delta II launches in 1997 have been baselined for the launch of CSI-Star as a secondary payload. The first mission, ACE, is scheduled for launch in mid-1997 into a highly elliptical

28.7 degree orbit. The second mission, ATMOS, is scheduled for an late 1997 launch into a 792 km sun synchronous polar orbit. The CSI-Star program schedule is built around the flight-proven 24 month development schedule of the Ball QuickStar bus, shown in Figure 5-8. The entire program schedule, shown in Figure 5-9, predicts a July 1997 launch, although minor changes in scheduling would accommodate the October launch.
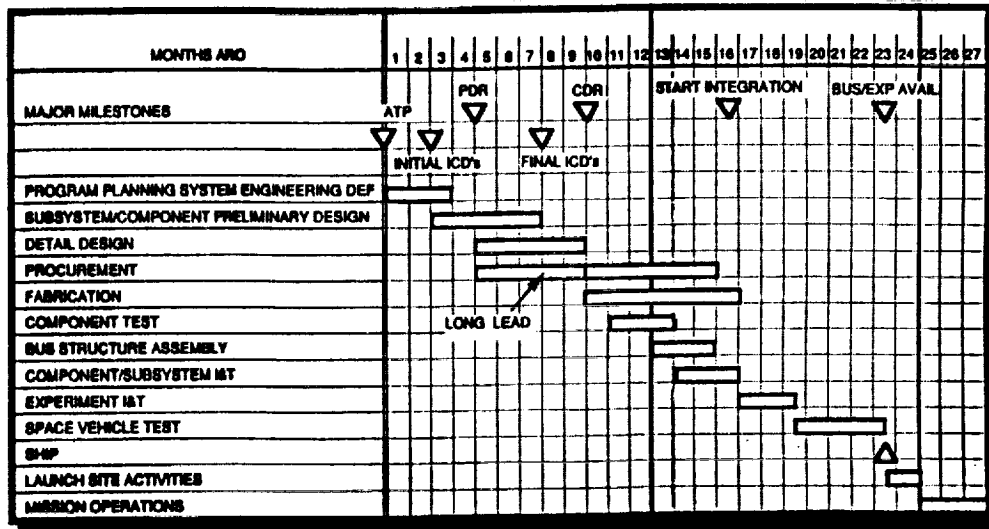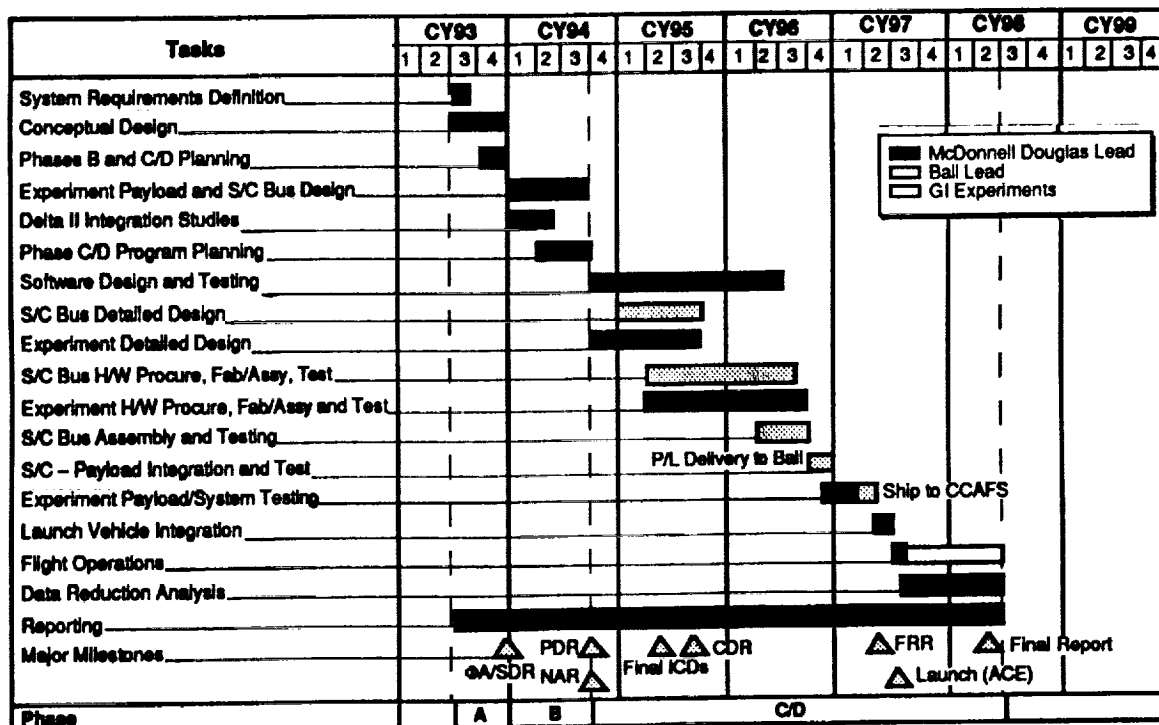

·Figure 5-8. QuickStar Satellite System Program Schedule

Figure 5-9. CSI-Star Program Schedule (July 1997 Launch)

5.3.1 Phase A : 6 months

Experiment and system requirements will be defined and a conceptual design will be developed based on the feasibility study. Beginning in third quarter CY93, the CSI-Star mission objectives, design drivers and ground rules will be established. Experiment design options will be further explored, conceptual designs will be generated, and operations timelines, risk and cost estimates will be better quantified. System requirements and the resulting conceptual designs will be presented in a System Design Review (SDR) and report.

5.3.2 Phase B : 9 months

The preliminary design of the experimental payload will commence first quarter CY94, and will be performed by the prime contractor. During this 9 month period, trades will be conducted on initial selections of commercially built hardware. Experimental payload performance requirements will be elaborated based on control and system identification experiment objectives. Concurrently, control software requirements will be defined to meet experiment performance objectives while providing flexibility in operation. Mass and power budgets will be better defined, initial interface control documents (ICDs) will be generated, and preliminary designs for non-commercial hardware will be created. Further Delta II integration studies will be conducted.

The preliminary design of the Quickstar bus will also begin in the first quarter CY94. Based on existing designs, the bus design will be altered to conform to the launch vehicle mass and space constraints as well as accommodate the revised payload requirements laid down by the ICDs. These alterations will be kept to a minimum to lessen the cost impact on the bus development. In addition, operational requirements for the Quickstar bus will be better defined through the examination of the candidate orbital environments. This will partially drive the selection of a primary launch date.

The results of Phase B will be presented in the Preliminary Design Review (PDR) at the end of third quarter CY94.

5.3.3 Phases C/D : 33-45 months

The detailed designs of both the experimental payload and Quickstar bus will begin in the fourth quarter CY94. Commercial hardware selections will be finalized and integrated into the ICDs. Designs for custom-made hardware, such as the active struts and reaction mass actuators, will be completed. ICDs between the payload and bus will be finalized. Software design and testing will continue through Phase C. Selection of launch date will be made, and coordination with the primary payload customer will begin. Experiment and operational timelines will be completed, and manufacturing drawings will be made for all custom-made components. Also,

initial control software designs will be developed and evaluated. The results of the detailed design will be presented at the Critical Design Review (CDR) at the end of third quarter of CY95.

Procurement of bus and payload hardware will begin in the second quarter of CY95, followed by initial fabrication, assembly and testing of hardware. The custom-made components of the experimental payload will be contracted out for fabrication, and then tested on a component level before assembly with the commercial hardware. The experimental payload will be tested as a system at several stages of assembly before integration into the Quickstar bus. The selected control software design will be programmed into the bus processors, and tested before integration with the experiment payload.

Payload-bus integration will begin by the fourth quarter CY96 with the delivery of the experimental payload to bus manufacturer. During the next seven months, assembly of the experiment will be completed, payload-bus interfaces will be examined, and system level operations and procedures will be tested. In June 1997, CSI-Star will be shipped to CCAFS for integration with the entire launch vehicle. Integration will begin with the Delta II second stage skirt and support truss. During the six week integration period, the spacecraft and payload will be tested to verify operation of all system level functions. During integration, a Flight Readiness Review (FRR) will be held to address final operational issues. After integration, CSI-Star will be launched as a secondary payload on the Delta II-ACE mission in July 1997.

Post-launch CSI-Star power-up and system check-.out will be conducted by the contractor. Once the Quickstar bus is operating nominally, the contractor will conduct the baseline series of control experiments to generate dynamic models of the spacecraft on orbit, as well as verify the correct operation of all experimental hardware. Once the initial data has been collected and analyzed, the control of CSI-Star will be turned over to NASA LaRC for Guest Investigator operation during the following year. The contractor will remain active in the program as technical consultants.

6.0 CONCLUSIONS AND RECOMMENDATIONS

The primary objective of this Pre-Phase A study was to define a free-flying concept that satisifies many of the CSI technology validation objectives at the lowest cost. This has been done by using the Ball QuickStar spacecraft bus. It was determined that QuickStar's flight-tested capabilities offered the best potential for a CSI orbital lab that had cost and risk minimized. A CSI experiment package was defined that will integrate into the QuickStar bus to provide a CSI orbital laboratory for the entire CSI community, which includes NASA, DoD, academia, and industry. This is the CSI-Star concept. The total cost through launch in 1997 and on-orbit checkout was estimated to be in the range of $20M to $26M. The CSI-Star one year reliability was estimated to be in the range of 0.90 to 0.95.

CSI-Star is a technology demonstration and validation program, not a technology development program. The current state-of-the-art for this technology is such that it is ready to be and must be tested on orbit if it is to be useful to and used on future programs. CSI-Star fills the gap between Shuttle middeck and other secondary non-free-flying experiments and the future NASA science missions such as Mission-to-Planet-Earth. The CSI-Star concept is worthwhile and feasible within the current fiscal environment.

It is recommended that a Phase A/B program proceed to further define and develop the concept into a realistic design that has the greatest chance to fly in the near future. During Phase A, potential guest investigator (GI) inputs are required. This could be implemented through a single representative GI or through a GI technical advisory panel. This would ensure that resulting CSI-Star design would meet, to the greatest extent possible within all other constraints, the CSI GI community's engineering science requirements.

REPORT DOCUMENTATION PAGE

1. AGENCY USE ONLY (Leave blank)	2. REPORT DATE August 1993	3. REPORT TYPE AND DATES COVERED Contractor Report

4. TITLE AND SUBTITLE

Feasibility Study of An Orbiting Laboratory for Testing CSI Technology

5. FUNDING NUMBERS

C NAS1-18763

WU 585-03-11-08

6. AUTHOR(S)

Andrew S. Bicos
Gregory G. Loboda

7. PERFORMING ORGANIZATION NAME(S) AND ADDRESS(ES)

McDonnell Douglas Aerospace
5301 Bolsa Avenue
Huntington Beach, CA 92647

8. PERFORMING ORGANIZATION REPORT NUMBER

MDC 93H0100

9. SPONSORING / MONITORING AGENCY NAME(S) AND ADDRESS(ES)

National Aeronautics and Space Administration
Langley Research Center
Hampton, VA 23681-0001

10. SPONSORING / MONITORING AGENCY REPORT NUMBER

NASA CR-191524

11. SUPPLEMENTARY NOTES

Langley Technical Monitor: Anthony Fontana
Final Report - Task 18

12a. DISTRIBUTION / AVAILABILITY STATEMENT

Unclassified - Unlimited
Subject Category 18

12b. DISTRIBUTION CODE

13. ABSTRACT (Maximum 200 words)

A concept for an orbiting laboratory for testing Controls-Structures Integration (CSI) technology is described. The CSI-Star concept reflects a lower cost, higher risk approach. The concept supports demonstration and validation testing for critical CSI technologies at a cost of $20M to $26M with a 1-year reliability of approximately 0.9. The Ball Aerospace QuickStar bus is the carrier for the CSI test article. QuickStar is launched as a secondary payload on the McDonnell Douglas Delta II. The QuickStar/Delta II approach is flight proven. The CSI test article is a 20 foot, 1 Hz., truss beam which is deployed from the QuickStar bus. The test article is well instrumented for quality system identification. The laboratory provides three layers of active control consisting of global vibration suppression along the truss beam, vibration isolation between the beam and instrument platforms, and vibration compensation through the use of gimbaled platforms which point lasers relative to optical sensor targets. The configuration simulates the dynamics of multi-instrument science platforms such as those of the Earth Observation System (EOS) while maintaining strong ties to astrophysics missions such as the Optical Interferometer. Uplink/downlink services and a reprogramable computer provide flexibility for long-term investigations by members of the CSI community (NASA, DoD, academia, and industry). CSI-Star fills the gap between short-term experiments, which have been conducted primarily on the Shuttle, and future science missions which require the technology. The on-orbit maturity of CSI technology must be established to obtain acceptance by project managers and to promote injection of the technology into future science missions.

14. SUBJECT TERMS

Flight Experiments, Control Systems, System Identification, Controls-Structures Integration

15. NUMBER OF PAGES

107

16. PRICE CODE

A06

17. SECURITY CLASSIFICATION OF REPORT	18. SECURITY CLASSIFICATION OF THIS PAGE	19. SECURITY CLASSIFICATION OF ABSTRACT	20. LIMITATION OF ABSTRACT
Unclassified	Unclassified		